NASA CONTRACTOR REPORT

ANALYSIS AND DOCUMENTATION OF QCSEE (QUIET CLEAN SHORT-HAUL EXPERIMENTAL ENGINE) OVER-THE-WING EXHAUST SYSTEM DEVELOPMENT

R. C. Ammer and J. T. Kutney

Prepared by
GENERAL ELECTRIC COMPANY
Cincinnati, Ohio 45215
for Langley Research Center

NATIONAL AERONAUTICS AND SPACE ADMINISTRATION • WASHINGTON, D. C. • JUNE 1977

1. Report No.	2. Government Accession No.	3. Recipient's Catalog No.
NASA CR-2792		

4. Title and Subtitle	5. Report Date
ANALYSIS AND DOCUMENTATION OF QCSEE (QUIET CLEAN SHORT-HAUL EXPERIMENTAL ENGINE) OVER-THE-WING EXHAUST SYSTEM DEVELOPMENT	June 1977
	6. Performing Organization Code

7. Author(s)	8. Performing Organization Report No.
R.C. Ammer and J.T. Kutney	R76AEG407
	10. Work Unit No.

9. Performing Organization Name and Address	11. Contract or Grant No.
General Electric Company Aircraft Engine Group, AE&TPD Cincinnati, Ohio 45215	NAS1-14270
	13. Type of Report and Period Covered
12. Sponsoring Agency Name and Address	Contract Report
National Aeronautics and Space Administration Washington, D.C. 20546	14. Sponsoring Agency Code

15. Supplementary Notes

Final Report
NASA Technical Representative: A.E. Phelps III
NASA-Langley Research Center, Hampton, Virginia

16. Abstract

A static scale model test program was conducted in the static test area of the NASA-Langley 9.14- by 18.29 m (30- by 60-ft) Full-Scale Wind Tunnel Facility to develop an over-the-wing (OTW) nozzle and reverser configuration for the Quiet Clean Short-Haul Experimental Engine (QCSEE). Three nozzles and one basic reverser configuration were tested over the QCSEE take-off and approach power nozzle pressure ratio range between 1.1 and 1.3. The models were scaled to 8.53% of QCSEE engine size and tested behind two 13.97-cm (5.5-in.) diameter tip-turbine-driven fan simulators coupled in tandem.

An OTW nozzle and reverser configuration was identified which satisfies the QCSEE experimental engine requirements in terms of nozzle cycle area variation capability and reverse thrust level, and provides good jet flow spreading over a wing upper surface for achievement of high propulsive lift performance.

17. Key Words (Suggested by Author(s))		18. Distribution Statement
Nozzle	Reverse Thrust Ratio	
Reverser	Airflow Ratio	
Exhaust System	Static Test	
Velocity Coefficient	QCSEE	
Flow Coefficient	Over-the-Wing	
Reverser Effectivity		Subject Category 07

19. Security Classif. (of this report)	20. Security Classif. (of this page)	21. No. of Pages	22. Price*
UNCLASSIFIED	UNCLASSIFIED	143	$6.00

* For sale by the National Technical Information Service, Springfield, Virginia 22161

FOREWORD

The contributions of J.L. Johnson, Jr. and A.E. Phelps, III, both from the Dynamic Stability Branch, Subsonic-Transonic Aerodynamics Division of NASA-Langley, are acknowledged. Messrs. Johnson and Phelps were responsible for all the scale model detail design, fabrication, and testing required for this experimental program.

The assistance of W.H. Hoelmer and R.G. Siegfried, both from the General Electric Company, is also acknowledged. Messrs. Hoelmer and Siegfried made significant contributions throughout the extended test period and established the methods used in the analysis of data in this report.

TABLE OF CONTENTS

Section		Page
1.0	INTRODUCTION	1
2.0	SUMMARY	2
3.0	MODEL AND TEST DESCRIPTION	4
	3.1 Test Facility	4
	3.2 Model Test Hardware	4
	3.2.1 Propulsion Simulator - General Arrangement	4
	3.2.2 Calibration Nozzles	4
	3.2.3 QCSEE Duct and Scale Model Simulation	8
	3.2.4 "D" Nozzle Configurations	8
	3.2.5 Reverser Configurations	16
	3.2.6 Wing Simulation	22
	3.3 Instrumentation	22
	3.4 Method of Test	25
4.0	ROUND NOZZLE CALIBRATION TEST RESULTS AND DATA ADJUSTMENTS	26
5.0	FORWARD THRUST NOZZLE DEVELOPMENT	34
	5.1 Test Matrix	34
	5.2 Internal Nozzle Performance	34
	5.2.1 Flow Coefficient Results	34
	5.2.2 Velocity Coefficient Results	39
	5.2.3 Nozzle Kickdown Angle	43
	5.2.4 Side Door Angle Derivatives for Flow and Velocity Coefficients	43
	5.3 Nozzle Configuration Recommendation	48
6.0	THRUST REVERSER PERFORMANCE	54
	6.1 Performance Basis	54
	6.2 Initial Parameter Sensitivity Screening	54
	6.2.1 Side Skirt Effects	57
	6.2.2 Blocker Spacing Effects	57
	6.2.3 Blocker Height Effects	65
	6.3 Parametric Matrix	65
	6.3.1 Side Skirt Angle Effects	65
	6.3.2 Blocker Inclination Angle Effects	69
	6.3.3 Lip Length Ratio Effects	69
	6.3.4 Lip Angle Effects	69

TABLE OF CONTENTS (Concluded)

Section		Page
	6.4 Other Performance Effects	69
	6.4.1 Lip Cutback Effects	69
	6.4.2 Reingestion Shield Effects	77
	6.4.3 Ground Plane Effects	77
	6.5 Reverser Configuration Recommendations	78
7.0	CONCLUSIONS	82
8.0	NOMENCLATURE	84
	APPENDIX A - Preliminary Static Turning Performance Data and Test Methodology	87
	APPENDIX B - Data Reduction Summary	98
	APPENDIX C - Forward Thrust Test Results	105
	APPENDIX D - Reverse Thrust Test Results	116
9.0	REFERENCES	133

LIST OF ILLUSTRATIONS

Figure		Page
1.	Static Test Setup.	5
2.	Test Hardware Elements.	6
3.	Calibration Nozzles.	7
4.	Comparison of QCSEE Exhaust Ducts and Single-Flow Stream Test Configuration.	9
5.	QCSEE Scale Model "D" Nozzle Geometry.	10
6.	Thrust Reverser Scale Model Geometry.	19
7.	OTW Thrust Reverser Static Test Installation.	20
8.	Reverser Configurations on Test.	21
9.	Simulated Wing Configurations.	23
10.	Test Instrumentation Sketch.	24
11.	Calibration Nozzle Measured Flow Coefficients.	28
12.	Calibration Nozzle Measured Velocity Coefficients.	29
13.	Calibration Nozzle Adjusted Flow Coefficients.	30
14.	Calibration Nozzle Adjusted Velocity Coefficients.	31
15.	Comparison of Calibration Nozzle Data with QCSEE Nozzle and Reverser.	32
16.	QCSEE Baseline OTW Nozzle Flow Coefficients.	36
17.	QCSEE RC-1 Nozzle Flow Coefficients.	37
18.	QCSEE RC-2 Nozzle Flow Coefficients.	38
19.	QCSEE Baseline OTW Nozzle Velocity Coefficients.	40
20.	QCSEE RC-1 Nozzle Velocity Coefficients.	41
21.	QCSEE RC-2 Nozzle Velocity Coefficients.	42
22.	Jet Spreading Characteristics of the QCSEE Nozzle at Takeoff.	44

LIST OF ILLUSTRATIONS (Continued)

Figure		Page
23.	QCSEE Baseline OTW Nozzle Exhaust Flow Angle.	45
24.	QCSEE RC-1 Nozzle Exhaust Flow Angle.	46
25.	QCSEE RC-2 Nozzle Exhaust Flow Angle.	47
26.	Effect of Side Door Position on Flow Coefficient, QCSEE Baseline OTW Nozzle.	49
27.	Effect of Side Door Position on Flow Coefficient, QCSEE RC-1 Nozzle Configuration.	50
28.	Effect of Side Door Position on Flow Coefficient, QCSEE RC-2 Nozzle Configuration.	51
29.	Effect of Side Door Position on Velocity Coefficients, QCSEE Baseline, RC-1 and RC-2 Configurations.	52
30.	Forward Mode Reference "D" Nozzle Thrust and Airflow Characteristics.	55
31.	Effect of Reverser Side Skirt Geometry and Angle on Reverse Thrust and Airflow Characteristics, L/D_{TH} = 0.4.	58
32.	Effect of Reverser Side Skirt Geometry and Angle on Reverse Thrust and Airflow Characteristics, L/D_{TH} = 0.8.	59
33.	Effect of Reverser Side Skirt Geometry and Angle on Effective Efflux Angle.	60
34.	Effect of Nominal and Extended Side Skirts on Reverse Thrust and Airflow Characteristics for Lip Length Ratios of 0.4 and 0.8.	61
35.	Effect of Nominal and Extended Side Skirts on Reverse Thrust and Airflow Characteristics for Lip Length Ratios of 0.4 and 0.8.	62
36.	Effect of Blocker Spacing on Reverse Thrust and Airflow Characteristics.	63
37.	Effect of Blocker Spacing on Effective Efflux Angle.	64
38.	Effect of Blocker Height on Reverse Thrust and Airflow Characteristics at L/D_{TH} = 0.4 and 0.8.	66

LIST OF ILLUSTRATIONS (Continued)

Figure		Page
39.	Change in Reverse Thrust and Airflow Characteristics with Side Skirt Angle.	68
40.	Change in Reverse Thrust and Airflow Characteristics with Blocker Door Angle.	70
41.	Change in Reverse Thrust and Airflow Characteristics with Lip Length Ratio.	71
42.	Change in Reverse Thrust and Airflow Characteristics with Lip Angle.	72
43.	Reingestion Pipe, Full Scale.	73
44.	Effect of Lip Cutback on Reverse Thrust and Airflow Characteristics.	75
45.	Effects of Ground Plane and Reingestion Shielding on Reverse Thrust.	76
46.	OTW Reverser Configuration Recommendation.	79
47.	Effect of Lip Length Ratio and Blocker Door Angle on Reverse Thrust Performance for Various Pressure Ratios.	80
48.	Effect of Side Skirt Angle and Blocker Door Angle on Airflow Performance for Various Pressure Ratios.	81
49.	Preliminary Exploratory Test Configurations for Static Turning Performance.	91
50.	Preliminary Static Turning Performance, Configuration 1, QCSEE OTW Baseline Nozzle.	92
51.	Preliminary Static Turning Performance, Configuration 2.	93
52.	Preliminary Static Turning Performance, Configuration 3.	94
53.	Preliminary Static Turning Performance, Configuration 4.	95
54.	Preliminary Static Turning Performance, Configuration 5.	96
55.	Preliminary Static Turning Performance, Baseline and Recontoured Nozzle, RC-1.	97

LIST OF ILLUSTRATIONS (Continued)

Figure		Page
56.	Effect of Nozzle Side Door Angle on Performance, QCSEE Baseline Configuration, Large Plate On.	106
57.	Effect of Nozzle Side Door Angle on Performance, QCSEE Baseline Configuration, Small Plate On.	107
58.	Effect of Nozzle Side Door Angle on Performance, QCSEE Baseline Configuration, Plate Off.	108
59.	Effect of Nozzle Side Door Angle on Performance, RC-1 Configuration, Large Plate On.	109
60.	Effect of Nozzle Side Door Angle on Performance, RC-1 Configuration, Small Plate On.	110
61.	Effect of Nozzle Side Door Angle on Performance, RC-1 Configuration, Plate Off.	111
62.	Effect of Nozzle Side Door Angle on Performance, RC-2 Configuration, Large Plate On.	112
63.	Effect of Nozzle Side Door Angle on Performance, RC-2 Configuration, Small Plate On.	113
64.	Effect of Nozzle Side Door Angle on Performance, RC-2 Configuration, Plate Off.	114
65.	Effect of Side Door Removal, Large Plate On.	115
66.	Effect of Lip Length Ratio and Side Skirt Configuration on Reverse Thrust and Airflow, $\alpha = 95°$, $\beta = 25°$.	117
67.	Effect of Lip Length Ratio and Side Skirt Configuration on Reverse Thrust and Airflow, $\alpha = 95°$, $\beta = 35°$.	118
68.	Effect of Lip Length Ratio and Skirt Configuration on Effective Efflux Angle, $\alpha = 95°$, $\beta = 25°$.	119
69.	Effect of Lip Length Ratio and Skirt Configuration on Effective Efflux Angle, $\alpha = 95°$, $\beta = 35°$.	120
70.	Effect of Lip Length Ratio and Side Skirt Configuration on Reverse Thrust and Airflow, $\alpha = 105°$, $\beta = 25°$.	121
71.	Effect of Lip Length Ratio and Side Skirt Configuration on Reverse Thrust and Airflow, $\alpha = 105°$, $\beta = 15°$.	122

LIST OF ILLUSTRATIONS (Concluded).

Figure		Page
72.	Effect of Tabbed Side Skirt Angle on Reverse Thrust and Airflow, α = 105°, β = 35°.	123
73.	Effect of Lip Length Ratio and Side Skirt Configuration on Effective Efflux Angle, α = 105°, β = 25°.	124
74.	Effect of Lip Length Ratio and Side Skirt Configuration on Effective Efflux Angle, α = 105°, β = 15°.	125
75.	Effect of Tabbed Side Skirt Angle on Effective Efflux Angle, α = 105°, β = 35°.	126
76.	Effect of Lip Length Ratio and Side Skirt Configuration on Reverse Thrust and Airflow, α = 115°, β = 15°.	127
77.	Effect of Side Skirt Configuration on Reverse Thrust and Airflow, α = 115°, β = 25°.	128
78.	Effect of Lip Length Ratio and Side Skirt Configuration on Effective Efflux Angle, α = 115°, β = 15°.	129
79.	Effect of Side Skirt Configuration on Effective Efflux Angle, α = 105°, β = 25°.	130
80.	Effect of Blast Shield on Reverse Thrust and Airflow Characteristics.	131
81.	Effect of Inlet Type on Reverse Thrust.	132

LIST OF TABLES

Table		Page
1.	Constants for Polynomial Curve Fit for Total Pressure Bias Correction.	27
2.	Constants for Polynomial Curve Fit for Cruise and Reverse Thrust Total Pressure Corrections.	33
3.	Forward Thrust Test Matrix.	35
4.	Nozzle Performance Summary.	53
5.	Reverser Parameter Sensitivity Screening Matrix.	56
6.	Reverser Parametric Test Matrix.	67
7.	Supplementary Reverser Test Configurations.	74

SECTION 1.0

INTRODUCTION

The Langley Research Center of the National Aeronautics and Space Administration and the General Electric Company have conducted a scale model experimental development program for an over-the-wing (OTW), powered lift, propulsion system in support of the NASA-Lewis Research Center QCSEE (Quiet, Clean, Short-Haul Experimental Engine) contract with the General Electric Company. This program was structured to utilize the significant propulsive lift background and experience of the Langley Dynamic Stability Branch in the design of the QCSEE OTW exhaust system. The program was conducted in the time period of 1975 and early 1976.

The exhaust system concept, which evolved under the QCSEE contract for the OTW installation, combined the requirements for engine cycle area variation and thrust reversal with the requirement of jet flow spreading for good jet/flap flow turning under powered-lift landing approach conditions. The large cycle area variation (about 20%) between takeoff and cruise was required to provide takeoff thrust at low pressure ratio (open nozzle) for QCSEE noise consideration, and high pressure ratio thrust (closed nozzle) for more efficient high speed cruise performance. This integrated OTW nozzle/reverser exhaust system employed new features about which there were some technical concerns:

- The new side door area variation concept lacked a sufficient data base to ensure adequate cycle area variation capability and flow spreading enhancement for wing/flap flow attachment at approach flap settings.

- The thrust reverser single blocker door and exit lip geometry lacked a sufficient data base to assess reverse thrust performance; and, axial placement of the blocker needed better aerodynamic definition from the standpoint of engine cycle area matching.

The scale model program, therefore, was initiated at Langley to provide an adequate data base in response to these technical concerns, from which final design of the QCSEE OTW exhaust system could proceed.

General Electric engineering coverage during the test period was under direct QCSEE Contract (NAS3-18021) funding. Documentation and comprehensive analysis of the nozzle and thrust reverser internal performance data included in this report were funded under separate contract to NASA-Langley (NAS1-14270).

SECTION 2.0

SUMMARY

A static scale model test program was conducted by NASA-Langley in the static test area of NASA-Langley's 9.14- by 18.29-m (30- by 60-ft) Full-Scale Wind Tunnel Facility to develop an over-the-wing (OTW) nozzle and reverser configuration for the Quiet, Clean Short-Haul Experimental Engine (QCSEE). The subject contract effort consisted of the engineering analysis and documentation of the major aspects of this test program. The objectives of the program being reported were to develop an OTW nozzle/reverser system which met the QCSEE demonstrator engine requirements in terms of nozzle area variation capability and reverse thrust level, and which provided good jet flow spreading over the wing upper surface for a high jet/flap static turning angle and turning efficiency at landing approach conditions. The models were scaled to 8.53% of QCSEE engine size and tested behind two 13.97-cm (5.5-in.) tip-turbine-driven fan simulators coupled in tandem. Three nozzles: the QCSEE baseline, Recontour No. 1 (RC-1), and Recontour No. 2 (RC-2), and one basic reverser configuration were tested over a takeoff and approach power range of pressure ratios between 1.1 and 1.3. The principal nozzle design variables were internal flowpath contouring to increase exhaust flow kickdown angle (requirement for high jet/flap static turning performance), and nozzle area variation side door geometry (required for engine cycle/effective area matching and good flow spreading for static turning performance). The nozzles were tested over a range of side door area settings from cruise (closed) to beyond the takeoff setting (25° open), each configuration being evaluated with and without wing upper surface simulation. The principal reverser design variables investigated were blocker door axial spacing, blocker door height, blocker door inclination angle (rotation about the blocker pivot point), lip length, lip angle, and blocker door side skirt geometry.

OTW nozzle and reverser configurations have been identified which satisfy the QCSEE requirements. The variable area side door concept was shown to be a viable design demonstrating good area variation capability (20% takeoff to cruise) and good flow spreading characteristics. When employed with the recommended recontoured, high kickdown internal flowpath (RC-1), the nozzle shows promise of achieving high static turning angles and high turning efficiencies at powered-lift approach conditions. The OTW thrust reverser design demonstrated reverser effectivity levels commensurate with the 35% reverse thrust QCSEE requirement when tabbed or extended side skirts, which rotate outward to capture blocker door side spillage flow, are employed. While reverse mode effective discharge area (airflow capacity) was found to be ~20% less than the QCSEE cycle takeoff power value, the recommended reverser configuration provides sufficient discharge area to maintain safe engine operating margins for full-scale experimental testing.

The nozzle and thrust reverser configuration which was experimentally developed under the QCSEE program, and whose analysis is reported herein, is considered to be fully representative of low speed OTW propulsive lift exhaust systems. It is recognized that further development of this experimental nozzle and thrust reverser configuration is required in order to arrive at a high performance flight configuration.

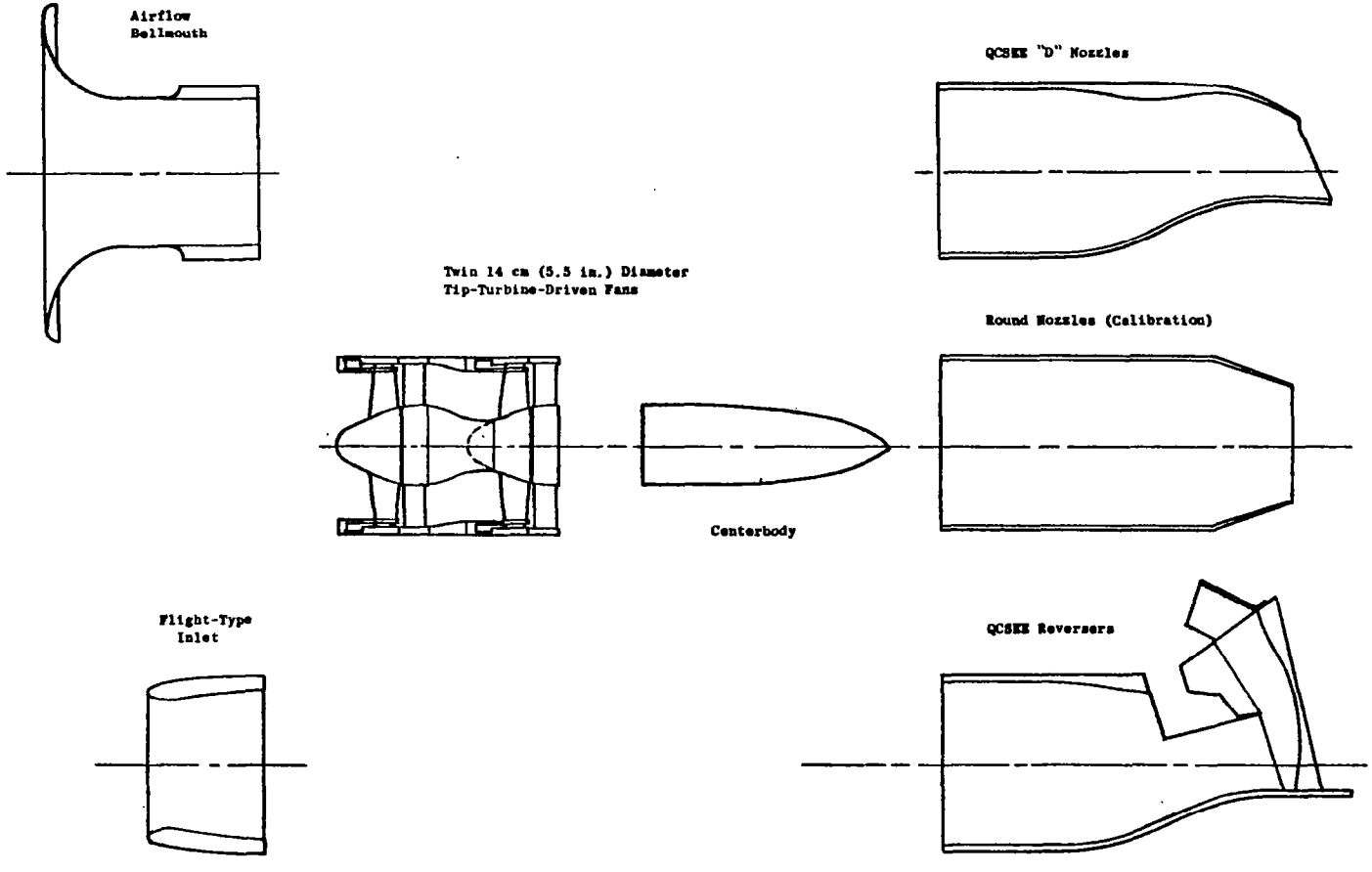

Figure 2. Test Hardware Elements.

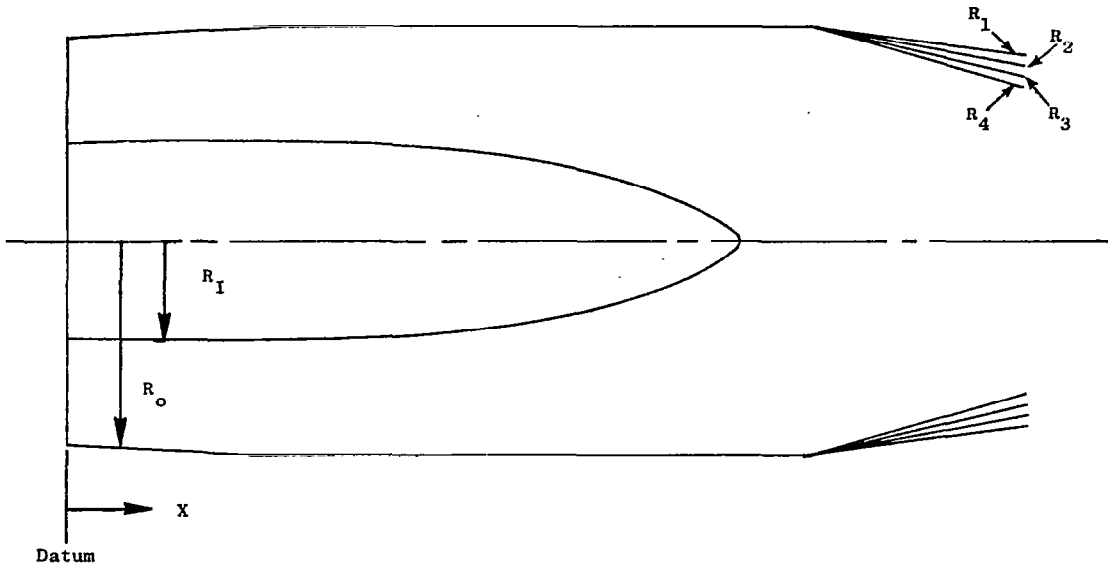

Axial Dimension X		Centerbody R_I		Nozzle R_o		
cm	(in.)	cm	(in.)	cm	(in.)	
0	(0)	3.734	(1.47)	7.62	(3.00)	
6.985	(2.75)	3.734	(1.47)	8.001	(3.15)	
8.382	(3.30)	3.708	(1.46)			
10.541	(4.15)	3.632	(1.43)			
12.725	(5.01)	3.493	(1.375)			
14.884	(5.86)	3.251	(1.28)			
17.043	(6.71)	2.946	(1.16)			
19.202	(7.56)	2.464	(0.97)			
21.387	(8.42)	1.753	(0.69)			
23.546	(9.27)	0.597	(0.235)			
23.978	(9.44)	0	0			
26.67	(10.5)	-	-			
34.29	(13.5)	-	-	6.934	(2.73) - R1	4 Calibration Nozzle Exit Configurations
				6.553	(2.58) - R2	
				6.147	(2.42) - R3	
				5.740	(2.26) - R4	

Figure 3. Calibration Nozzles.

3.2.3 QCSEE Duct and Scale Model Simulation

The QCSEE over-the-wing (OTW) engine is a high-bypass-ratio (10:1) mixed-flow turbofan with fan and core streams exhausting through a common "D" nozzle. Since the 14cm (5.5in.)-diameter fans selected for use during these QCSEE exhaust system development tests could not simulate the hot core stream, exhaust duct and centerbody geometries were defined which faired over the QCSEE core region. Figure 4 shows the faired model test configuration in relation to the real QCSEE duct geometry in the region between the full-scale engine fan exit guide vanes (Station 200) and the core nozzle centerbody trailing edge (Station 302). (Station notation applies to General Electric drawing number 4013174-198, design "B", as shown in Figure 5.) All engine dimensions which appear henceforth were referred to this reference drawing. The single-flow model centerbody was terminated at approximately the same engine station for better simulation of the flow field into the "D" nozzle, considering the single-flow constraints.

3.2.4 "D" Nozzle Configurations

The QCSEE scale models tested were developed from 1/4-scale undimensioned engine flowpath drawings with cross-sectional cuts photographically reduced to 0.0853 scale for model fabrication at Langley's model shop. All models were made of fiber glass. Hardware modifications were made on-site as required during the test, based on observed test results.

In all, three scale model "D" nozzle models were built. The first of these was a direct scale of the QCSEE Baseline engine flowpath as defined by GE drawing 4013174-198, a reduced sized copy of which is shown as Figure 5(a). Two nozzle area variation side door configurations were made as shown in Figure 5(b). The positions shown for both door geometries were designed to satisfy the QCSEE engine cycle discharge area requirements at takeoff; the two-door configurations were tested early in this program to determine their relative flow spreading characteristics for potential benefit to powered lift jet/flap static turning performance. Two interchangeable sets of small doors were made with door angles at 60° and 70°; five sets of interchangeable large doors (with angle settings of 20°, 25°, 30°, 40°, and 50°) were fabricated. Closed nozzle settings also were made for cruise nozzle simulation.

The two additional forward thrust nozzles, RC-1 and RC-2, were recontoured flowpaths designed for more downward flow direction (or kickdown angle) to improve jet spreading over the wing for increased static turning with the approach flap setting. The need for higher flow kickdown was established from the preliminary baseline nozzle test results shown in Appendix A. Both recontoured nozzles featured modified roof lines and steeper floor angles, as shown on Figures 5(c) and 5(d), which compare these two high-kickdown nozzle flowpaths with the baseline geometry. The baseline nozzle exit cross section was used in both recontoured nozzles, as shown in Figure 5(d).

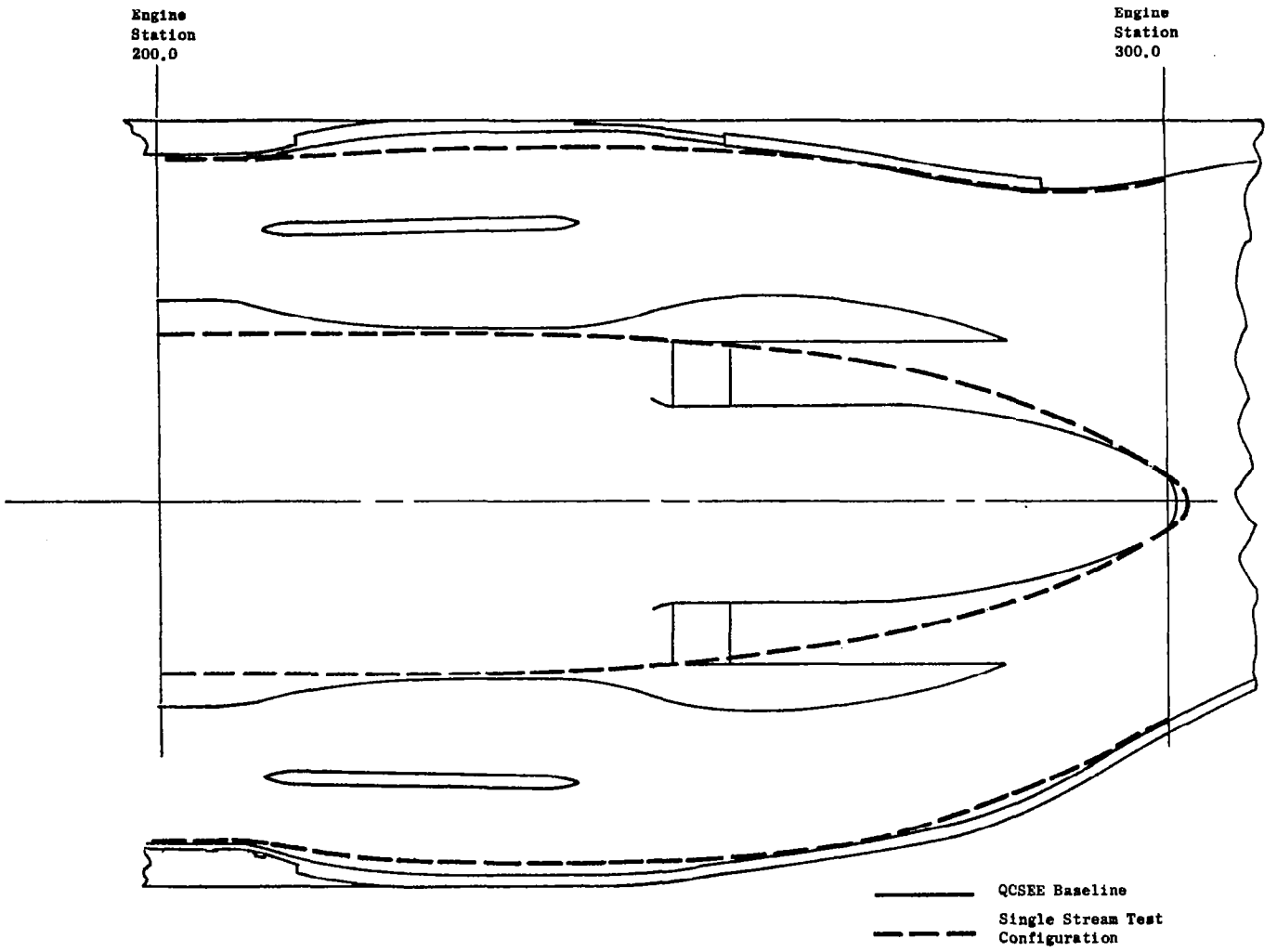

Figure 4. Comparison of QCSEE Exhaust Ducts and Single-Flow Stream Test Configuration.

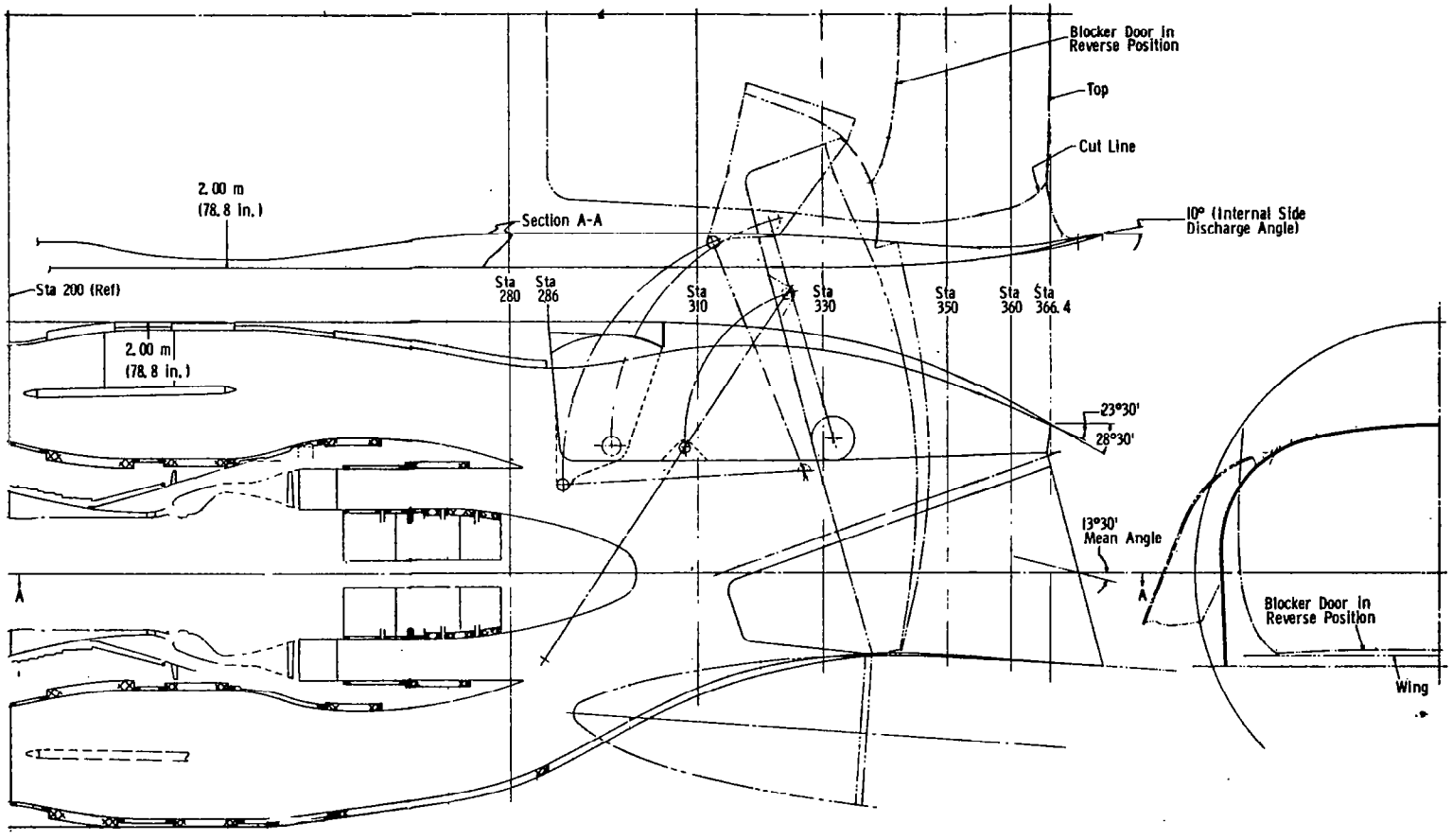

(a). Undimensioned Baseline Reference Drawing.

Figure 5. QCSEE Scale Model "D" Nozzle Geometry.

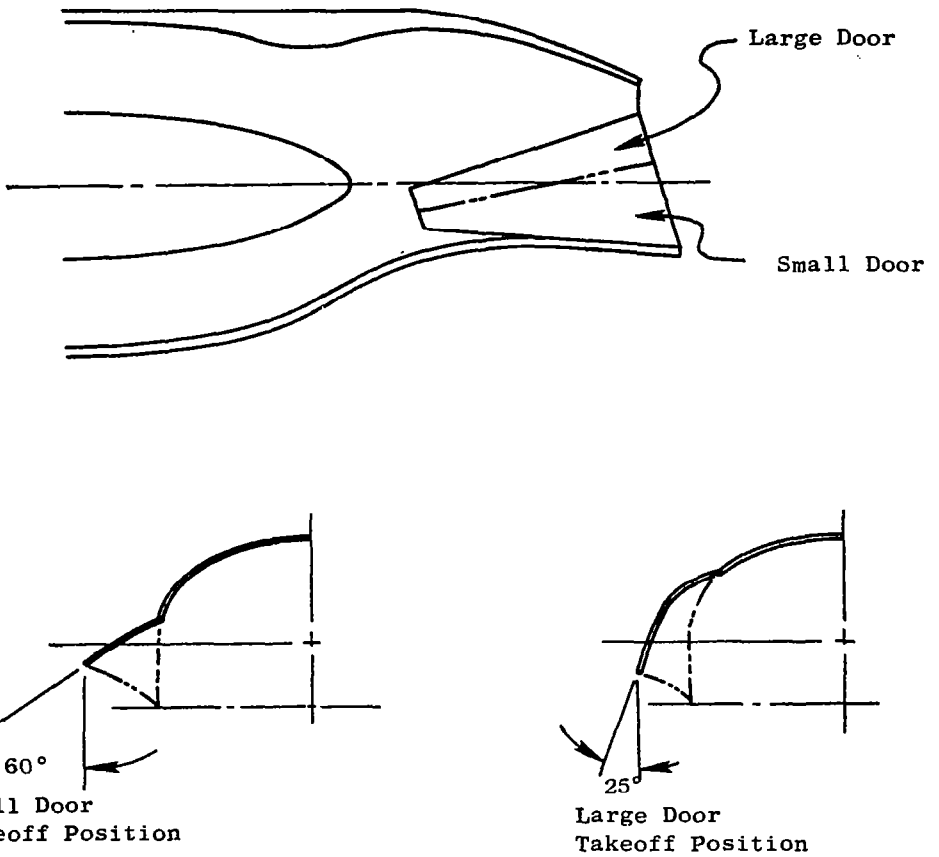

(b). Nozzle Side Door Designs.

Figure 5. QCSEE Scale Model "D" Nozzle Geometry (Continued).

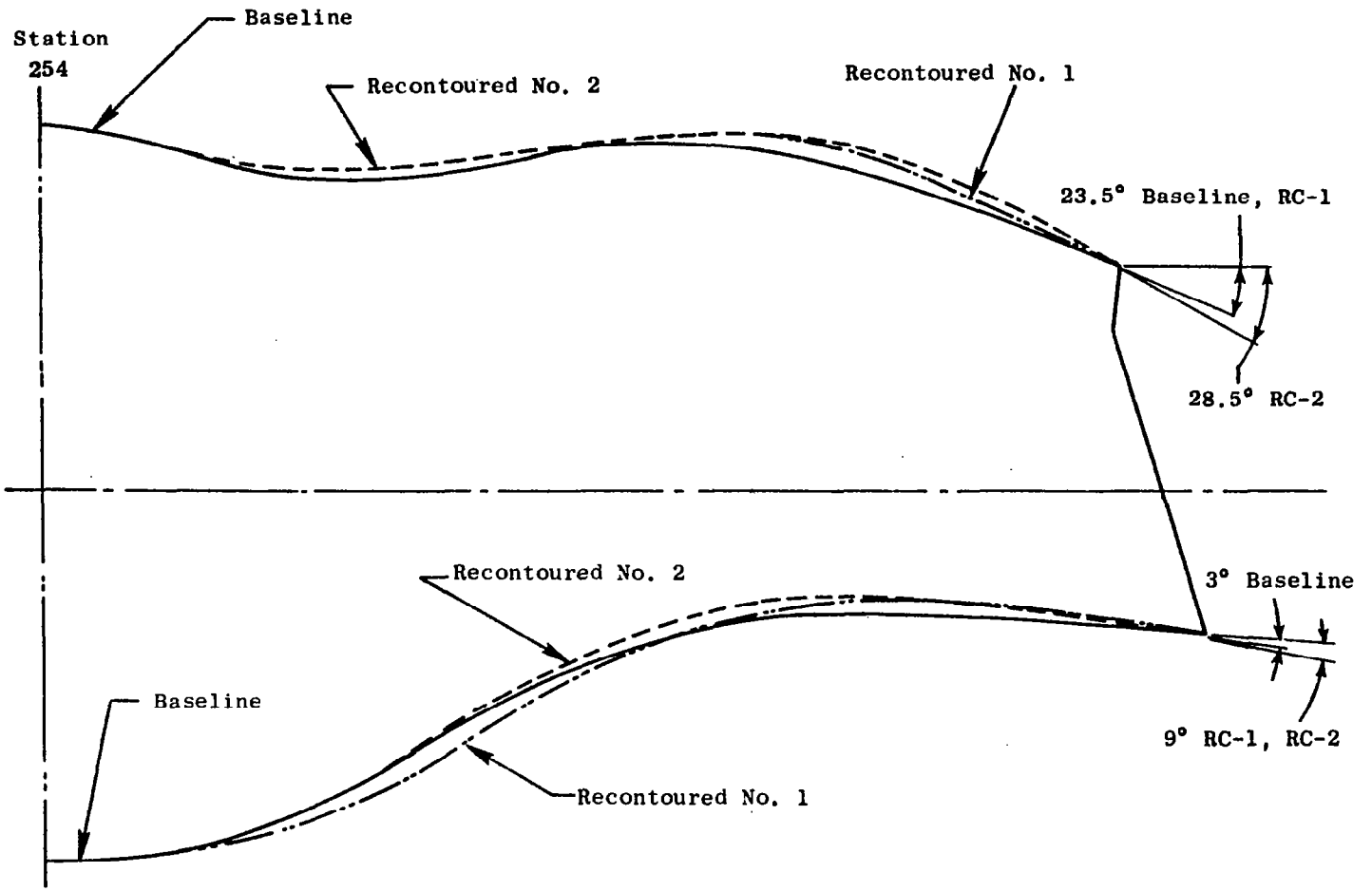

(c). Nozzle Internal Flowpaths, along Vertical Centerline.

Figure 5. QCSEE Scale Model "D" Nozzle Geometry (Continued).

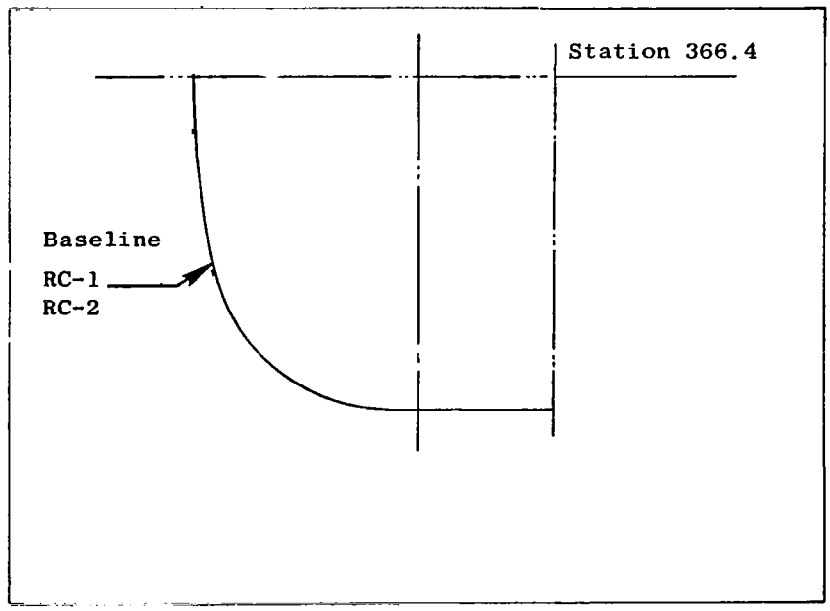

(d). Cross-Sectional Comparisons.

Figure 5. QCSEE Scale Model "D" Nozzle Geometry (Continued).

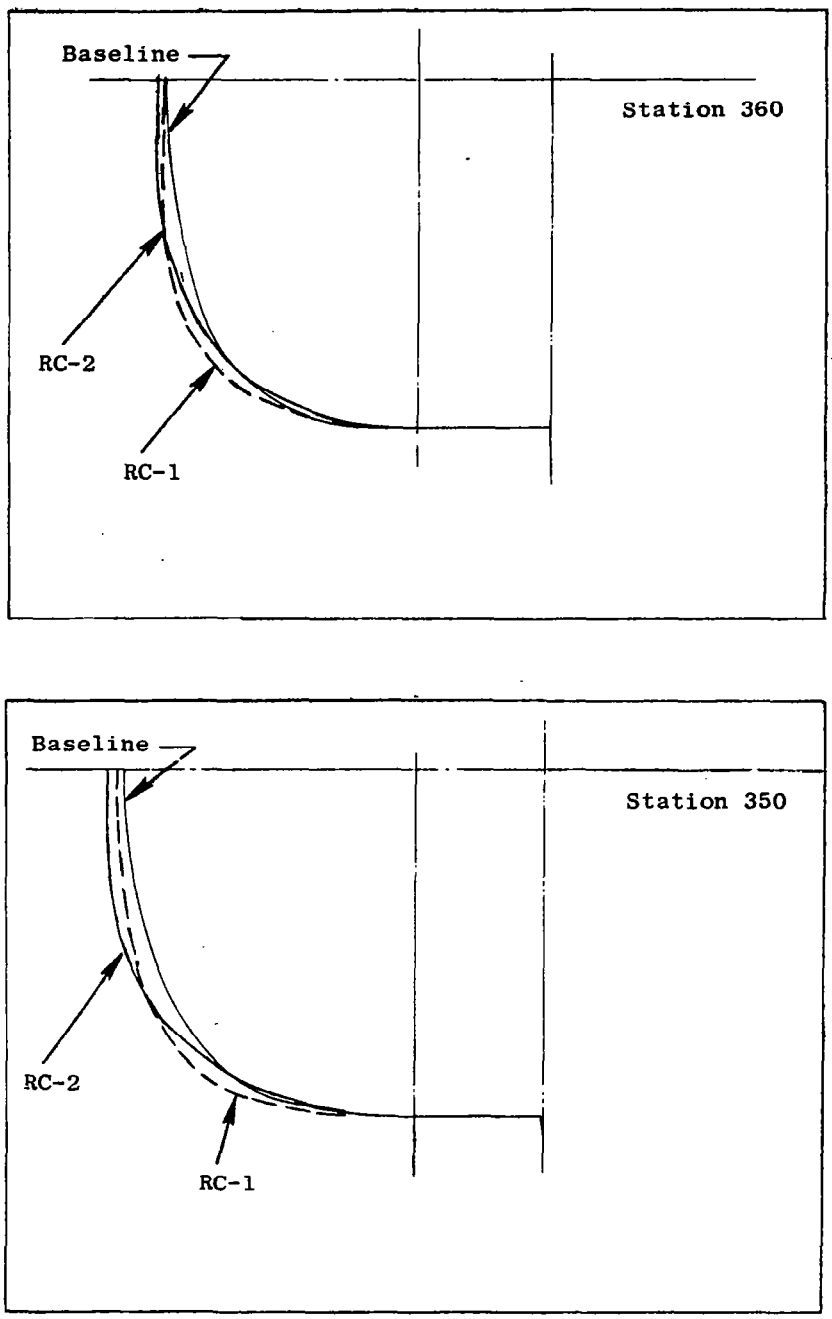

(d). Cross-Sectional Comparisons (Continued).

Figure 5. QCSEE Scale Model "D" Nozzle Geometry (Continued).

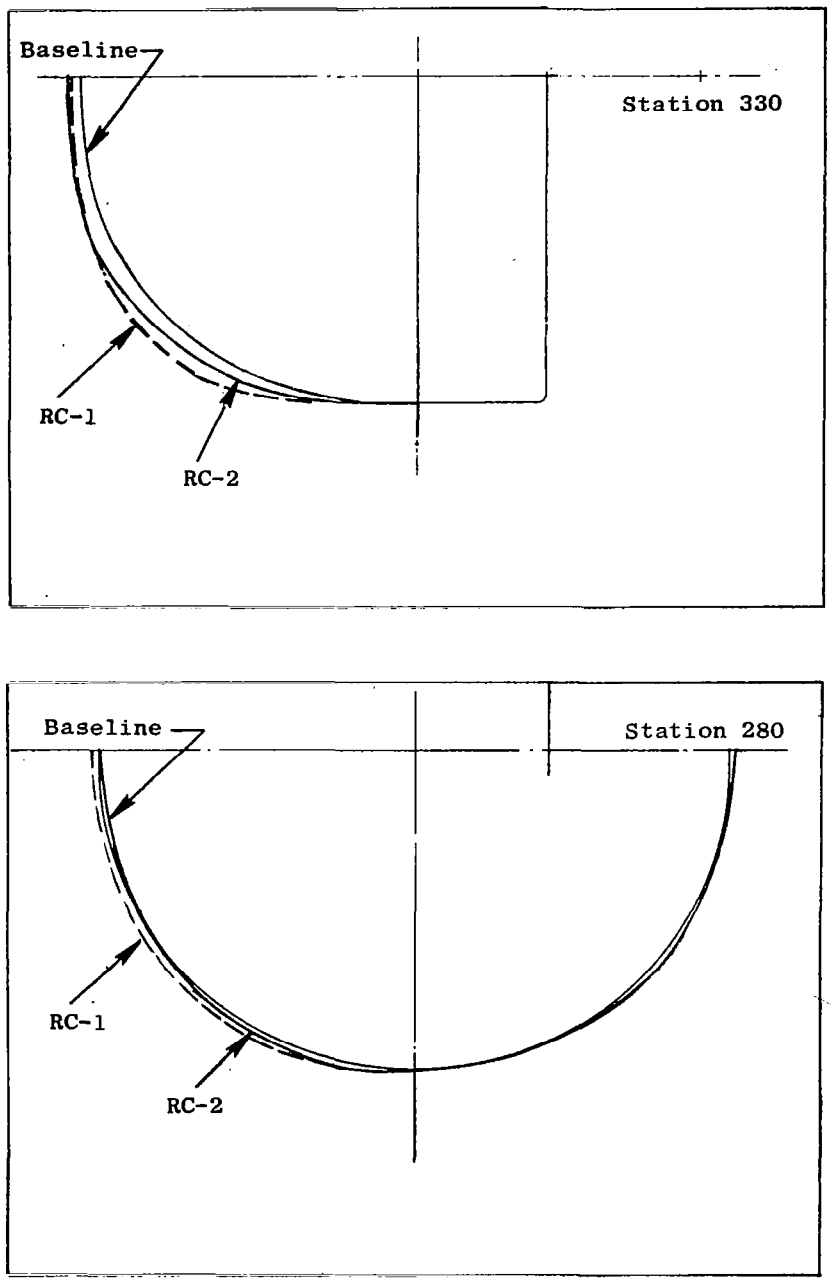

(d). Cross-Sectional Comparisons (Concluded).

Figure 5. QCSEE Scale Model "D" Nozzle Geometry (Continued).

Configuration RC-1 was modified from a foam core taken from the baseline pattern. Hand sketched nozzle roof templates were inserted into the foam core at selected axial stations, and epoxy filler was used to build up the new contour. The templates were designed to provide a steeper average flow angle over the nozzle roof as shown on Figure 5(e); as a result, the nozzle upper surface was flattened laterally with smaller corner radii employed to transition into the vertical side walls [Figure 5(d)].

The Recontour RC-2 flowpath was designed in 1/4-scale engine size, and then reduced photographically to 0.0853 scale for model construction. The RC-2 roof line was made steeper at the top (28.5°) and transitioned into the vertical side walls with larger radii (more like the baseline) to improve the nozzle external boattail lines. See Figures 5(d) and 5(e) for comparison with other configurations.

A typical nozzle model is shown in Figure 5(f). This picture shows the baseline configuration with large area variation side doors set at the 25° position.

3.2.5 Reverser Configurations

The thrust reverser scale model was made from the original baseline nozzle model, cut up to form the basic reverser opening and blocker door assembly. The reverser geometries and parameters tested are shown on Figure 6. Figure 7 shows one of the final configurations on test, while Figure 8 illustrates some of the preliminary screening test models which led to selection of the final test configurations.

Referring to Figure 6, the reverser model was built so that blocker door axial spacing (X_P, X_F), inclination angle (α), and height (H_B) were variable through the ranges indicated. Seven interchangeable blocker lips were made with varying lip length (L) and lip angle (β). These lips were selected such that 15°, 25°, and 35° β settings were obtained at blocker door inclination angle increments of 95°, 105°, and 115° α. As indicated from Figure 6, one lip was cut back to investigate its effect on reverse thrust; this configuration was a 0.4 L/D_{TH} lip which had a 35° lip angle as tested with the 105° blocker angle.

Interchangeable side skirts of varied design were added to the blocker during the development tests. These are shown in Figure 6 as the nominal side skirt, extended side skirt, and tabbed side skirt. These were made at 0° and 45° ϕ (with one extended skirt position at 25°). When skirt rotation was found to be beneficial to performance, the blocker door trim line was modified as shown by chamfering the door at a 45° angle (in line with 45° ϕ) and the piece removed was added back into the nacelle (Section E-E). Figure 7 shows a tabbed side skirt configuration on test, with some of the important model and facility features flagged for easy identification. The evolution of the tabbed side skirt geometry is shown on Figure 8, which shows (a) the basic blocker configuration without side skirts, and (b) the

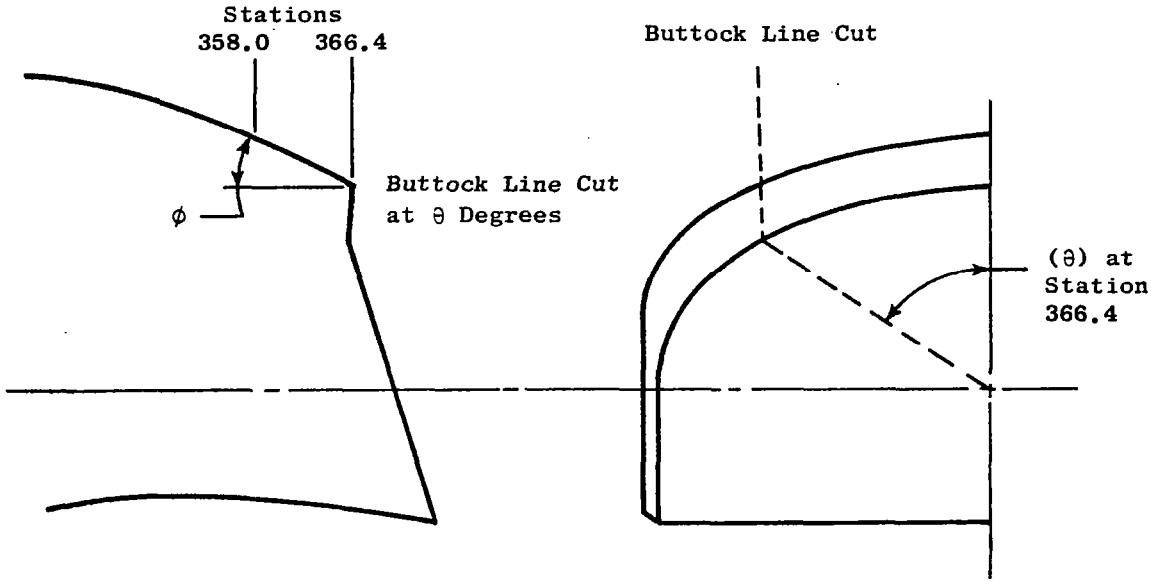

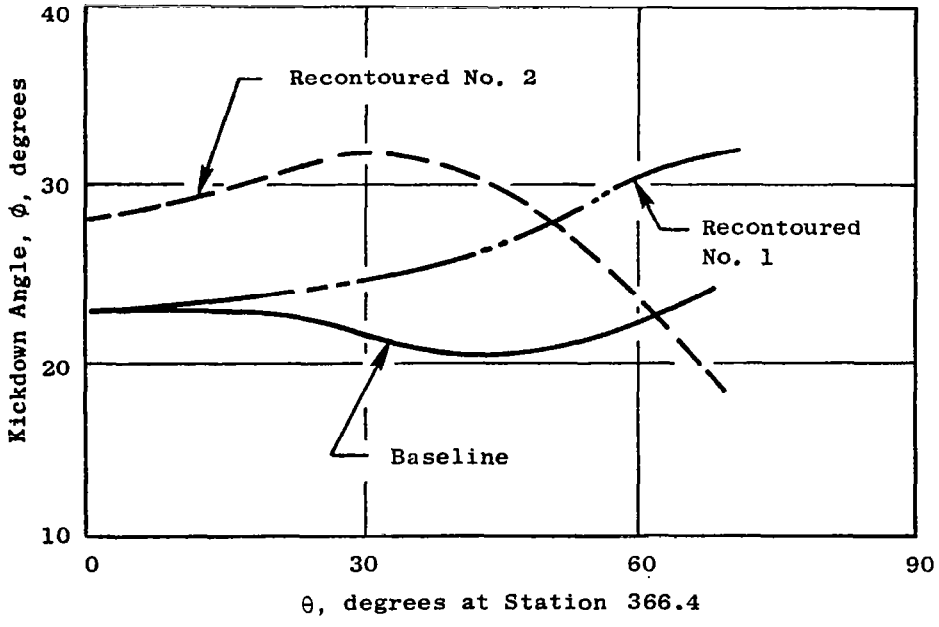

(e). Comparison of Nozzle Kickdown Angles.

Figure 5. QCSEE Scale Model "D" Nozzle Geometry (Continued).

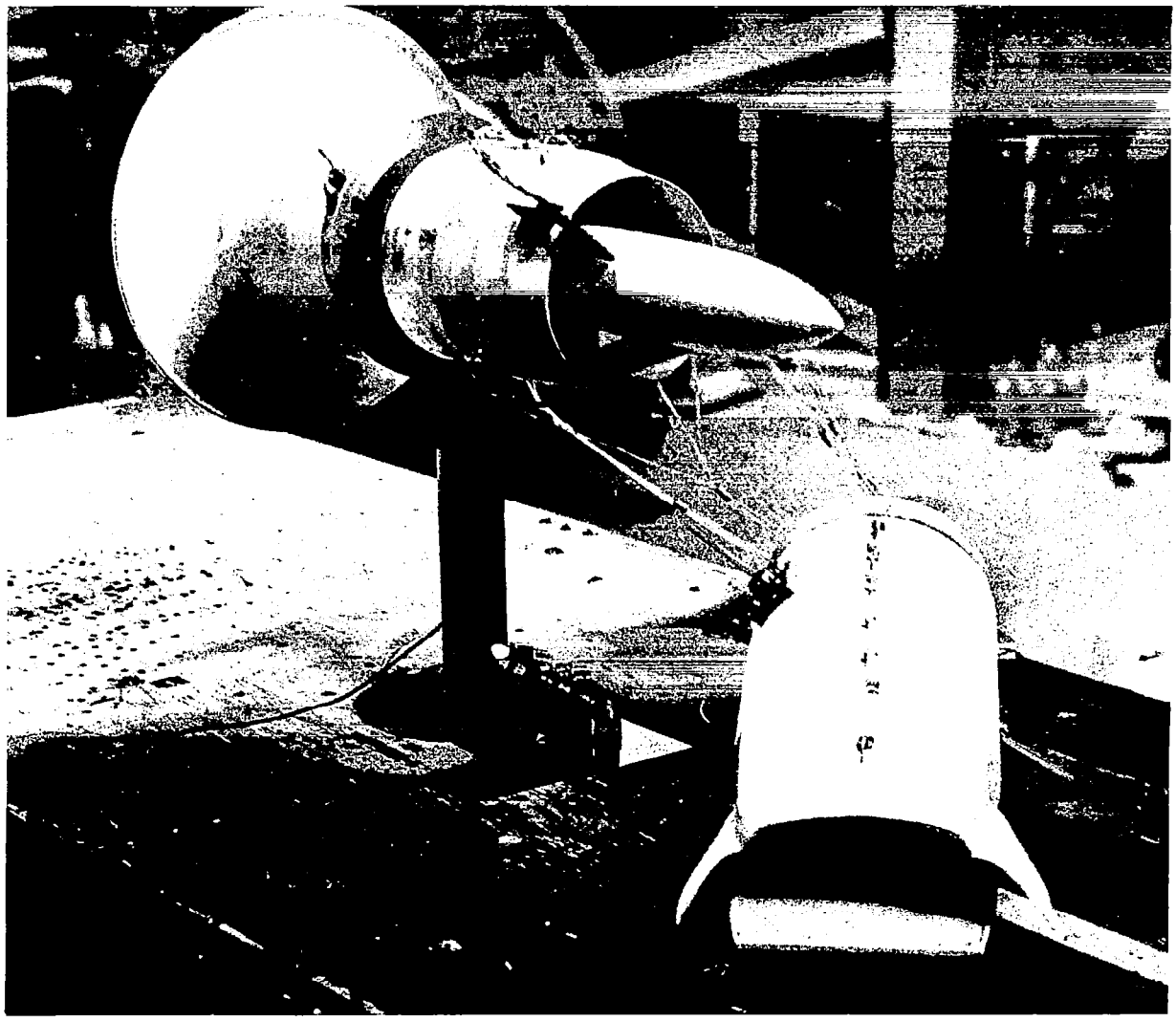

(f). Scale Model "D" Nozzle and Static Test Facility.

Figure 5. QCSEE Scale Model "D" Nozzle Geometry (Concluded).

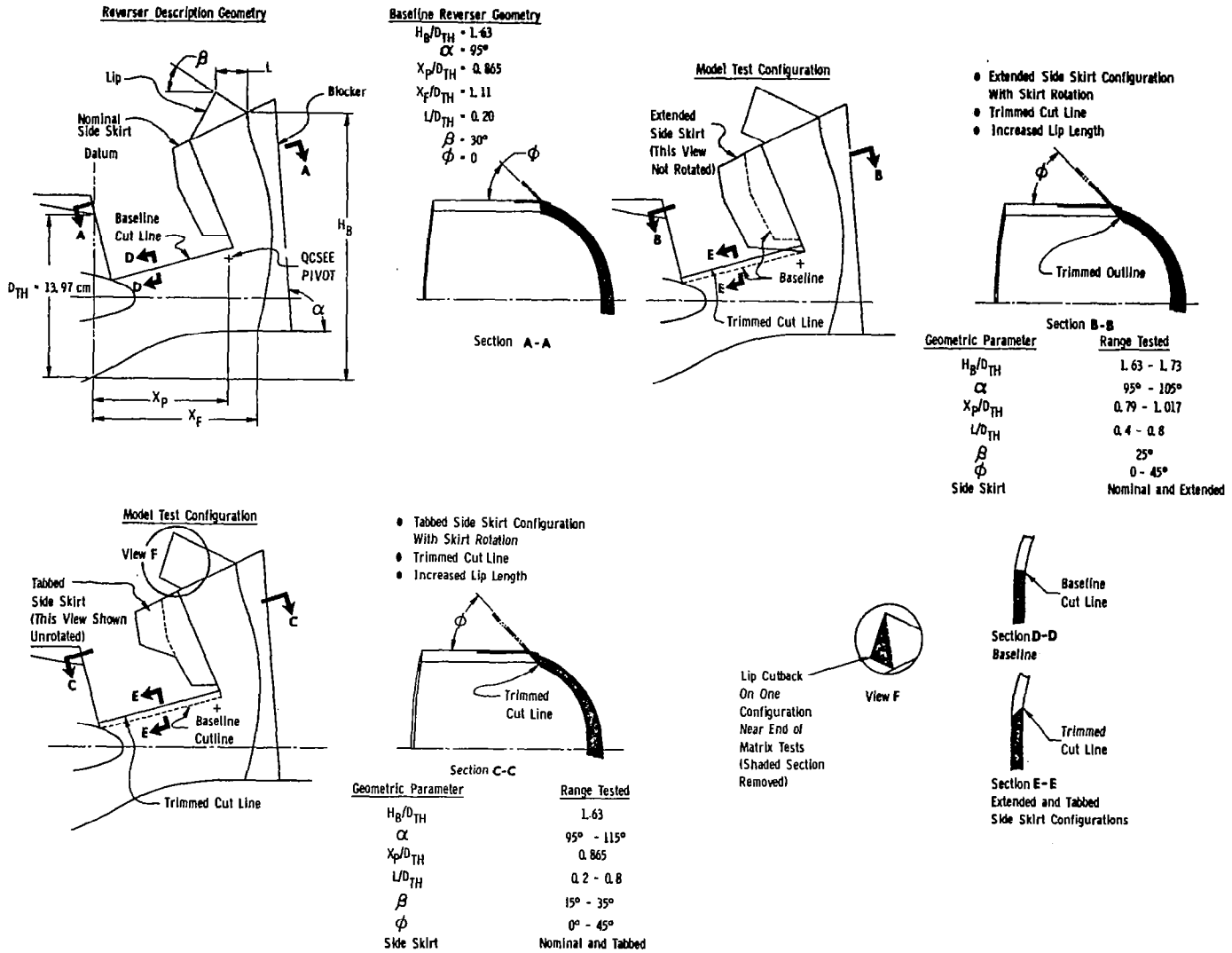

Figure 6. Thrust Reverser Scale Model Geometry.

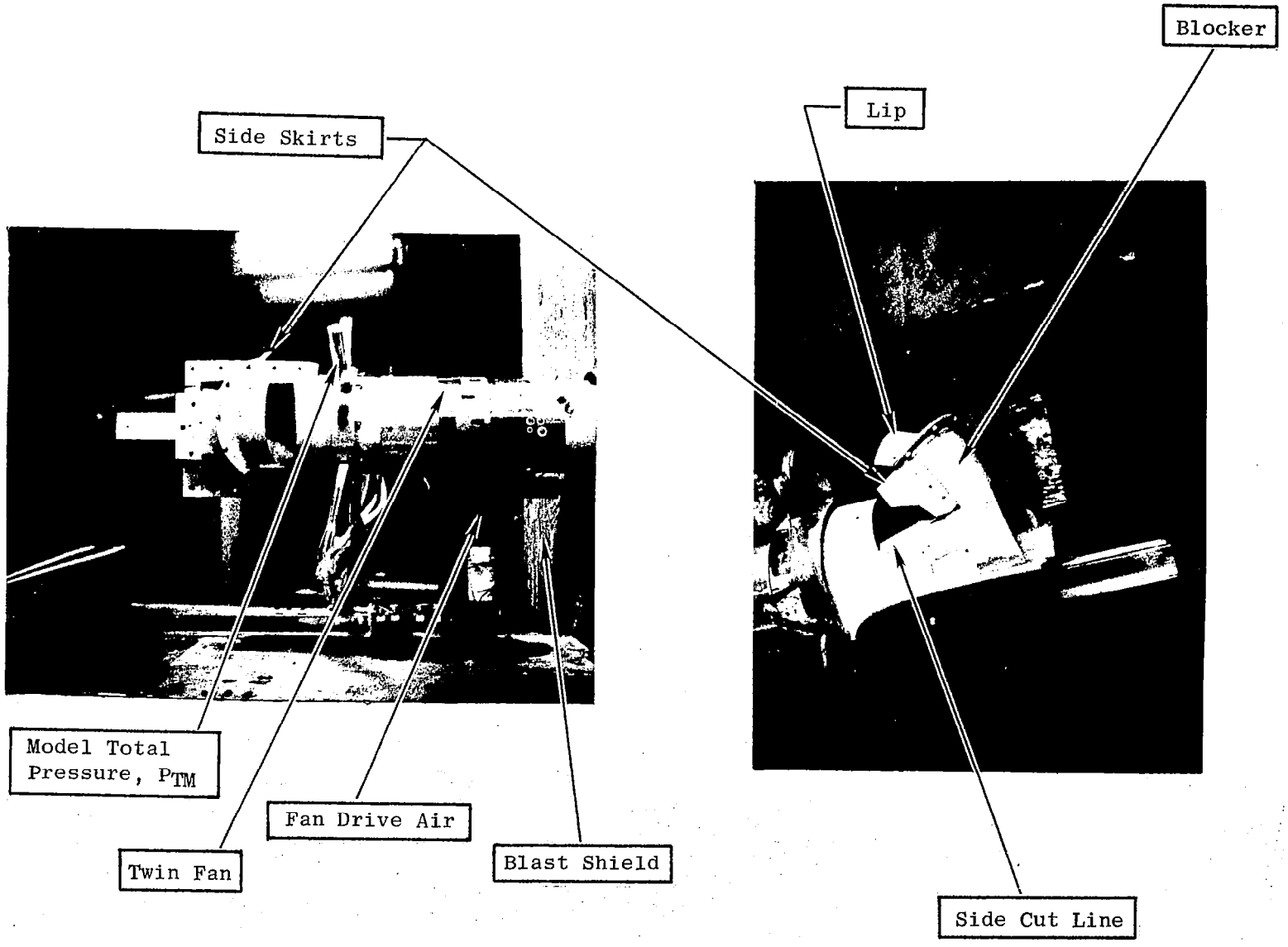

Figure 7. OTW Thrust Reverser Static Test Installation.

(a) Baseline Reverser with 0.4 L/D_{TH} Lip

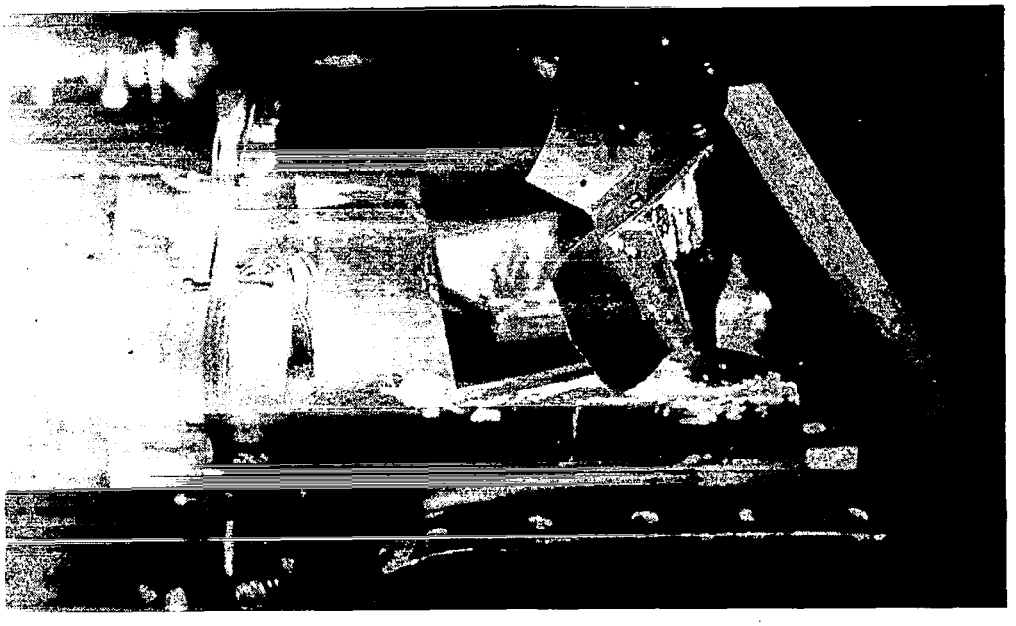

(b) Reverser with Extended Side Skirt Rotated to 45^{o}

Figure 8.- Reverser Configurations on Test

extended (2.54 cm model size) side skirt rotated outward 45°. The tabbed side skirt which finally evolved (Figure 7) was made by trimming off the aft portion of the extension to clear the nozzle area variation side doors when the reverser was stowed.

3.2.6 Wing Simulation

Three different wing configurations were employed during forward thrust nozzle development tests. Two of those configurations, as shown on Figure 9, were flat plates positioned parallel to the engine centerline and perpendicular to the vertical centerline plane. Each flat plate spanned three nozzle widths (one width either side). Flat plate leading edge location was 15.24 cm (6.0 inches) ahead of the "D" nozzle floor trailing edge to simulate the wing proximity effect on flow beneath the nozzle side doors. The small plate was cut at the nozzle floor trailing edge, while the large plate extended 25.4 cm (10.0 in.) aft (~3 nozzle heights) to explore wing/nozzle flow coefficient effects and to turn the exhaust flow to the axial direction. These plates were attached to the "D" nozzle test configurations, hence, their effects on exhaust system thrust forces were measured directly in the force balance readings.

The third wing configuration, also shown on Figure 9, represented a typical OTW wing/flap segment during powered-lift conditions at approach. This wing section was used during preliminary wing jet/flap static turning investigations as presented in Appendix A. The span of this wing section was 76.2-cm (30-in.) and the flap radius was 20.32-cm (8.0-in.) with a terminal angle of 73°. Placement of the nozzle floor trailing edge was at about 30% of wing chord.

3.3 INSTRUMENTATION

Test facility and scale model instrumentation used in these tests is shown on Figure 10.

Fan inlet airflow was measured during bellmouth tests only. For these tests, four wall static pressure ports were located at 90° spacing around the circumference of the cylindrical section of the bellmouth. These ports were manifolded into one recorded reading.

Turbine drive air was measured before being split between front and aft fan drive manifolds. A rotating vane-type flowmeter (not shown) was used for this measurement with the required meter upstream pressure and temperature measurements also being taken.

A two-component strain-gage load cell (not shown) was utilized to determine axial and normal force elements for all test configurations.

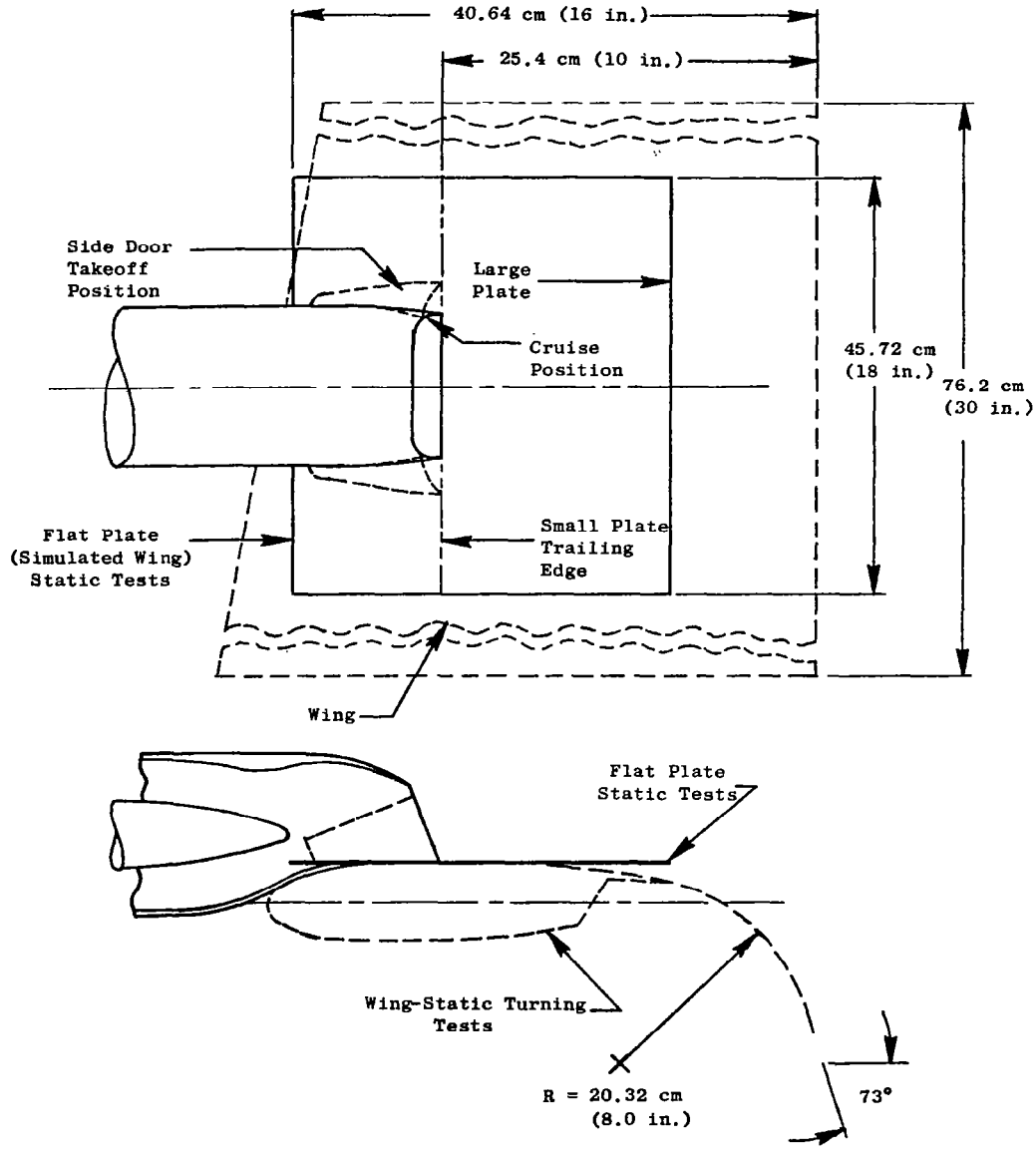

Figure 9. Simulated Wing Configurations.

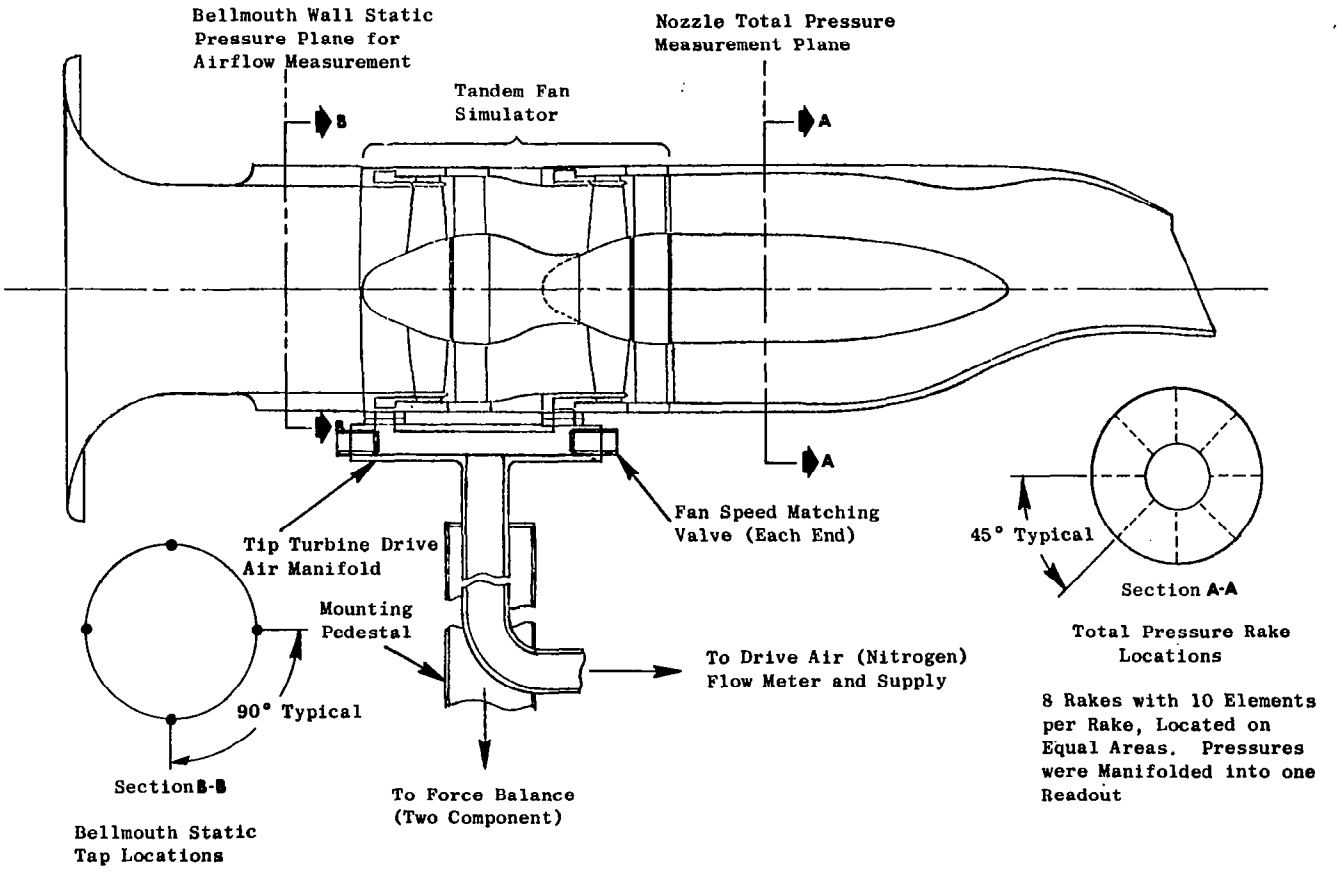

Figure 10. Test Instrumentation Sketch.

Nozzle total pressure was measured as a single manifolded reading from an 80-element sample (8 rakes with 10 elements per rake, positioned every 45°). This method of nozzle total pressure measurement was selected on the basis of limited facility read-out capability.

Fan speed (not shown) was measured using a magnetic pickup built into the simulator as standard equipment by the manufacturer.

Barometric pressure measurements were recorded for use as fan inlet bellmouth total pressure and nozzle discharge static pressure. Ambient temperature measured in the full-scale wind tunnel static test area was used as bellmouth inlet total temperature and also was assumed to represent fan discharge total temperature, since no measurement was made here, and the low temperature rise associated with the low pressure ratio fan was offset by the cold (expanded) tip turbine drive air.

3.4 METHOD OF TEST

The following procedures generally prevailed during the tests:

All QCSEE "D" nozzle configurations were installed on the thrust stand with the nozzle rotated 90° counterclockwise (looking forward); all reverse configurations were rotated clockwise 90° (looking forward). This orientation placed the model vertical and axial force components in line with the active force balance axes and in a plane parallel with the test table.

Test points were set by incrementally varying fan speeds between 20,000 and 30,000 rpm. For each point, fan speed was quickly brought up to the desired values by manually opening the turbine drive air supply valve. When stabilized, all data were recorded, and fan speed was reduced to a low sustaining value. This throttling back on fan speed between test points was required to prevent ice from forming on the exit guide vanes. Ice formation was found to occur during sustained fan operation at high speeds because of the prevalent low turbine drive air temperatures. Running under iced-up conditions was found to produce erratic airflow/thrust data.

Repeat points were taken as deemed necessary during the course of testing.

SECTION 4.0

ROUND NOZZLE CALIBRATION TEST RESULTS AND DATA ADJUSTMENTS

Flow coefficient and velocity coefficient data computed from measured airflow, thrust, and pressure ratio (as outlined in Appendix B) are presented on Figures 11 and 12, respectively, as functions of the measured nozzle pressure ratio. The measured coefficients were found to be in disagreement with past experience on round nozzles of similar geometry. Both the flow coefficient level (too high) and the trend of increasing flow coefficient with decreasing pressure ratio were in contradiction with reliable data presented in NACA Report 933 (Reference 1). Velocity coefficient levels (Figure 12) were found to be greater than unity, and they also exhibited an increasing trend with decreasing pressure ratio.

The observed coefficient characteristics of the round calibration nozzles resulted in reassessment of the measurement techniques employed during these tests, particularly with regard to the manifolded single reading of fan discharge total pressure. This parameter was measured using eight 10-element rakes (Section 3.3), all manifolded to provide a comprehensive, equal area sampling which was to account for the radial and circumferential pressure variations characteristic of the 14-cm (5.5-in.) fan design. It was theorized that the manifolded sampling technique was not sufficiently compensating for mass flow distribution effects in average total pressure because of the low turbine drive air total temperatures which existed in the outer annulus. Accounting for these mass flow distribution effects would weight the total pressure measured toward a higher value (higher pressures and higher weight flow per unit of flow area occur at the tip). It also was recognized that a small pressure ratio measurement error would have a large effect on both ideal weight flow and ideal velocity at low pressure ratios, and that an increase in measured pressure would produce the desired change in computed flow and velocity coefficients (lower in both cases, and with the greatest reduction at the lowest pressure ratios); therefore, a computational procedure was established to adjust the calibration nozzle flow coefficients to correspond with the referenced NACA Report 933 levels. The adjustment was made to each data point by applying a total pressure bias correction to computation of nozzle ideal weight flow to effect a match between calibration nozzle flow coefficients and the NACA data at their respective nozzle cone half angles (θ). The resultant total pressure bias correction amounted to nominally 0.9 percent at a measured pressure ratio of 1.1, and 1.3 percent at a measured pressure ratio of 1.25. The pressure measurement bias corrections were then curve fitted by computer using a polynomial equation of the form:

$$K_{PT} = k + A\,(P_{TM}/P_0) + B\,(P_{TM}/P_0)^2 + C\,(P_{TM}/P_0)^3$$

where:

$$K_{PT} = 1 + \frac{\Delta P_T}{P_{TM}}$$

ΔP_T = The pressure measurement adjustment

P_{TM} = The measured pressure

The corrected pressure ratio then was computed as:

$$P_T/P_0 \equiv K_{PT} \ (P_{TM}/P_0)$$

The constants k, A, B, and C for the four round nozzles are given in Table 1.

Table 1. Constants for Polynomial Curve Fit for Total Pressure Bias Correction.

Constant	Nozzle			
	R_1	R_2	R_3	R_4
k	-4.9861273	0.76635849	0.073401583	-2.122906
A	16.314239	0.50122243	2.217829	7.5142339
B	-14.813435	-0.33157444	-1.7606428	-6.0071377
C	4.4891577	0.07068393	0.4703686	1.6014451

The final flow and velocity coefficient data calculated using the polynomial curve fit for total pressure measurement bias are presented on Figures 13 and 14, respectively. Also shown on Figure 13 are the NACA reference report flow coefficient curves. The resultant calibration nozzle flow and velocity coefficient trends and level with the adjusted pressure ratio are reasonable and lend credence to the method used to correct the data.

All scale model flow and velocity coefficient data contained in this report have been adjusted using the corrections to total pressure developed from analysis of these round nozzle results. Note from Figure 15 that the round nozzle airflow-pressure ratio characteristics bracket the range observed from the QCSEE "D" nozzle and reverser tests. Because of the close proximity of the takeoff nozzle and round nozzle R_2 flow characteristics, the pressure correction curve fit for that calibration nozzle was applied for all takeoff test configurations. For the cruise and reverse thrust configurations, a pressure correction midway between R_3 and R_4 was applied. Polynomial equation constants for cruise and reverse thrust data reduction pressure corrections are given in Table 2.

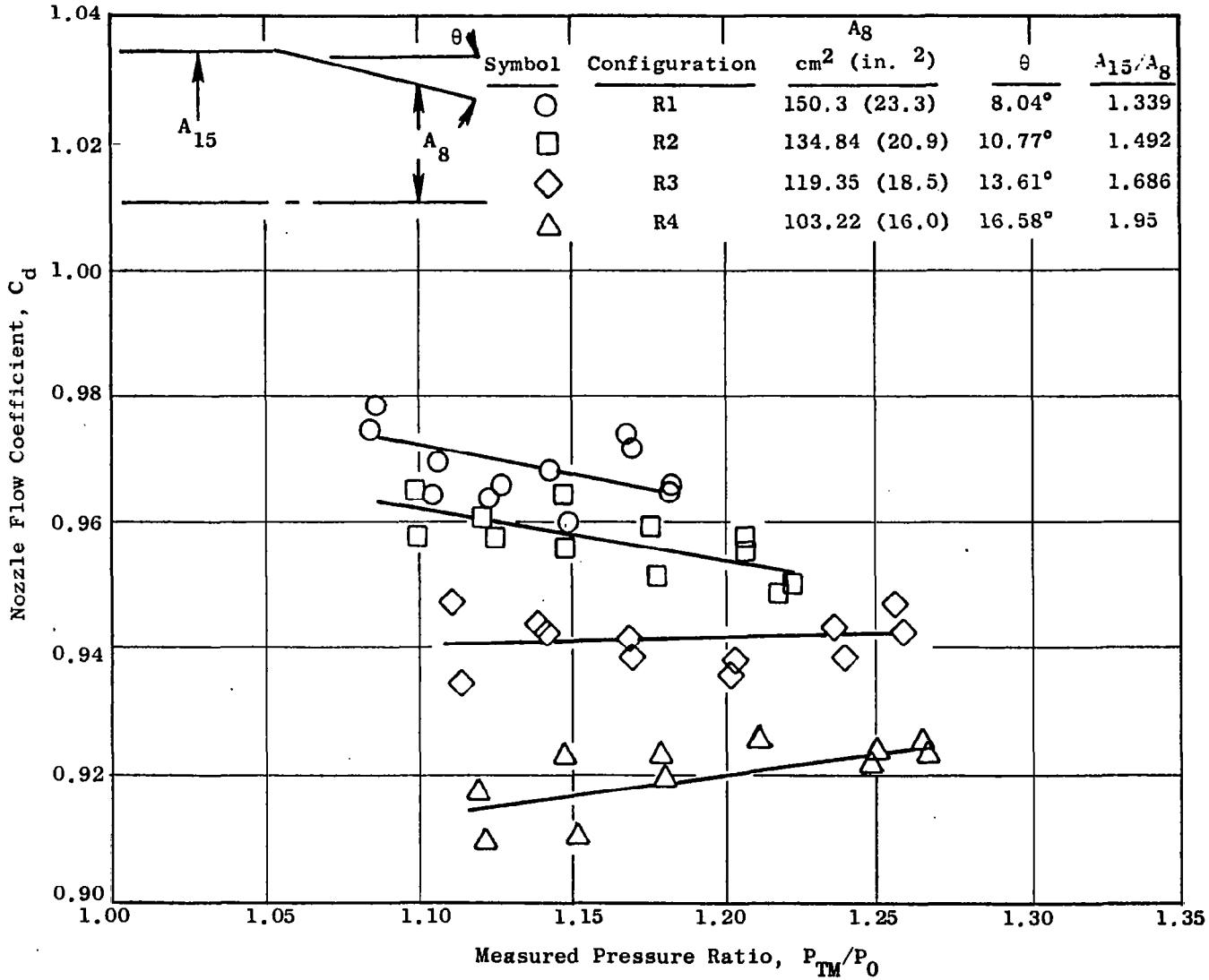

Figure 11. Calibration Nozzle Measured Flow Coefficients.

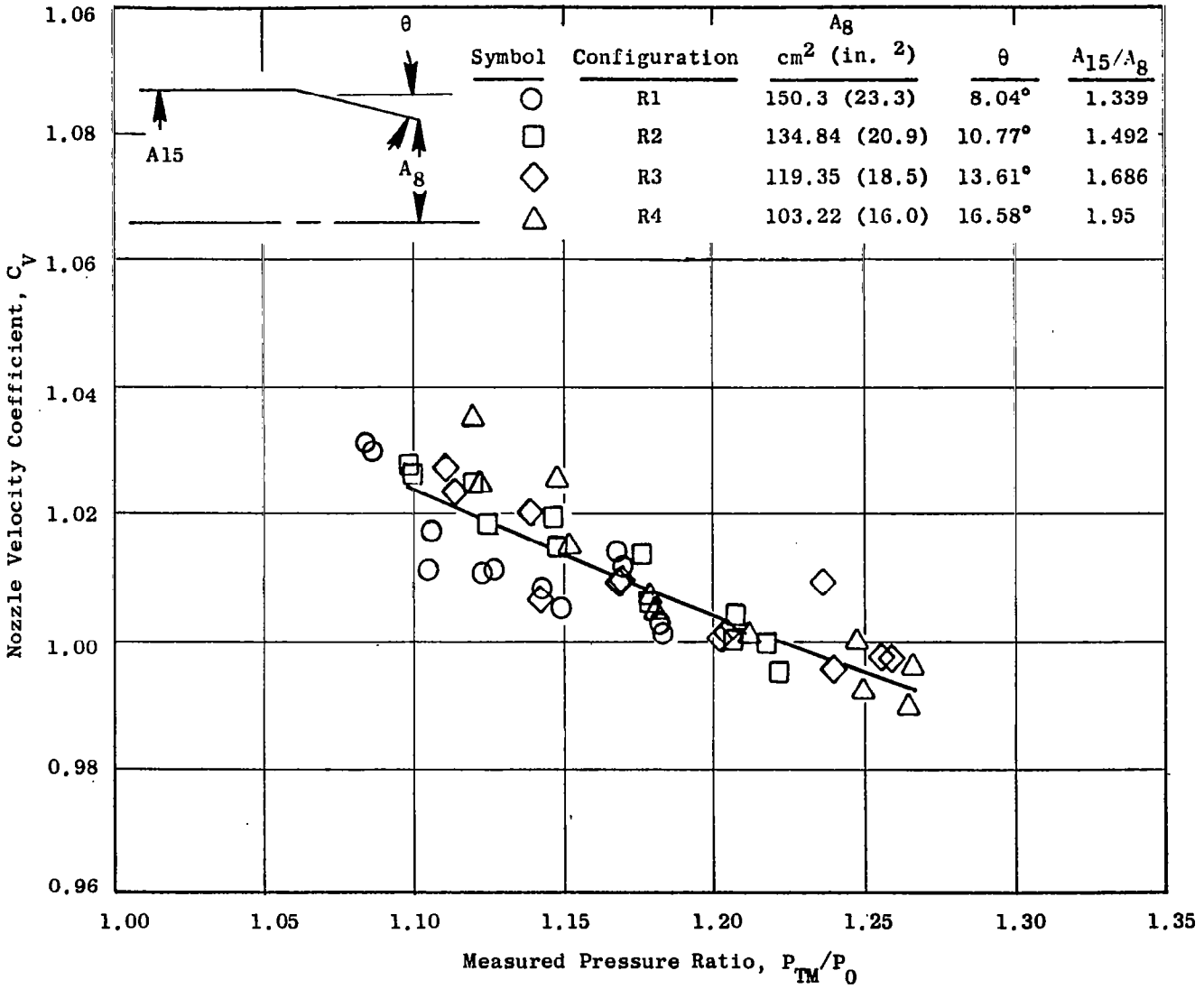

Figure 12. Calibration Nozzle Measured Velocity Coefficients.

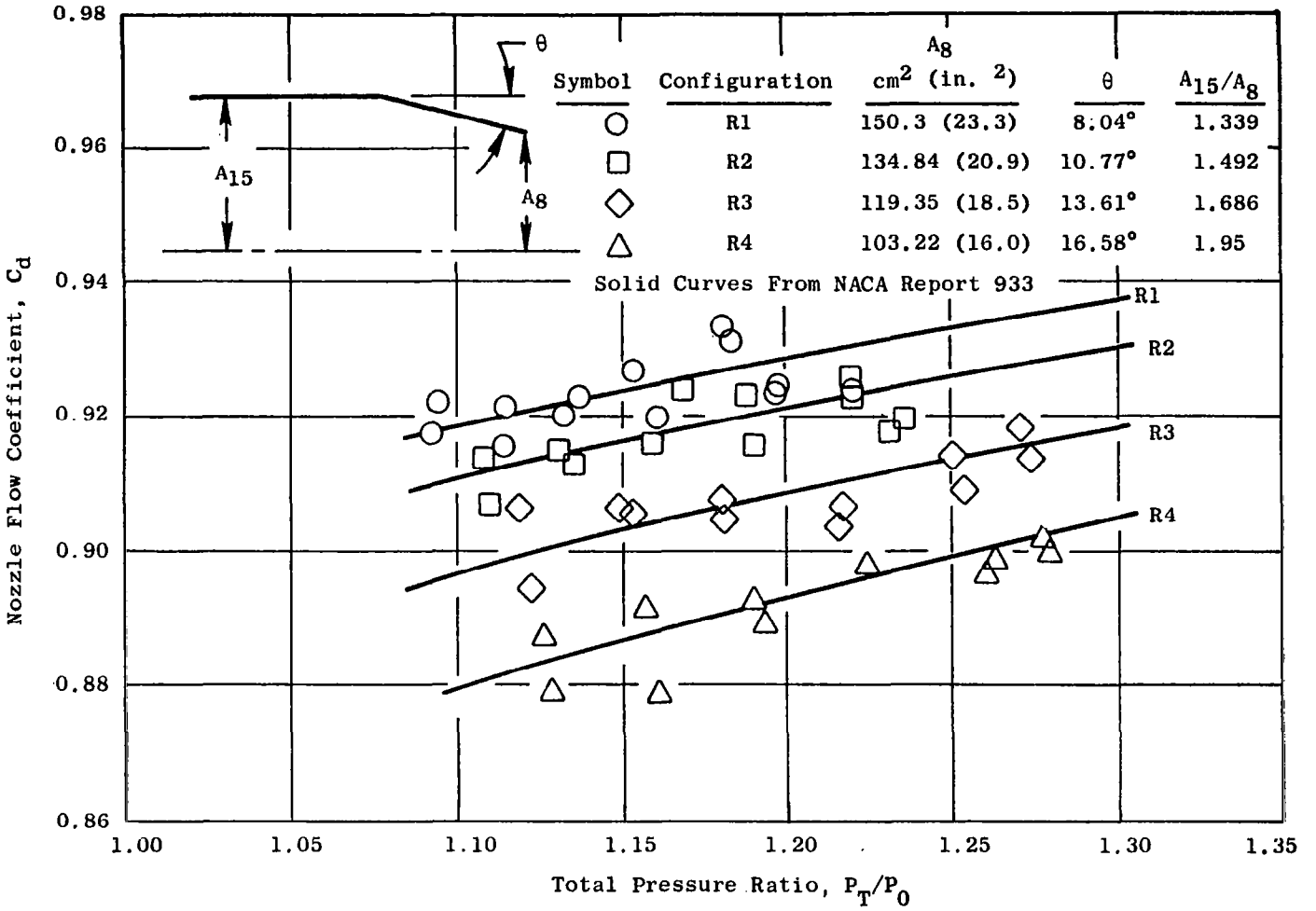

Figure 13. Calibration Nozzle Adjusted Flow Coefficients.

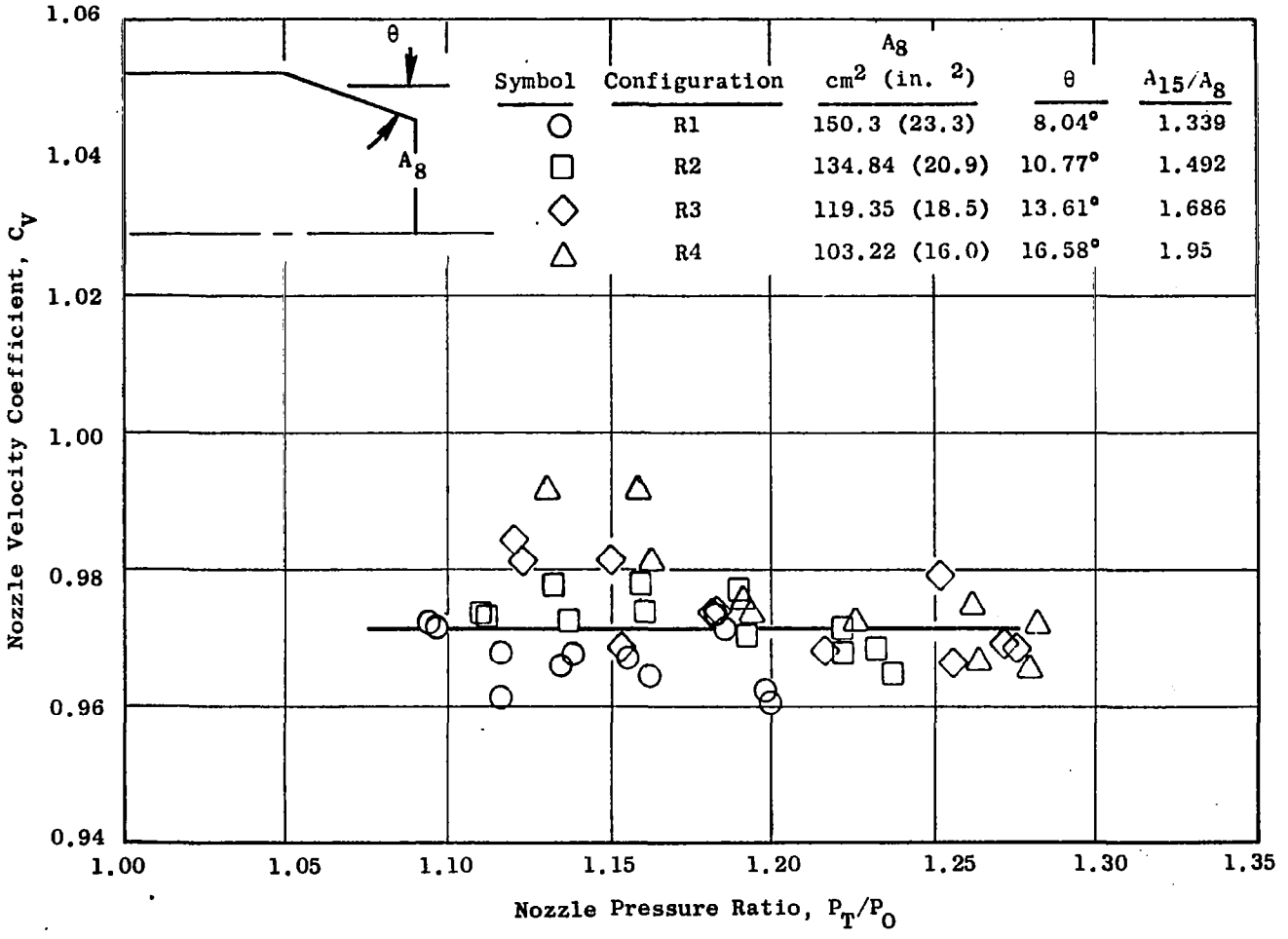

Figure 14. Calibration Nozzle Adjusted Velocity Coefficients.

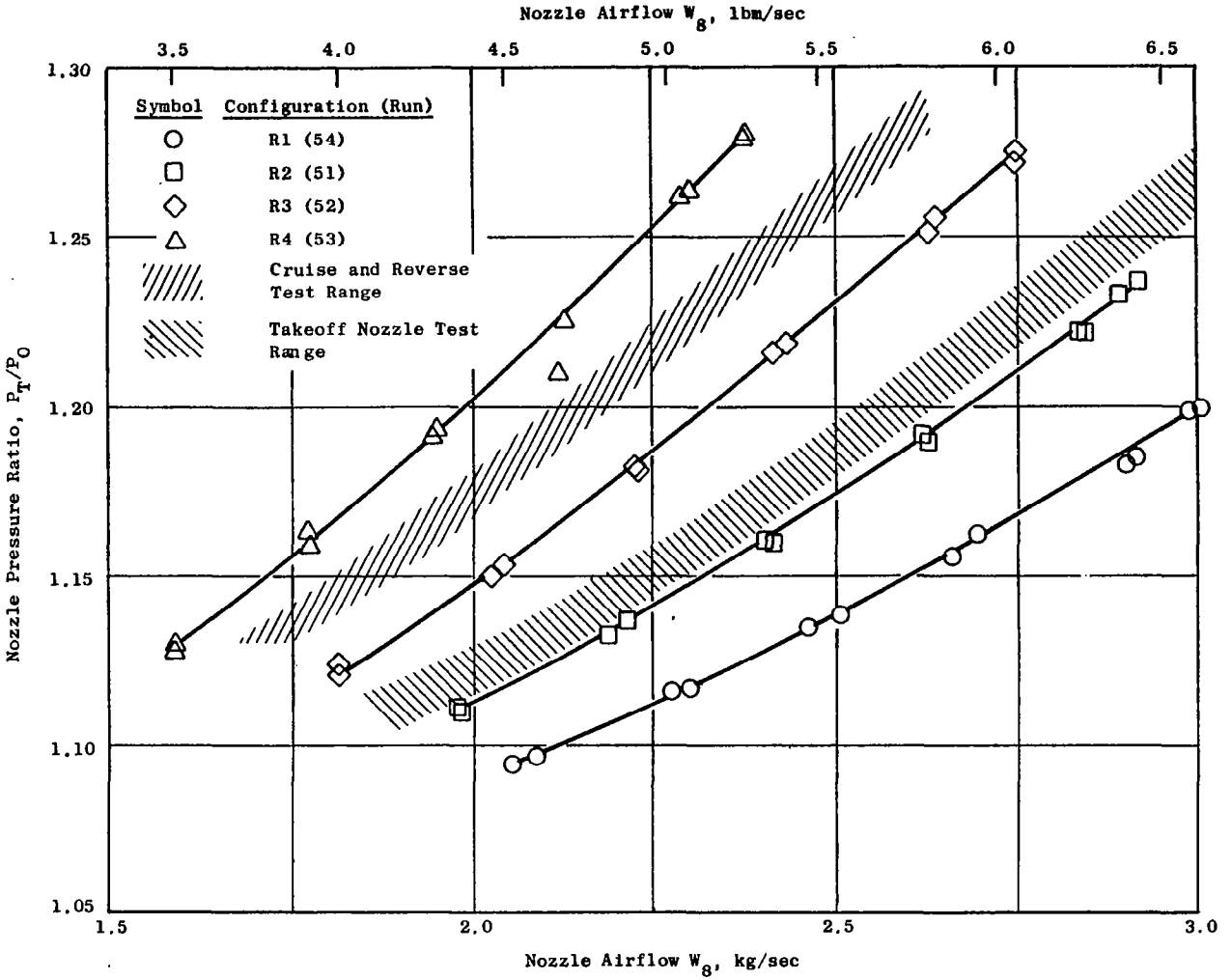

Figure 15. Comparison of Calibration Nozzle Data with QCSEE Nozzle and Reverser.

Table 2. Constants for Polynomial Curve Fit For Cruise and Reverse Thrust Total Pressure Corrections.

Constant	Value
k	-0.58932853
A	3.7516409
B	-2.9345061
C	0.7666686

SECTION 5.0

FORWARD THRUST NOZZLE DEVELOPMENT

5.1 TEST MATRIX

Final documentation of QCSEE nozzle performance was made using the tandem fan propulsion simulator to obtain higher nozzle pressure ratios which more closely matched the QCSEE mixed-flow takeoff pressure ratio of approximately 1.29. The test matrix shown in Table 3 was set up to evaluate the nozzle flow coefficients, velocity coefficients, and exhaust flow angle (or kickdown angle) over a range of pressure ratios. All three nozzle flowpaths (baseline, RC-1, and RC-2) were tested without wing simulation (for exhaust flow angle, primarily), with the small plate attached and with the larger plate installed to obtain internal performance data in a wing back-pressure environment. Each configuration was tested at the cruise nozzle position and at various side door areas in the vicinity of the takeoff area position (25° door setting for the baseline and RC-1; 30° for RC-2). Only the large door design was included in this final test matrix, the 60° small-door configuration having been eliminated in earlier model screening tests.

Preliminary static turning data obtained in baseline and RC-1 nozzles are shown in Appendix A.

5.2 INTERNAL NOZZLE PERFORMANCE

5.2.1 Flow Coefficient Results

Flow coefficients for the three "D" nozzle configurations are presented on Figures 16, 17, and 18 for the cruise and takeoff nozzle side door settings. The flow coefficients defined in these figures and elsewhere in this report were based on ideal exhaust flow calculated at each test pressure ratio using the cruise nozzle exit area of 109.68 cm^2 (17 in^2) as the reference. Hence, the takeoff flow coefficients shown are substantially greater than unity. The cruise nozzle area was selected for reference on the basis that it was a completely bounded area whose value was more readily determined with accuracy. Note from these figures that the area changes measured between takeoff and cruise nozzle positions with the large plate installed were between 18.74% (RC-2) and 21.3% (RC-1) at a pressure ratio of 1.25. This level of change was in the range expected to meet QCSEE takeoff cycle area requirements (see nozzle selection, Section 5.3).

The effect of wing proximity on nozzle flow coefficient (back pressure effect) also can be noted from a comparison of large plate data with small plate and "plate-off" results. Figures 16, 17, and 18 show only moderate wing back-pressure effects at either the takeoff or cruise condition; flow

Table 3. Forward Thrust Test Matrix.

Run	Nozzle	Door Angle	Plate
28	RC-1	50°	Large
29	RC-1	50°	Small
30	RC-1	50°	Off
31	RC-1	30°	Off
32	RC-1	30°	Small
33	RC-1	30°	Large
34	RC-1	40°	Large
35	RC-1	40°	Small
36	RC-1	40°	Off
37	RC-1	25°	Off
38	RC-1	25°	Small
39	RC-1	25°	Large
40	RC-1	Cruise	Large
41	RC-1	Cruise	Small
42	RC-1	Cruise	Off
43	RC-1	20°	Off
44	RC-1	20°	Small
45	RC-1	20°	Large
51	2	---	---
52	3	---	---
53	4	---	---
54	1	---	---
55	RC-2	Cruise	Large
57	RC-2	Cruise	Small
60	RC-2	Cruise	Off
61	RC-2	25°	Off
62	RC-2	25°	Large
63	RC-2	25°	Small
64	RC-2	30°	Small
65	RC-2	30°	Off
66	RC-2	30°	Large
67	RC-2	*	Large
68	RC-2	**	Large
69	RC-2	40°	Off
70	RC-2	40°	Large
71	RC-2	40°	Small
72	Baseline	Cruise	Large
73	Baseline	Cruise	Off
74	Baseline	Cruise	Small
75	Baseline	25°	Small
76	Baseline	25°	Off
77	Baseline	25°	Large
78	Baseline	30°	Large
79	Baseline	30°	Off
80	Baseline	30°	Small
81	Baseline	40°	Small
82	Baseline	40°	Off
83	Baseline	40°	Large

* Door Removed

** Door Removed, Opening Enlarged

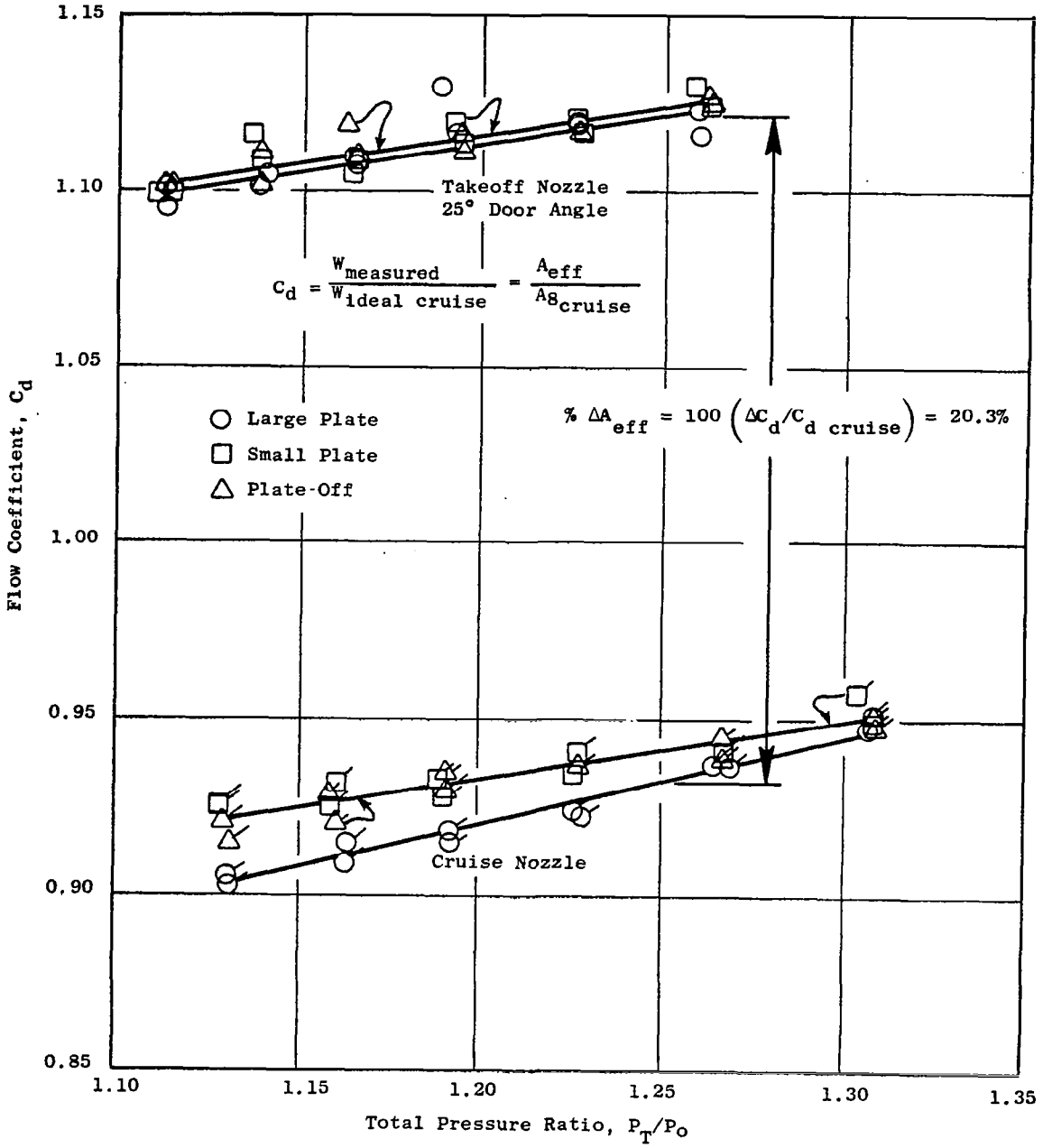

Figure 16. QCSEE Baseline OTW Nozzle Flow Coefficients.

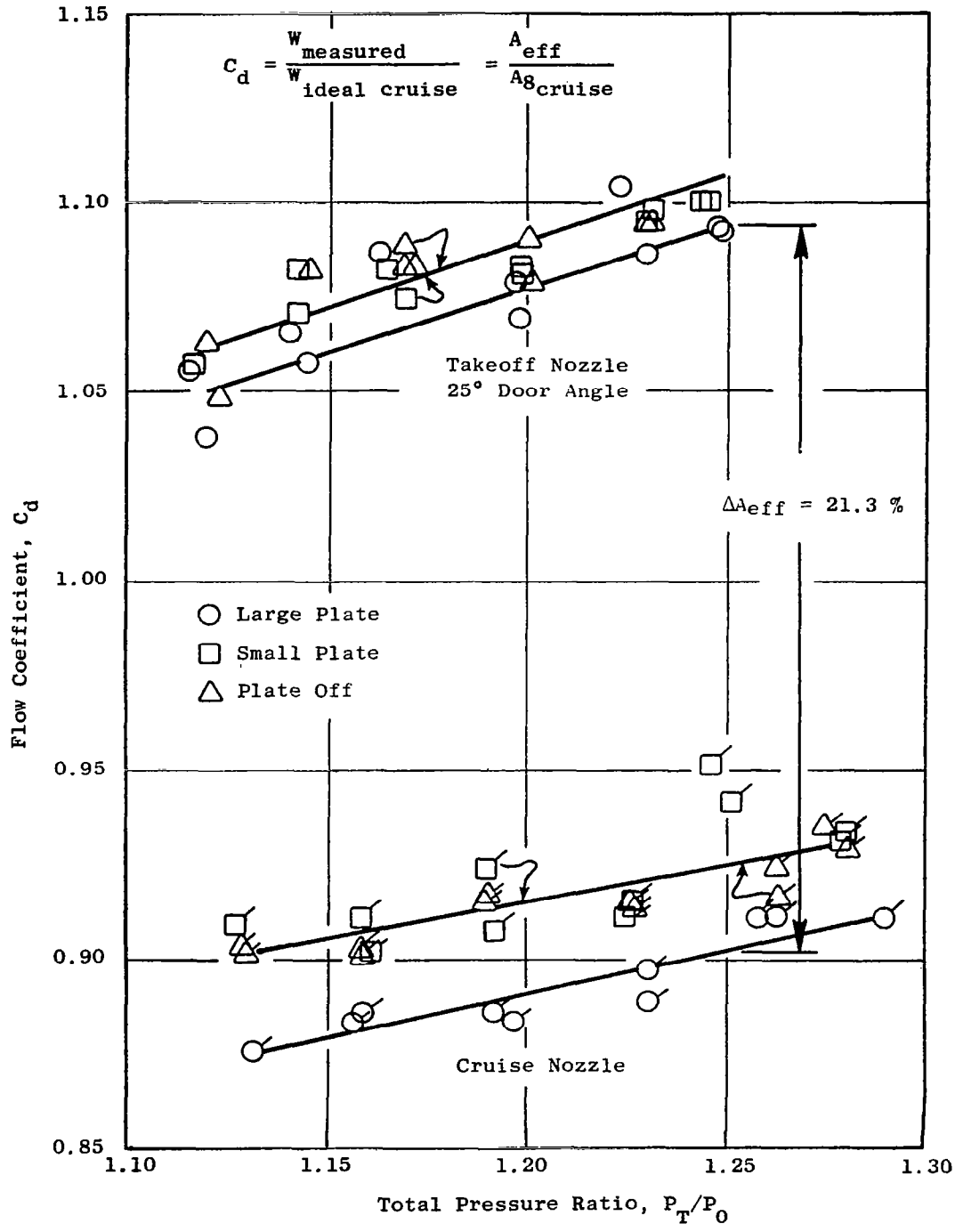

Figure 17. QCSEE RC-1 Nozzle Flow Coefficients.

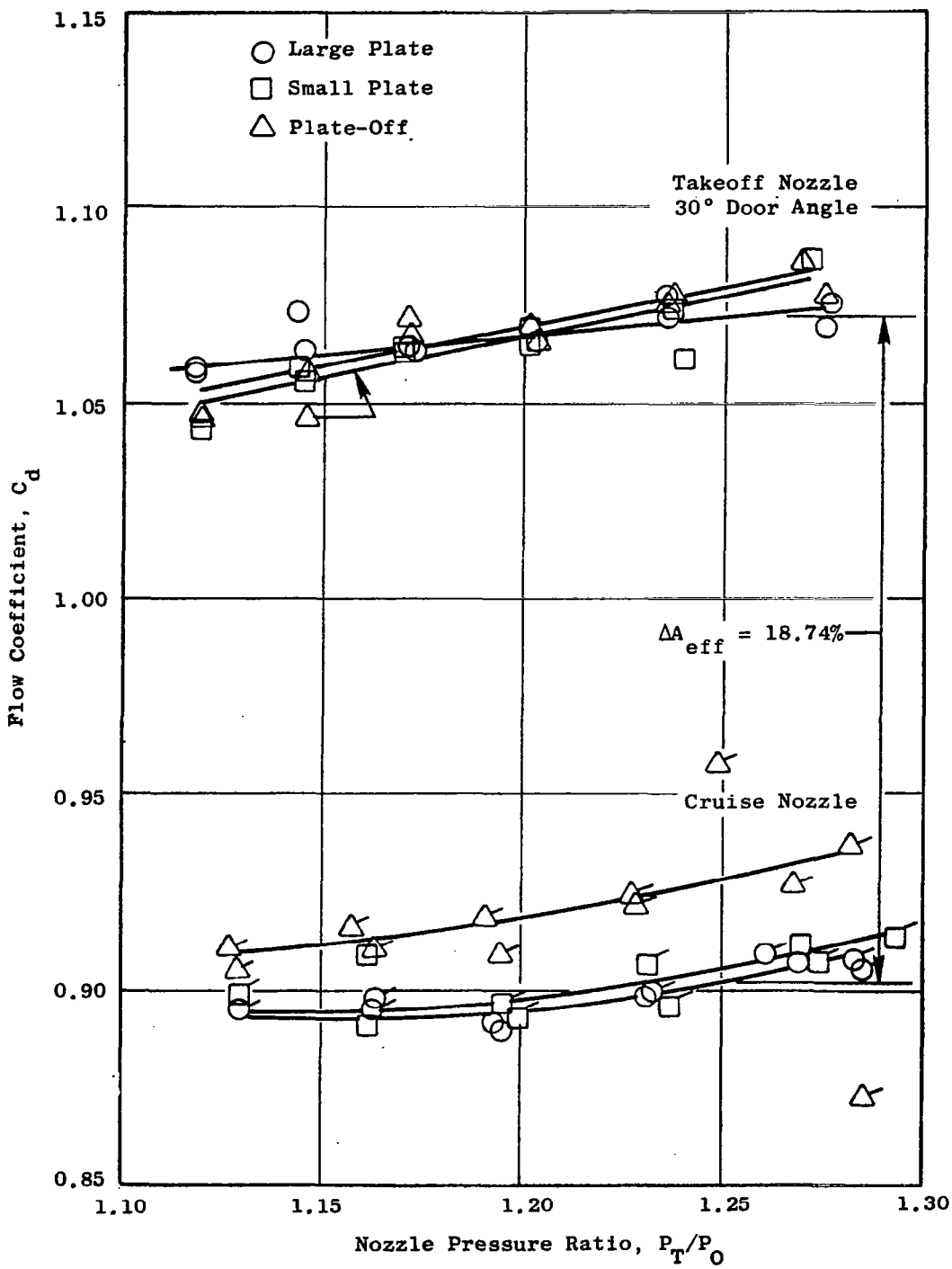

Figure 18. QCSEE RC-2 Nozzle Flow Coefficients.

coefficient changes observed for the three takeoff nozzles and plate configurations were 0.012 or less, while the cruise nozzle position indicated changes in flow coefficient of up to about 0.026.

The effect of recontouring the nozzle internal flowpath for higher kickdown angle also can be assessed from an examination of Figures 16 through 18. At 1.25 pressure ratio, these figures show both recontoured nozzles to have slightly lower flow coefficients than the baseline for the takeoff and cruise nozzle positions. For the large flat plate case, takeoff flow coefficient values measured were 1.12, 1.093, and 1.071 for baseline, RC-1, and RC-2, respectively; comparable measured values at cruise were 0.931, 0.902, and 0.903, respectively. The lower flow coefficients observed for the recontoured nozzle reflect the effects of steeper internal flow angles (duct convergence effect) and higher back-pressure levels which result from increased flow kickdown angle on the simulated wing. Similar trends can be noted from these figures for the small flat plate and plate-off cases, but the effects were of smaller magnitude, being predominantly due to the steeper internal duct geometry.

5.2.2 Velocity Coefficient Results

Velocity coefficients for the baseline, RC-1, and RC-2 nozzles are presented on Figures 19, 20, and 21, for the cruise and takeoff nozzle configurations. These coefficients are based on the resultant velocity, calculated from resolution of axial and normal force balance readings into a resultant thrust value, and then divided by the measured exhaust flow; the ideal velocity used in computing velocity coefficient was evaluated as a function of nozzle pressure ratio. The results from these three figures show that baseline and RC-1 takeoff velocity coefficients are essentially the same ($C_V \approx 0.914$) with the large plate installed, while comparable values for RC-2 were slightly lower on the average. A comparison of plate-off and small plate takeoff velocity coefficients shows the recontoured nozzles as having about the same performance, both being higher than the baseline by approximately 0.01. The difference in performance (0.03 to 0.06 ΔC_V) between the large plate and either the plate-off or the small plate takeoff configurations is attributed to a combination of: 1) large plate skin friction, 2) spanwise velocity components (flow angularity loss) which arise from the side door flow-spreading characteristics, and 3) jet impingement losses associated with turning the exhaust flow axially aft along the large plate surface. Also shown in these figures is that little difference in velocity coefficients was measured between plate-off and small plate configurations. For the takeoff nozzle data, plate-off performance was observed to be consistently slightly higher, indicating some small plate scrubbing friction losses from flow spreading underneath the nozzle side doors ahead of the nozzle exit plane.

Cruise nozzle velocity coefficients presented in Figures 19, 20, and 21 show trends similar to those observed for the takeoff values. Baseline and RC-1 configurations with large plates installed show comparable performance, with results for RC-2 being somewhat lower (~0.01). As with the takeoff

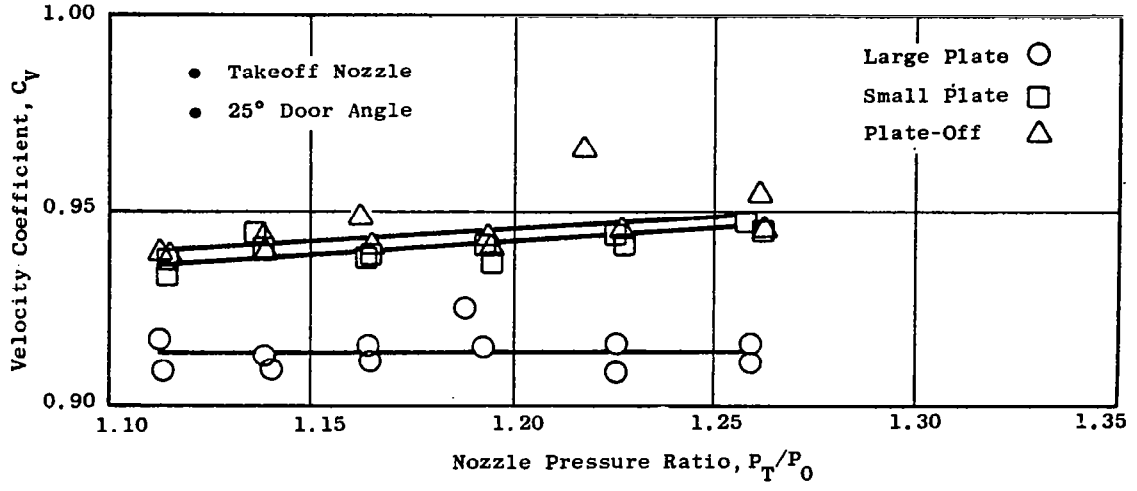

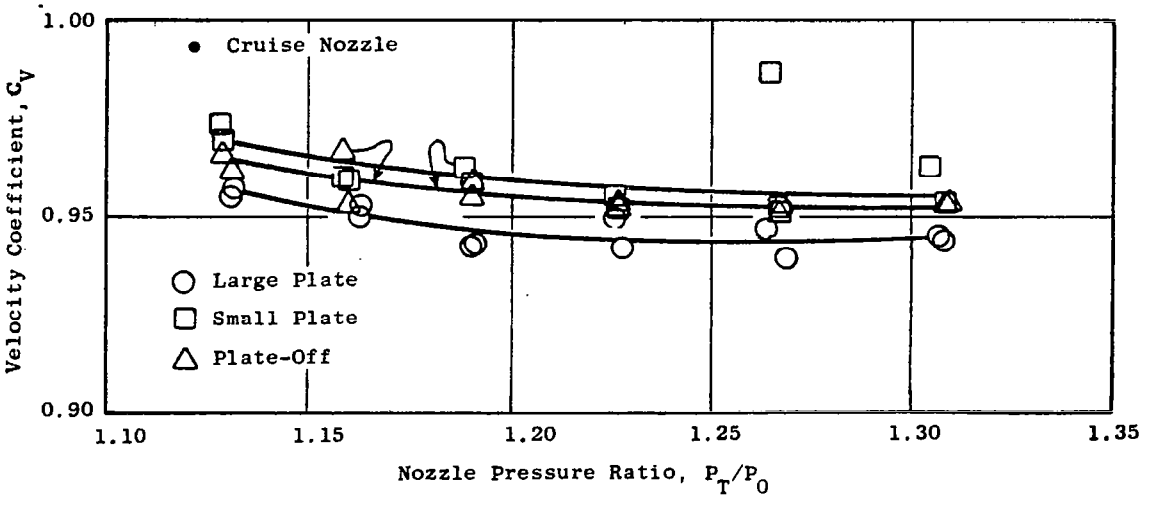

Figure 19. QCSEE Baseline OTW Nozzle Velocity Coefficients.

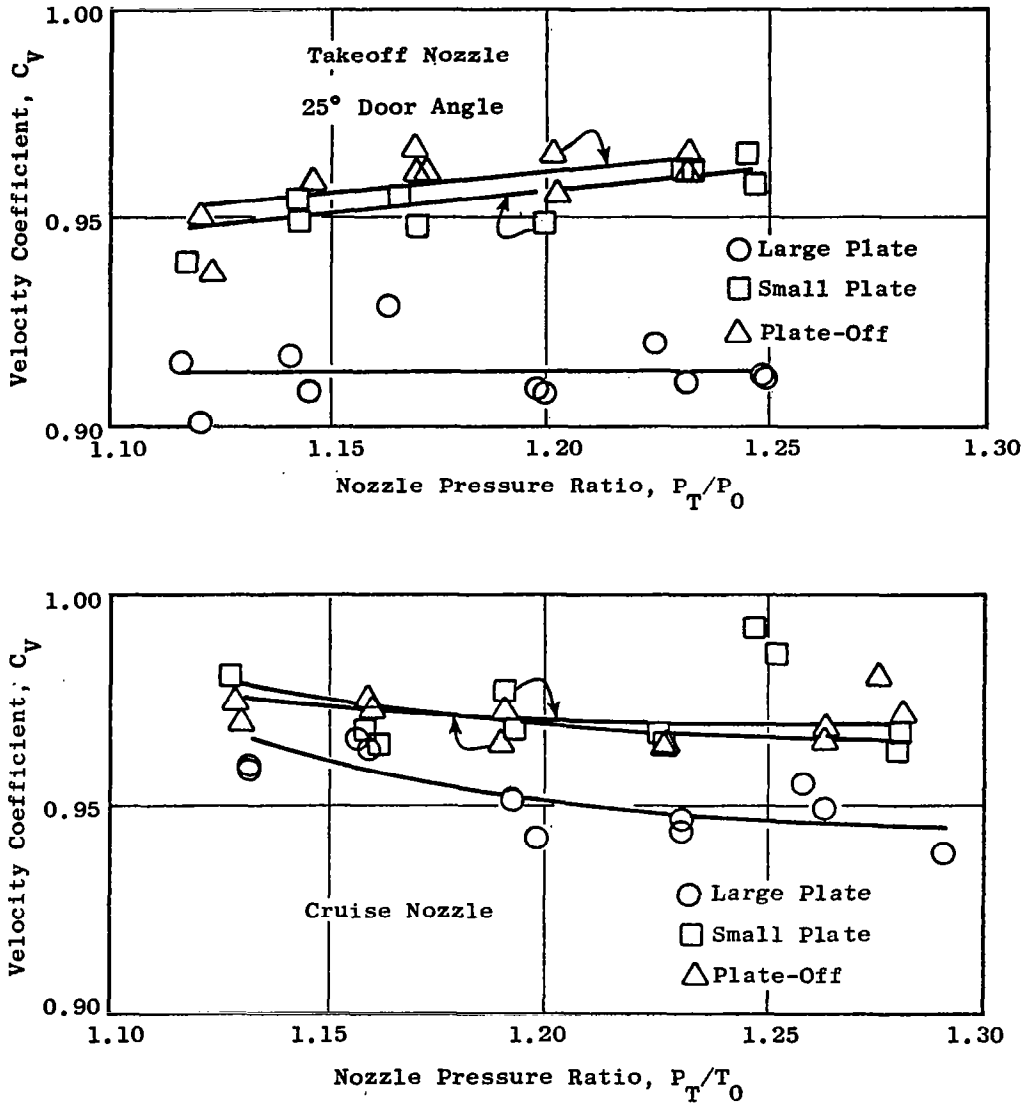

Figure 20. QCSEE RC-1 Nozzle Velocity Coefficients.

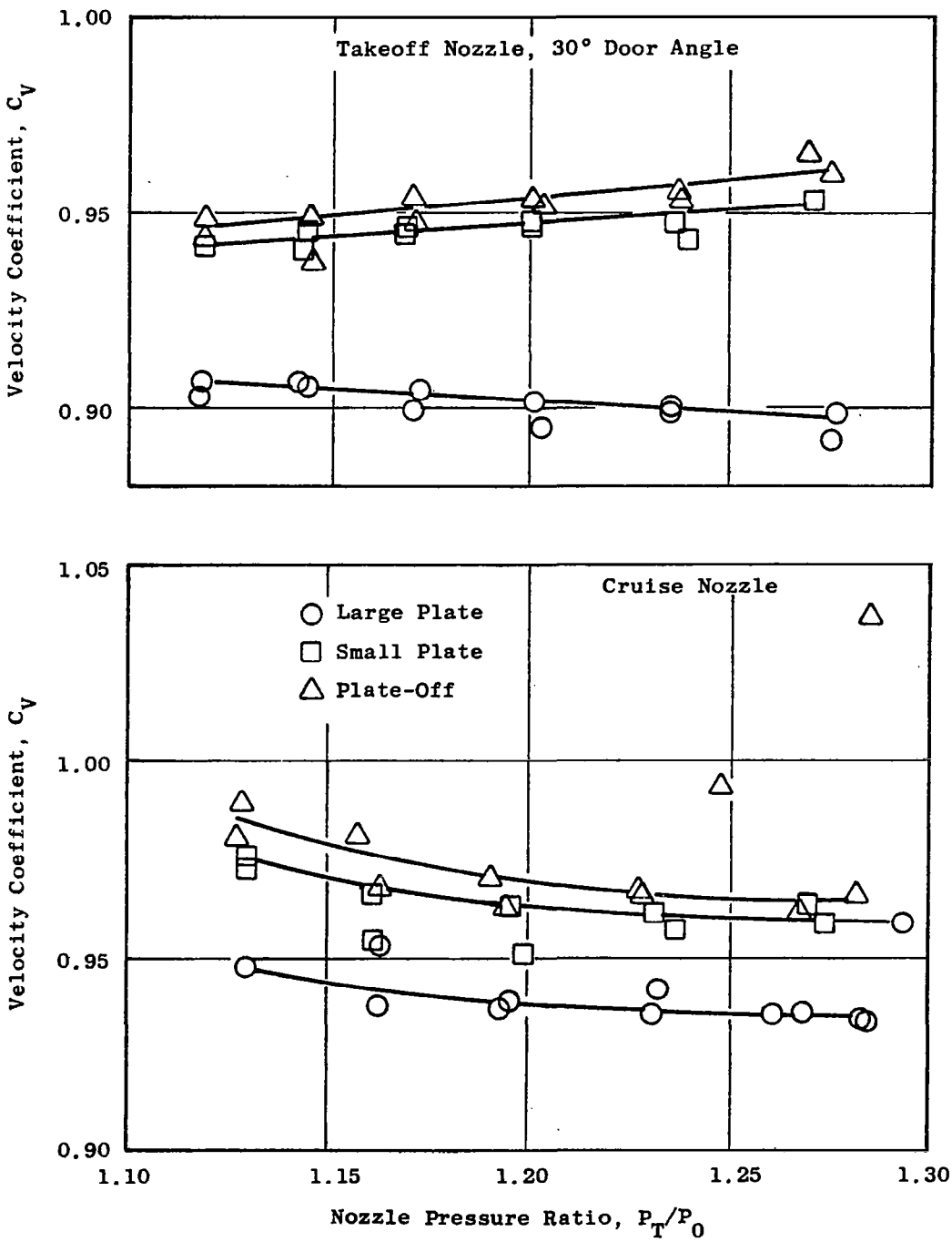

Figure 21. QCSEE RC-2 Nozzle Velocity Coefficients.

nozzles, differences in performance between large plate and small plate/plate-off configurations are attributed to large plate friction and jet impingement turning losses. Angularity losses, however, are considered to be eliminated when the side doors are closed to the cruise position. Note that the difference in performance between small plate/plate-off, and large plate configurations is less than that observed for takeoff; this is attributed to the fact that flow spreading is reduced substantially when the doors are closed. The trend of increasing C_V with reduced pressure ratio is not fully understood, but it may be attributable to small residual pressure measurement errors. Figure 22 compares the flow-spreading characteristics using the lamp black flow visualization technique.

5.2.3 Nozzle Kickdown Angle

One of the key parameters relating to achievement of good exhaust flow static turning angles at approach flap settings, as determined from preliminary configuration screening tests, was nozzle kickdown angle. It was from these early tests that the QCSEE baseline nozzle configuration was recontoured to the RC series to provide a higher wing impingement angle for better static turning performance. Figures 23, 24, and 25 present nozzle exhaust flow angle (θ_j), or kickdown angle for the baseline, RC-1, and RC-2 nozzles. The exhaust flow angle was determined trigonometrically from measured force balance axial and normal thrust components. While flow angles are shown for take-off and cruise nozzles with all three plate configurations, the plate-off takeoff nozzle exhaust flow angle data are most significant; these data show both recontoured nozzles to have higher kickdown angles than the baseline, with RC-1 indicating the highest value of the three configurations. Note that pressure ratio has little effect on exhaust flow angle in the range investigated. Final static turning and wind tunnel data will be published in a future report by the NASA Langley Research Center.

Large plate exhaust flow angle data on these figures indicate flow leaving angles at the trailing edge of the plate to be nominally between 1 to 2 degrees. These small leaving angles are considered to be attributable to either slight plate misalignment with the simulator axis or some slight downward trailing edge curvature on the plate. In either case, the unrecovered axial thrust component which results from these angles is negligible, being about 0.1 percent of the absolute thrust vector based on the 2° misalignment.

5.2.4 Side Door Angle Derivatives for Flow and Velocity Coefficients

Much of the data taken in the final forward thrust test matrix included nozzle side door angle settings to explore the area variation capability of the QCSEE "D" nozzle design. These data were taken with the large plate, small plate, and plate-off wing variants for a range of door angles between 20 and 50 degrees. In one case, the side doors were removed altogether, and

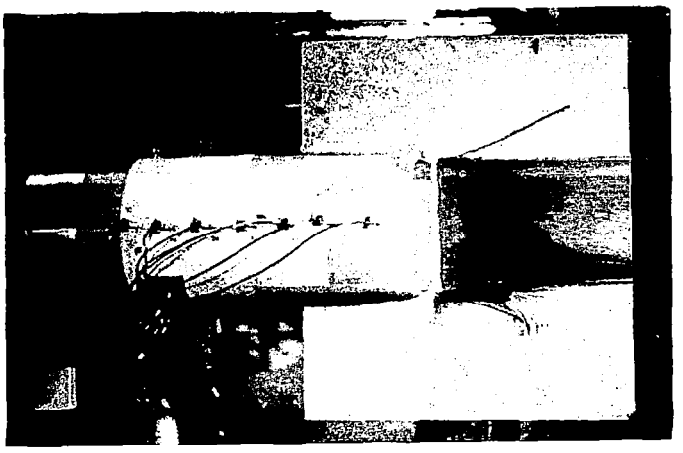

Cruise Nozzle

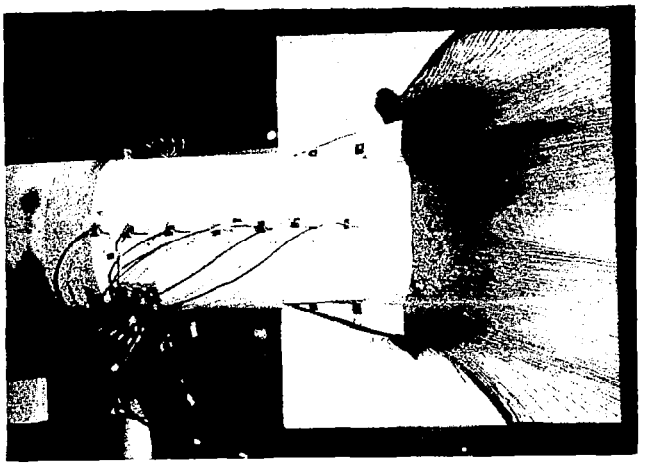

Baseline: Small Doors at 60°

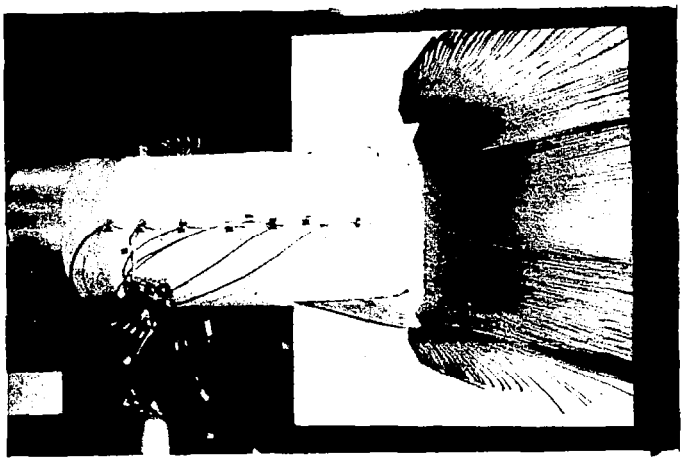

Baseline: Large Doors at 25°

Figure 22. Jet Spreading Characteristics of the QCSEE Nozzle at Takeoff.

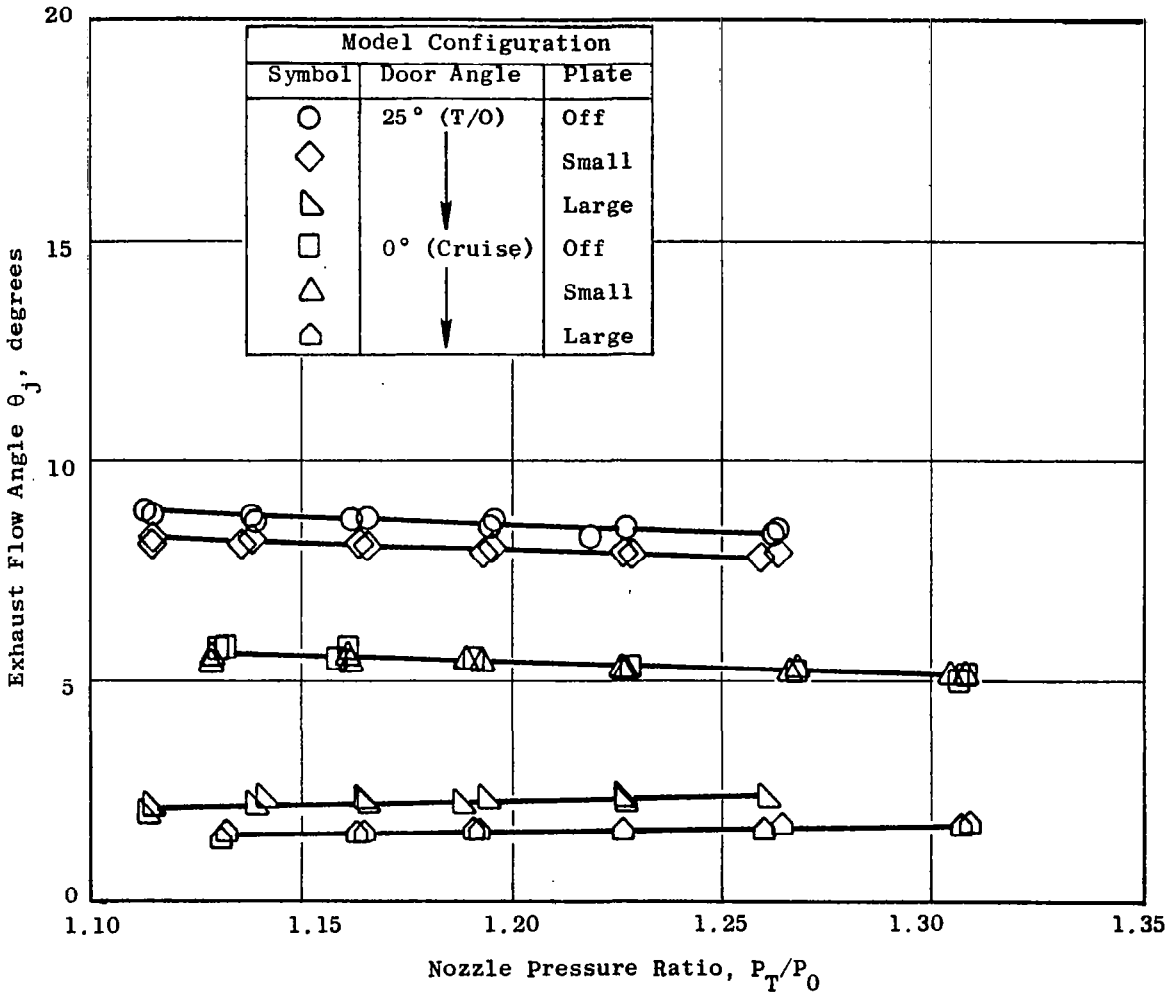

Figure 23. QCSEE Baseline OTW Nozzle Exhaust Flow Angle.

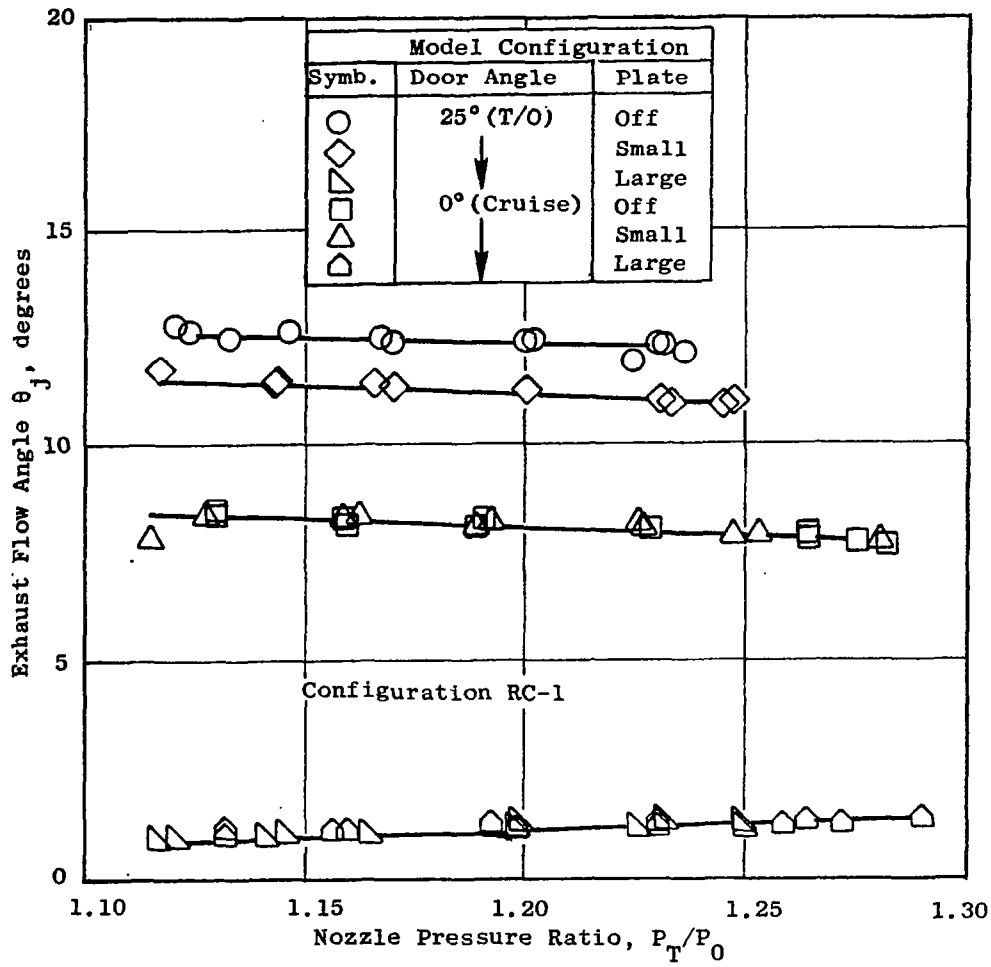

Figure 24. QCSEE RC-1 Nozzle Exhaust Flow Angle.

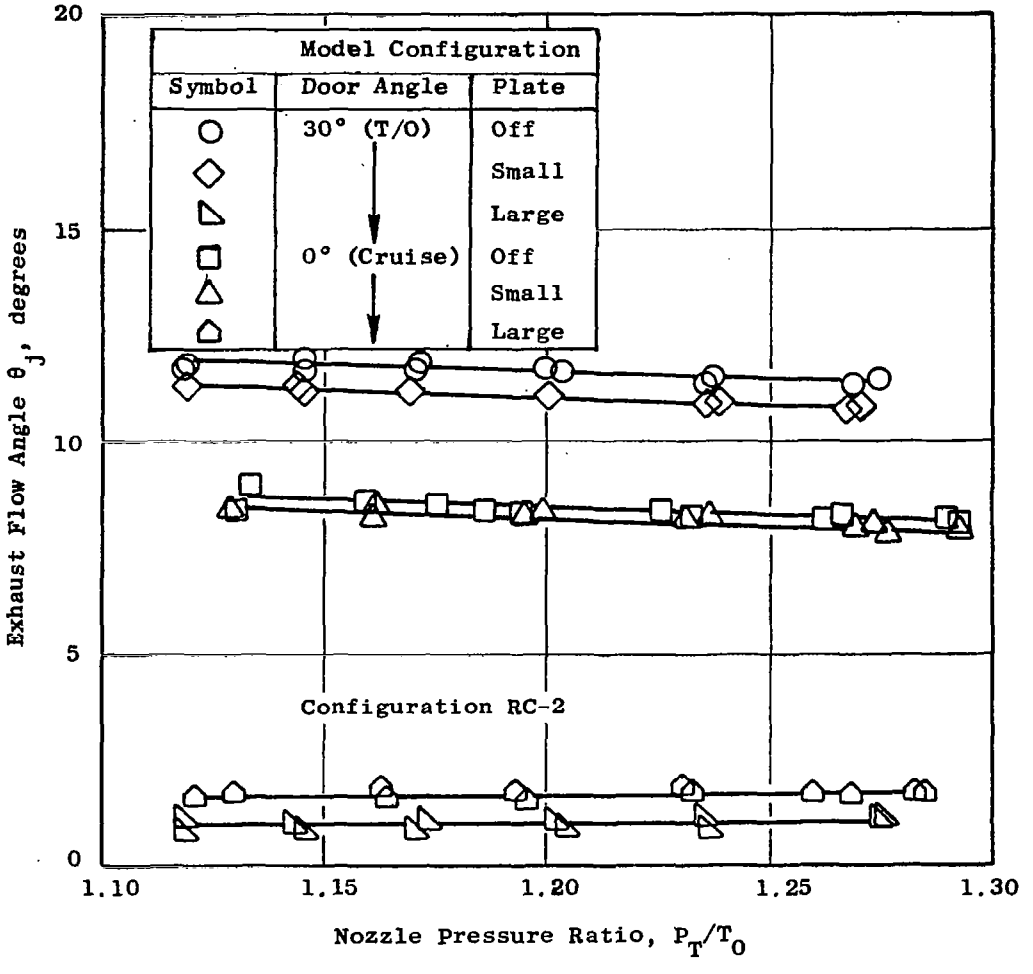

Figure 25. QCSEE RC-2 Nozzle Exhaust Flow Angle.

tests were made to evaluate the internal performance of this configuration and a modification to it which enlarged the opening (runs 67 and 68, Table 3). These test data, and all other internal performance test data not presented in Section 5.2.3, are included in Appendix C. The results from all of the side door area variation tests were condensed to derivative form and presented in this section.

Flow coefficient derivatives are shown on Figures 26, 27, and 28. These derivatives are all referenced to the 25° side door setting and include cruise nozzle data for more complete definition of area characteristics. One of the most important observations to be made from analysis of these data is that flow separation appears to occur at side door settings beyond 25° (30° for baseline and RC-2). This phenomenon presents an upper limit for potential full-scale QCSEE engine tests aimed at exploration of open nozzle use at approach conditions. It also should be noted from these figures that neither pressure ratio nor plate configuration greatly influenced the flow coefficient derivative characteristics for either model tested.

Velocity coefficient derivatives presented on Figure 29 are referenced to the 25° side door setting. Except for the cruise nozzle case, these derivatives show little dependency on side door position, pressure ratio, or plate configuration. For the cruise case with the large plate installed, the rise in velocity coefficient increment is attributed to wing scrubbing reduction or reduced flow-spreading angularity losses, or both, as discussed in Section 5.2.2.

5.3 NOZZLE CONFIGURATION RECOMMENDATION

On the basis of internal nozzle performance results and from preliminary indications of the static turning characteristics of the three nozzle configurations evaluated, configuration RC-1 is recommended for use on the QCSEE OTW experimental engine. The basis for selecting this nozzle design is summarized on Table 4. As indicated from this table, RC-1 was shown to rate best in terms of nozzle velocity coefficient, and it provided the largest exhaust flow angle (12.5°) for best jet/flap turning. It also met the QCSEE cycle area requirements (0.026 greater than required), as calculated from scale-model effective area (17.0 times C_d) versus pressure ratio characteristics extrapolated to the QCSEE takeoff fan pressure ratio of 1.32 and scaled to full size by dividing by the model linear scale factor squared (0.0853^2). The QCSEE cycle reference area used for comparison in Table 4 was 16355 cm^2 (2535 $in.^2$). This value was determined from the QCSEE fan and core engine stream flow properties (flow rate, pressure, and temperature) converted to a single equivalent stream value at the takeoff fan pressure ratio, considering temperature, pressure, and flow function differences between streams.

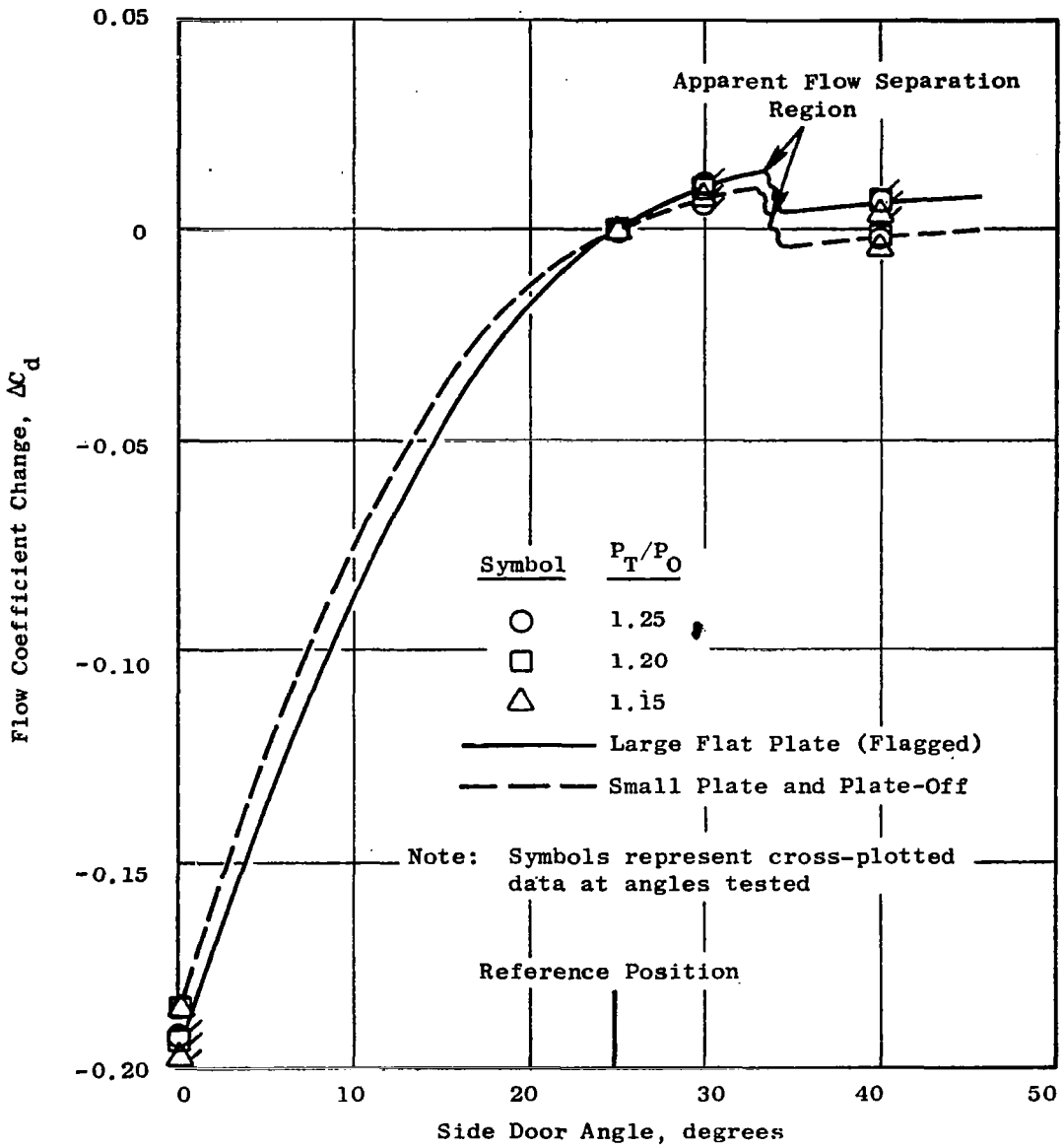

Figure 26. Effect of Side Door Position on Flow Coefficient, QCSEE Baseline OTW Nozzle.

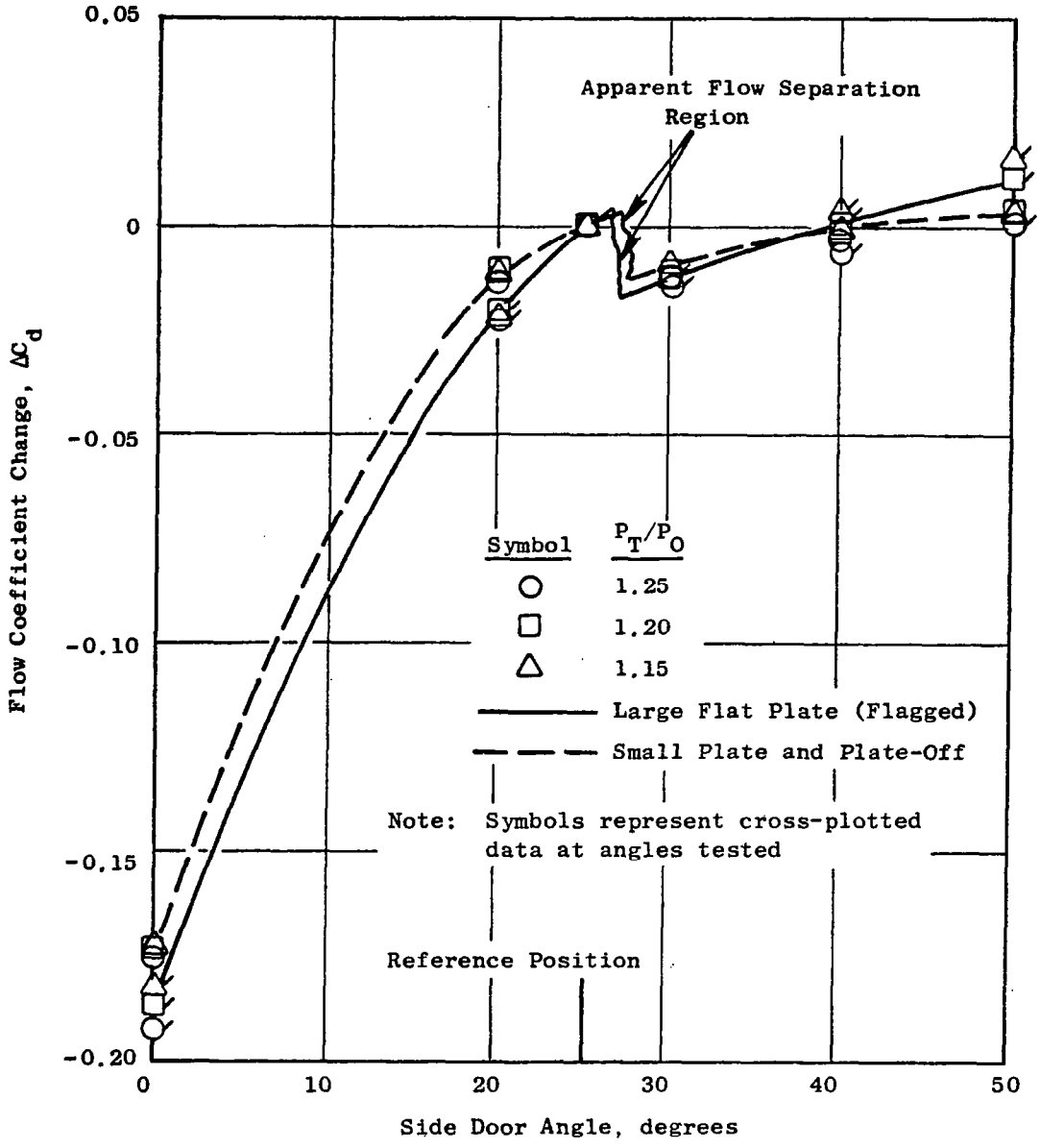

Figure 27. Effect of Side Door Position on Flow Coefficient, QCSEE RC-1 Nozzle Configuration.

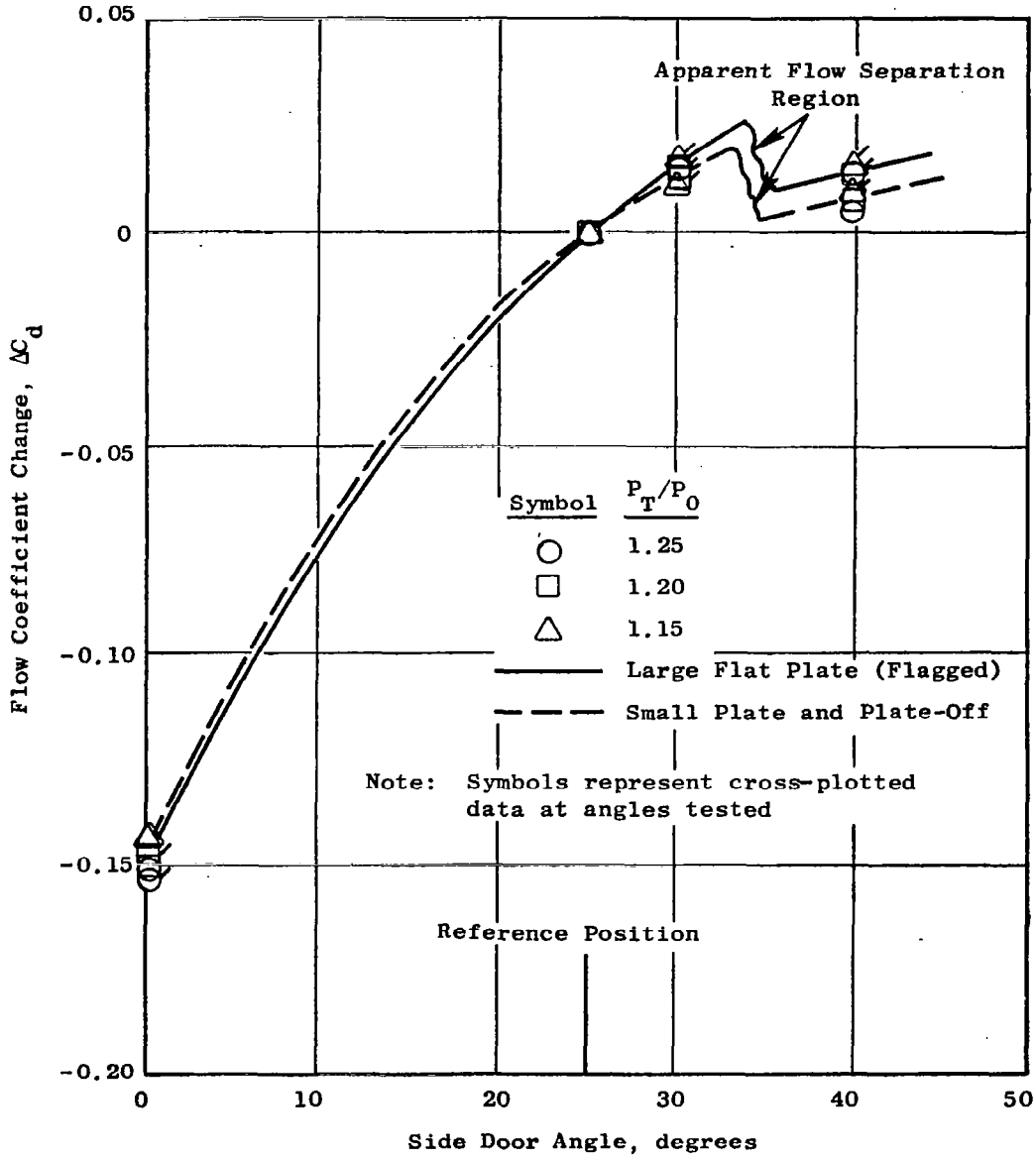

Figure 28. Effect of Side Door Position on Flow Coefficient, QCSEE RC-2 Nozzle Configuration.

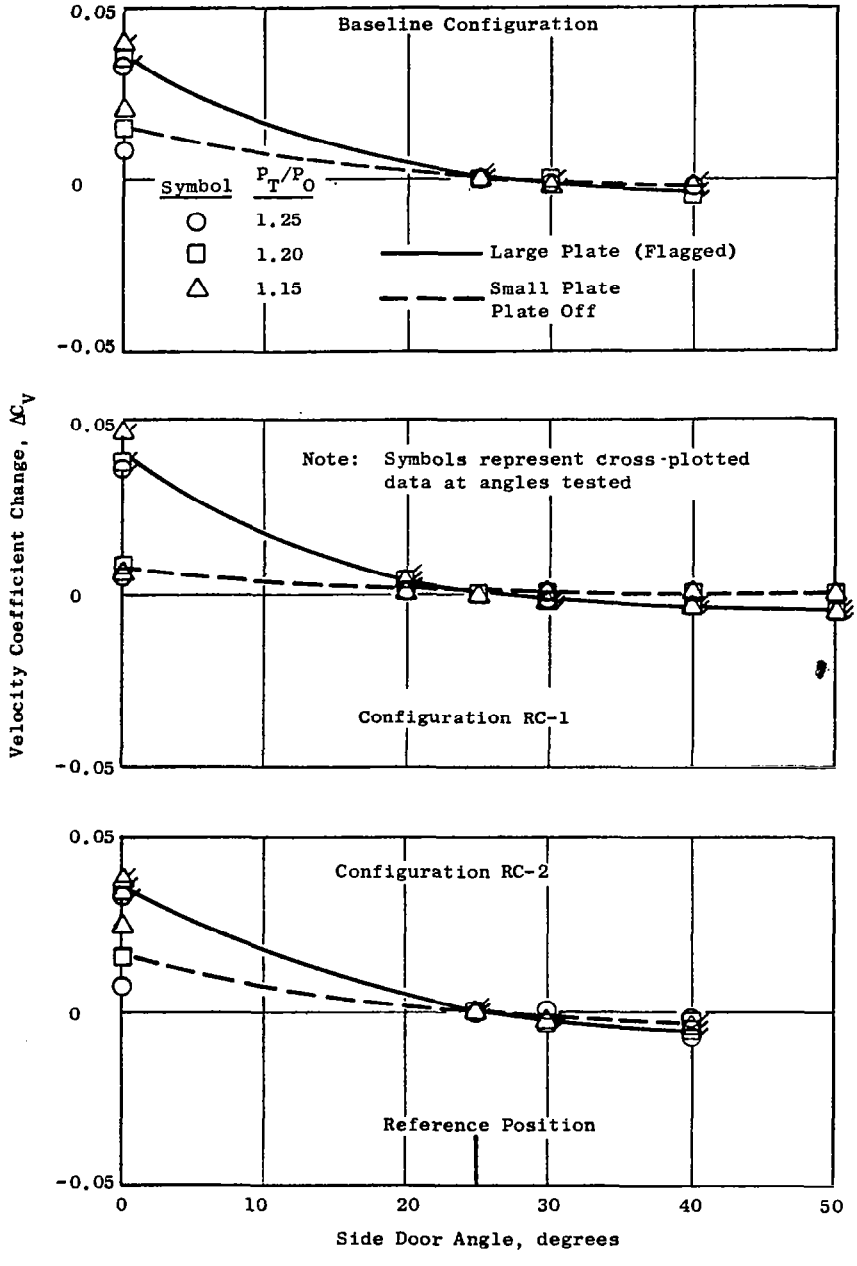

Figure 29. Effect of Side Door Position on Velocity Coefficients, QCSEE Baseline, RC-1 and RC-2 Configurations.

Table 4. Nozzle Performance Summary.

Nozzle Configuration	Calculated Takeoff Effective Area Relative to QCSEE Cycle Reqmt	Exhaust Flow Angle, θ_j	Internal Performance*			
			Takeoff C_V		Cruise C_V	
			Large Plate	Plate-Off	Large Plate	Plate-Off
Baseline	1.037	8.5°	0.914	0.948	0.944	0.952
RC-1	1.026	12.5°	0.914	0.966	0.946	0.969
RC-2	0.994	11.5°	0.898	0.957	0.934	0.965

* Evaluated at a nozzle pressure ratio of 1.25, the highest pressure attainable for takeoff nozzle test configurations.

SECTION 6.0

THRUST REVERSER PERFORMANCE

6.1 PERFORMANCE BASIS

The scale-model thrust reverser test results presented in this section were referenced to forward thrust performance data from configuration RC-1 as tested with 25° side doors and the small plate attached. Airflow ratio (W_{REV}/W_{FWD}) and effectivity (F_{REV}/F_{FWD}) data given are defined as measured flow and reverse thrust at the test pressure divided by forward-mode airflow and resultant forward thrust, respectively, at the same pressure ratio. Resultant thrust and airflow characteristics for the reference nozzle are given on Figure 30. These data, presented as a function of nozzle pressure ratio adjusted for measurement bias (Section 4.0), were curve fitted and incorporated into the final reverser data reduction program for computation of reverser airflow ratio and effectivity. Variations in prevailing ambient test conditions (barometric pressure and test facility room temperature) were compensated for by normalizing all forward and reverse mode thrust and airflow input data to standard sea level atmospheric conditions prior to computation of reverser performance parameters.

Reverser efflux angles (β_E) also were calculated from force balance normal and axial thrust readings. These calculated angles indicate the average reverser efflux angle as affected by blocker lip geometry and side skirt configuration. This angle is referenced to the model centerline, which is consistent with the blocker lip angle definition. Therefore, lower angles are indicative of higher reverse thrust.

6.2 INITIAL PARAMETER SENSITIVITY SCREENING

Initial tests conducted at the Langley static facility were informal explorations to improve reverser performance when the basic reverser performance without side skirts [Figures 6 and 8(a)], and with a short blocker lip ($L/D_{TH} = 0.2$) set at a 30° lip angle, showed low reverse thrust and airflow relative to the takeoff nozzle, with indications that a large fraction of flow was spilling out the sides of the blocker. These informal tests (many not recorded) were conducted to establish the direction for further reverser development effort. Significant reverse thrust improvement was noted with lip extension (up to $L/D_{TH} = 0.8$), and by addition of extended side skirts (including one configuration, the full skirt, which totally blocked off the two sides) rotated outward to capture the spillage flow previously observed. Increasing the blocker door inclination angle also was found to substantially increase reverse thrust. The results from these early tests led to formulation of the reverser parameter sensitivity screening matrix on Table 5. This matrix was established to further explore the effects of blocker door inclination angle, lip angle and length, and various

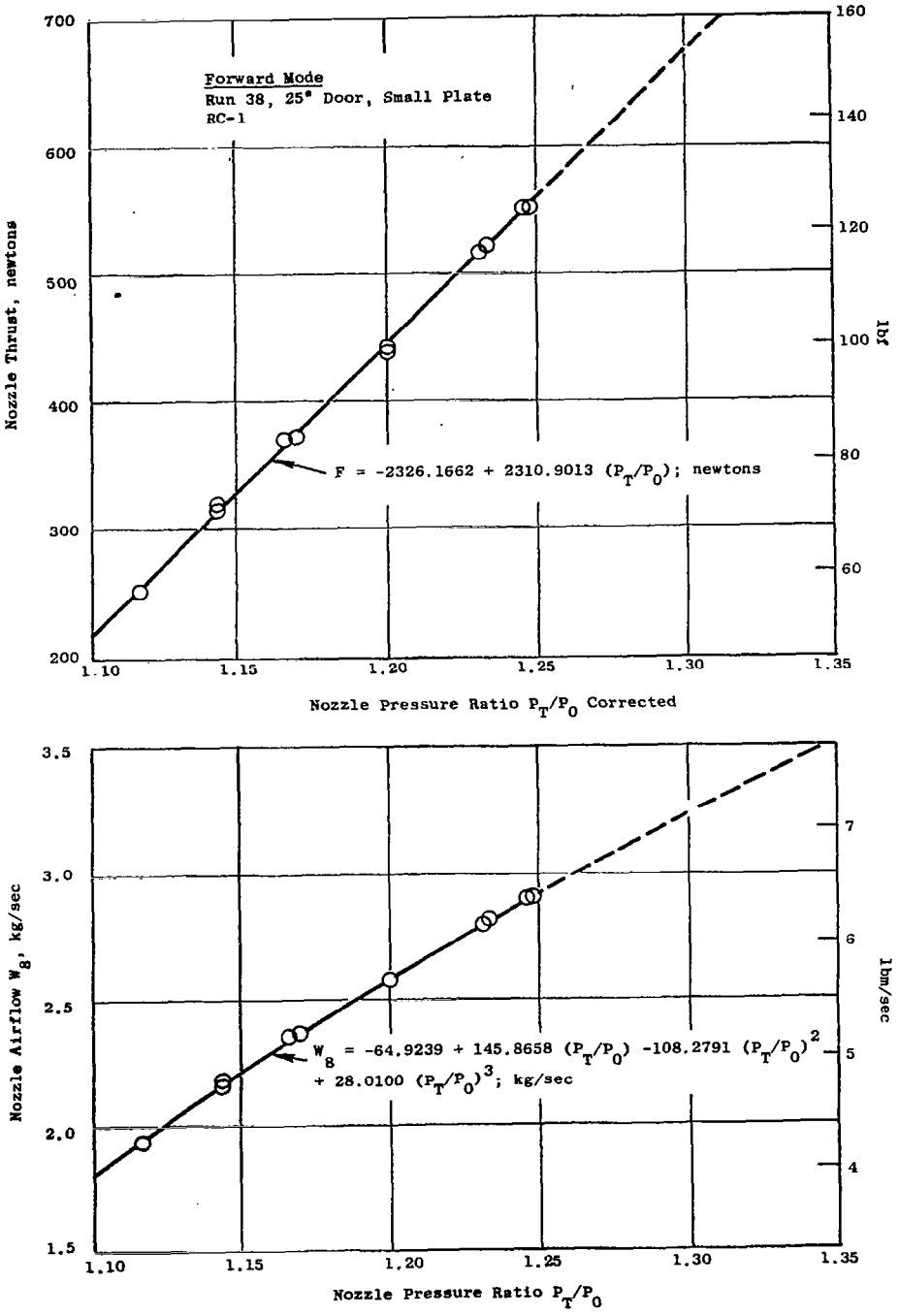

Figure 30. Forward Mode Reference "D" Nozzle Thrust and Airflow Characteristics.

Table 5. Reverser Parameter Sensitivity Screening Matrix.

Untrimmed Cut Line									
Run No.	$\frac{X_P}{D_{TH}}$	α	β	$\frac{H_B}{D_{TH}}$	$\frac{L}{D_{TH}}$	Inlet	Blast Shield	Skirt	Skirt Angle, ϕ
9	0.915	95	25	1.63	0.8	Bellmouth	On	Full	0
10	0.915	95	25	1.63	0.8	Bellmouth	On	Nominal	0
11	0.915	95	25	1.63	0.4	Bellmouth	On	Nominal	0
12	0.915	95	25	1.63	0.4	Bellmouth	On	Extended	45
13	0.915	95	25	1.63	0.4	Bellmouth	On	Extended	25
14	0.915	95	25	1.63	0.4	Bellmouth	On	Nominal	45
15	0.915	95	25	1.63	0.8	Bellmouth	On	Extended	45
16	0.915	95	25	1.73	0.8	Bellmouth	On	Extended	45
17	0.915	95	25	1.73	0.4	Bellmouth	On	Extended	45
18	1.017	95	25	1.63	0.4	Bellmouth	On	Extended	45
19	0.823	95	25	1.63	0.4	Bellmouth	On	Extended	45
20	0.790	105	25	1.63	0.4	Bellmouth	On	Extended	45
21	0.790	105	25	1.63	0.4	Bellmouth	On	Nominal	45
22	0.790	105	25	1.63	0.4	Bellmouth	Off	Nominal	45
23	0.790	105	25	1.63	0.4	Flight	Off	Nominal	45
24	0.790	105	25	1.63	0.8	Bellmouth	Off	Nominal	45
25	0.790	105	25	1.63	0.8	Bellmouth	Off	Extended	45
26	0.790	105	25	1.63	0.8	Bellmouth	On	Extended	45

Note: Refer to Figure 6 for definition of parameters.

side spillage flow containment skirts on reverse thrust and airflow. Blocker axial spacing variation and blocker door height increases were investigated also to determine what effect these parameters would have on the previously observed low reverse mode airflow characteristics.

6.2.1 Side Skirt Effects

Figures 31 through 35 present the effects of side skirt geometry and rotation angle on reverser performance. Data shown are for lip length ratios of 0.4 and 0.8 L/D_{TH}, blocker door angles of 95° and 105°, and spacing ratios of 0.915 and 0.79.

These data show a significant improvement in reverse thrust with the extended side skirt rotated to 45°; an increase in reverser effectivity of about 0.12 was observed with this configuration relative to the nominal, unrotated skirt (Figures 31 and 32). Intermediate effectivity improvements were noted for the full-skirt case and for the nominal skirt rotated outward 45°.

Little variation was seen in reverse-mode airflow ratio (0.02 and less) for these configurations except for the full-skirt extension, which showed a reduction in flow ratio of about 0.06 (Figure 32) relative to the nominal, unrotated-skirt design. All configurations indicated airflow capacity considerably below the forward takeoff nozzle levels, with ratios generally in the 0.84 to 0.88 range for the 95° blocker angle (Figures 31 and 32) and between 0.79 and 0.83 for the 105° angle with spacing ratio of 0.79 (Figure 34).

The reverse thrust effective efflux angles shown on Figures 33 and 35 confirm the observed trend of increased performance with decreasing pressure ratio, with lower angles indicating more forward direction of reverser efflux (more turning, hence, higher reverse thrust).

6.2.2 Blocker Spacing Effects

The effects of blocker door spacing ratio on reverse-mode airflow ratio and reverser effectivity are presented on Figure 36, while Figure 37 shows the effect on effective efflux angle. Blocker spacing ratio was investigated in an attempt to obtain a better match between reverse and takeoff nozzle airflow levels. For the blocker, lip, and side skirt configuration tested, it was found that increasing the spacing ratio from 0.823 to 1.017 improved airflow capacity by about 0.075; but, at the highest spacing, the reverse-mode flow ratio was increased to only 0.91, with a corresponding loss to reverser effectivity amounting to about 0.075.

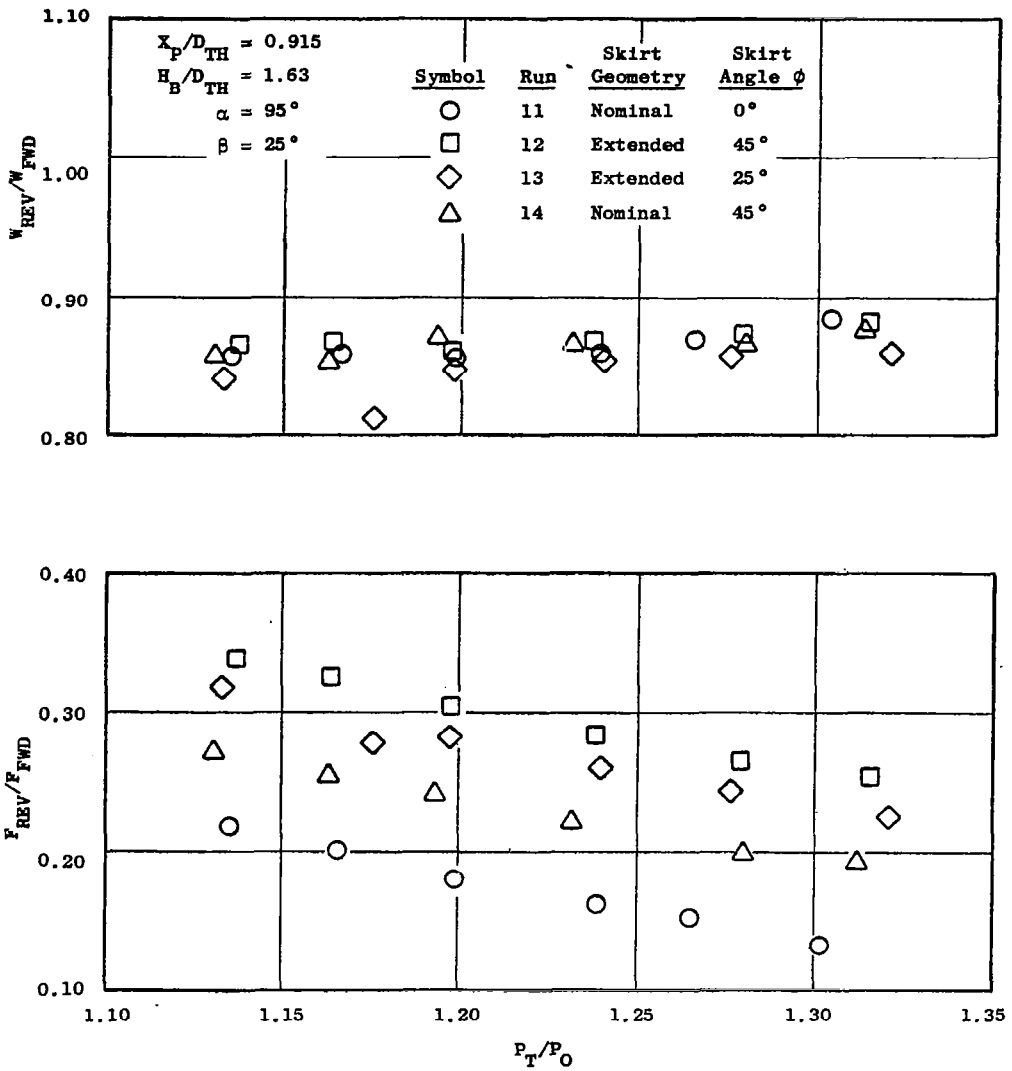

Figure 31. Effect of Reverser Side Skirt Geometry and Angle on Reverse Thrust and Airflow Characteristics, L/D_{TH} = 0.4.

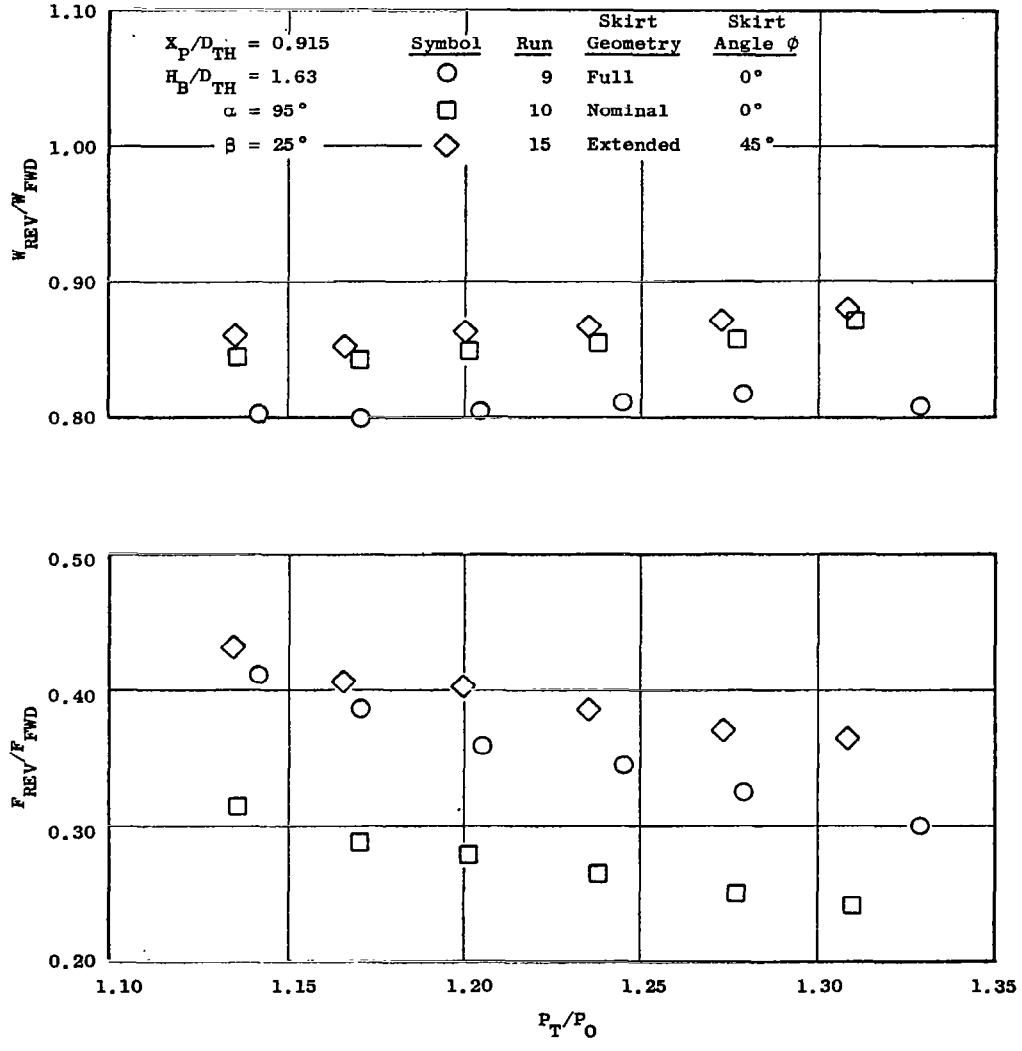

Figure 32. Effect of Reverser Side Skirt Geometry and Angle on Reverse Thrust and Airflow Characteristics, L/D_{TH} = 0.8.

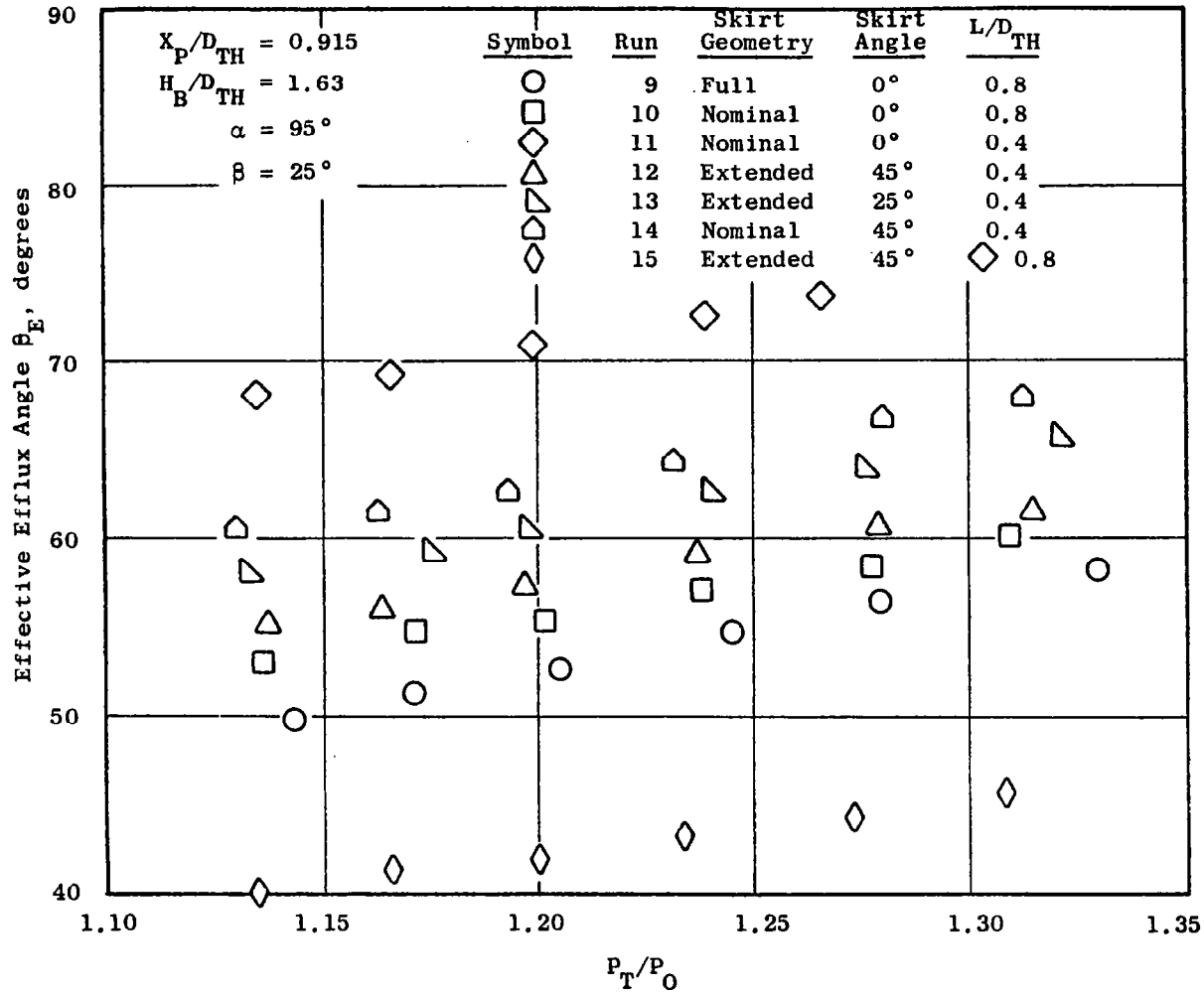

Figure 33. Effect of Reverser Side Skirt Geometry and Angle on Effective Efflux Angle.

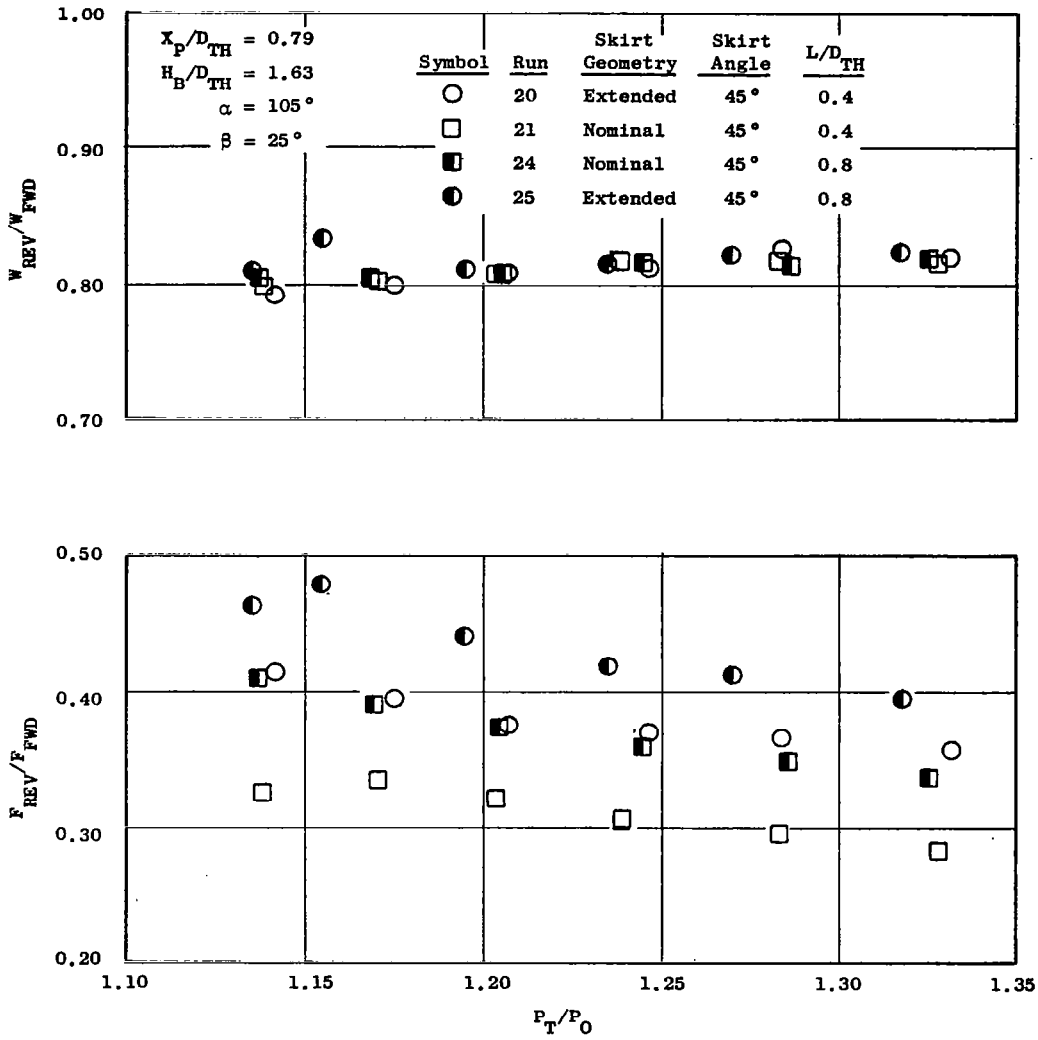

Figure 34. Effect of Nominal and Extended Side Skirts on Reverse Thrust and Airflow Characteristics for Lip Length Ratios of 0.4 and 0.8.

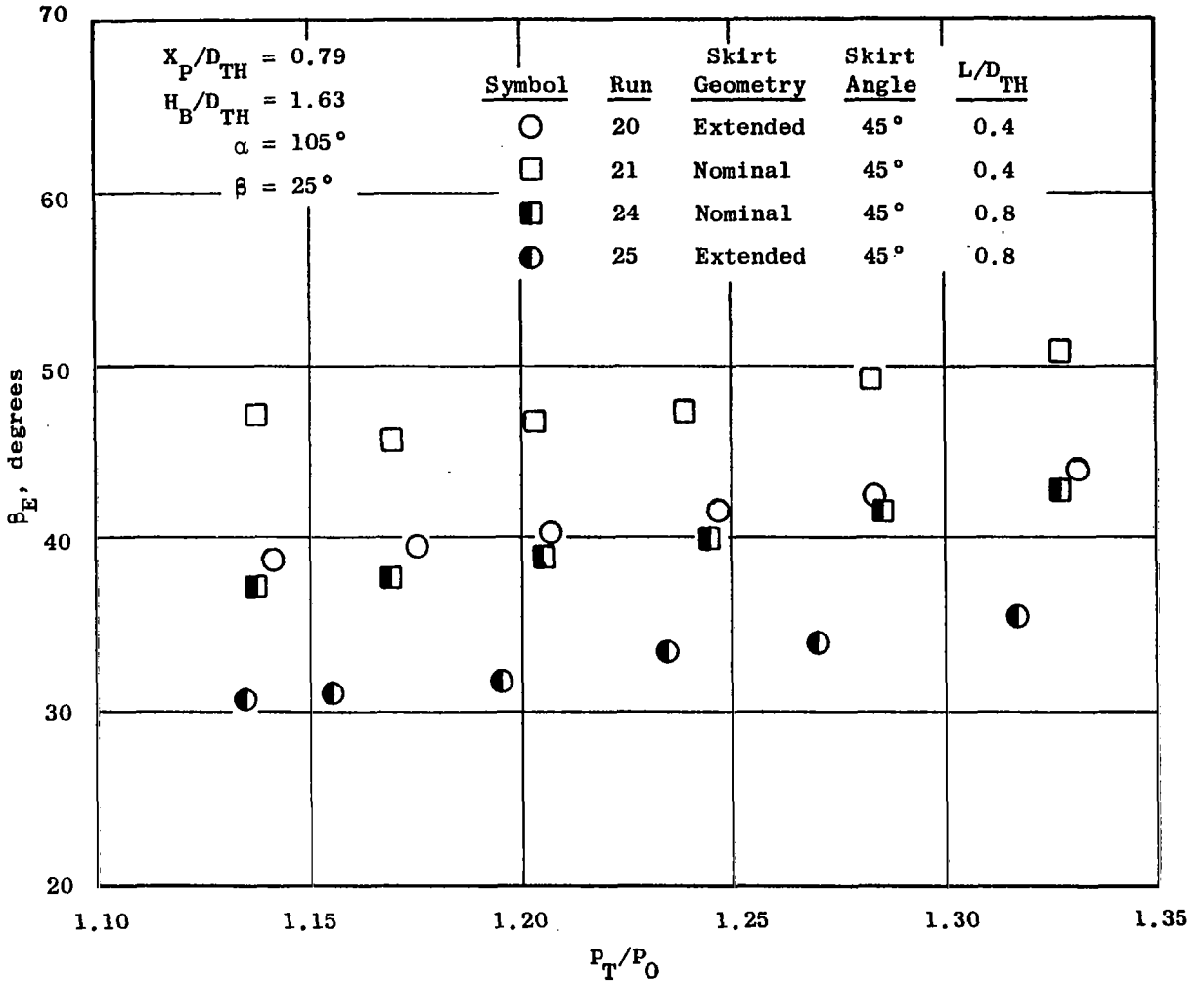

Figure 35. Effect of Nominal and Extended Side Skirts on Reverse Thrust and Airflow Characteristics for Lip Length Ratios of 0.4 and 0.8.

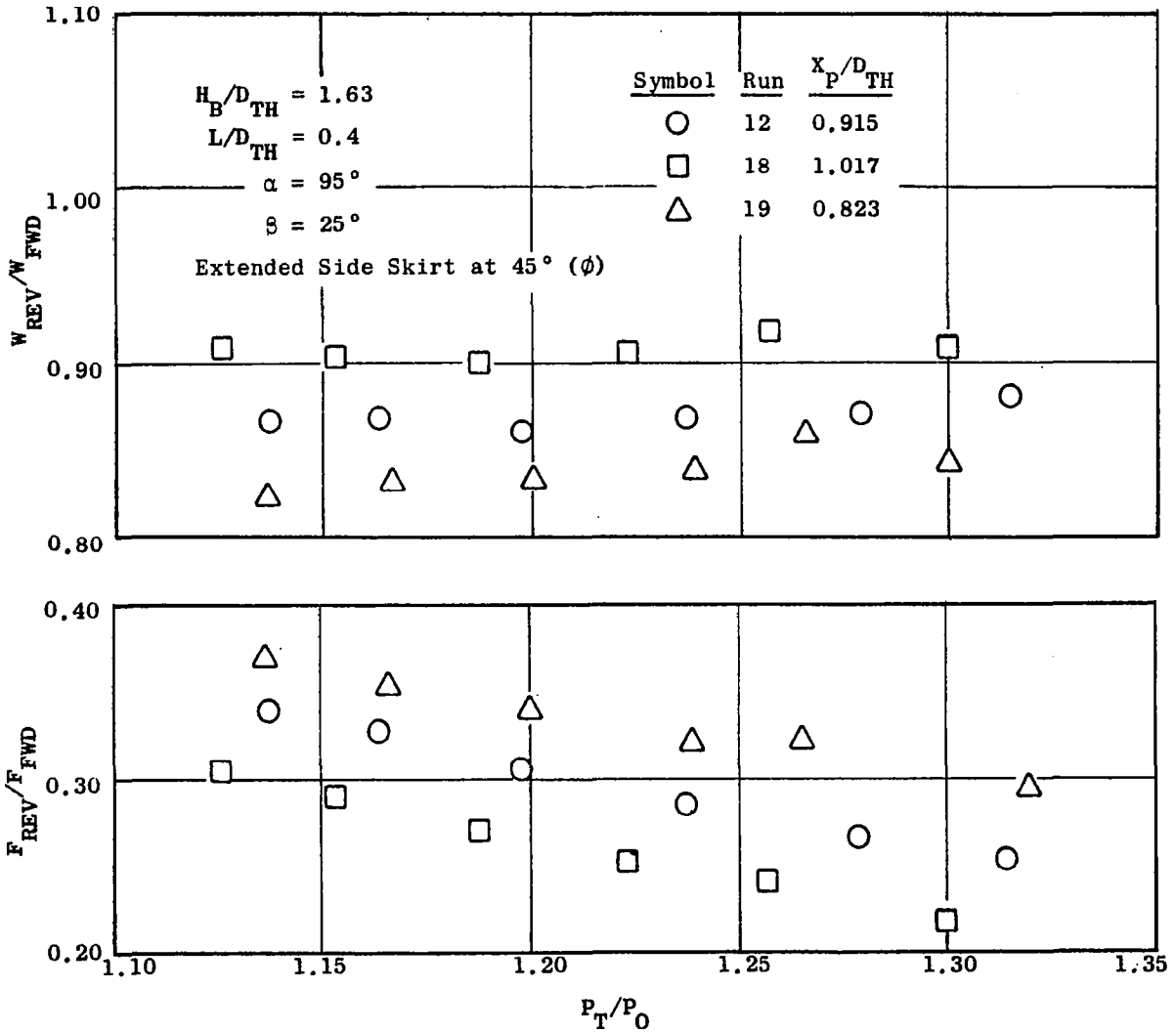

Figure 36. Effect of Blocker Spacing on Reverse Thrust and Airflow Characteristics.

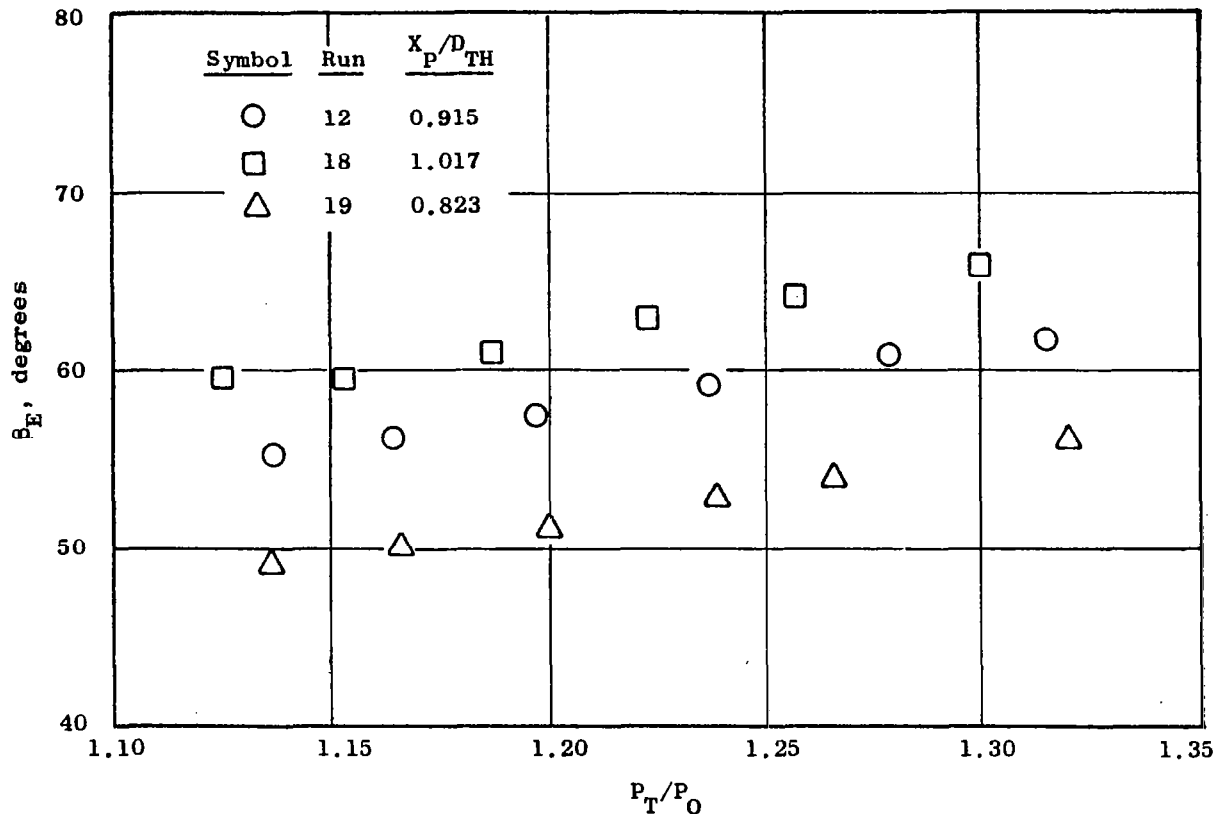

Figure 37. Effect of Blocker Spacing on Effective Efflux Angle.

6.2.3 Blocker Height Effects

Blocker door height was varied between 1.63 and 1.73 H_B/D_{TH} during the parameter screening tests. Results from these tests, as presented on Figure 38, show little effect on either reverse-mode airflow ratio or reverse thrust ratio for lip lengths of 0.4 and 0.8 L/D_{TH}. At increased blocker height, airflow ratio improved about 0.02 for both lip lengths, while reverse thrust increased 0.01 to 0.02 for the 0.4 L/D_{TH} lip configuration. No reverser effectivity change was observed for the 0.8 lip length ratio.

6.3 PARAMETRIC MATRIX

The parametric test matrix, Table 6, was established on the basis of results obtained from earlier screening tests and the QCSEE reverser geometry which began to emerge from these results. For these parametric investigations, a blocker spacing ratio of 0.865 Xp/D_{TH} was chosen, corresponding with the blocker spacing ratio selected for the QCSEE full-scale experimental nacelle. Blocker height was fixed at 1.63 H_B/D_{TH} to match the QCSEE blocker design. Side skirt geometry evolved from the extended design to the tabbed configuration (see Figure 6, Section 3.0) in order to eliminate side skirt and nozzle side door interference which would otherwise occur when stowing the reverser with the extended skirt concept. Blocker door inclination angle and lip angle were included as major parametric variables with a range of variation between 95° and 115°, and between 15° and 35°, respectively. Lip length ratio was varied between 0.2 and 0.8, with primary emphasis given to a value of 0.4.

All test results obtained from this test matrix may be found in Appendix D. From these data, reverse airflow ratios and reverser effectivity trends were reduced to derivative form for presentation in this section. While these derivatives were found to be independent of pressure ratio effects, some secondary effects were observed which could not be sorted out systematically for presentation individually; these effects are indicated by use of symbols on the derivative curves (Figures 39 through 42) and by shading the regions affected. Test run numbers and important geometric parameters also are given for easy reference.

6.3.1 Side Skirt Angle Effects

The effects of side skirt angle on reverse thrust and airflow are shown on Figure 39, with the 45° skirt angle position as the reference. These derivatives show higher airflow capacity (by 0.03) and higher reverse thrust (by 0.05) when the side skirts are rotated outward 45°. Although the trends appear linear with rotation angle, some earlier unrecorded tests with extended side skirts rotated to beyond 45° showed no additional gains.

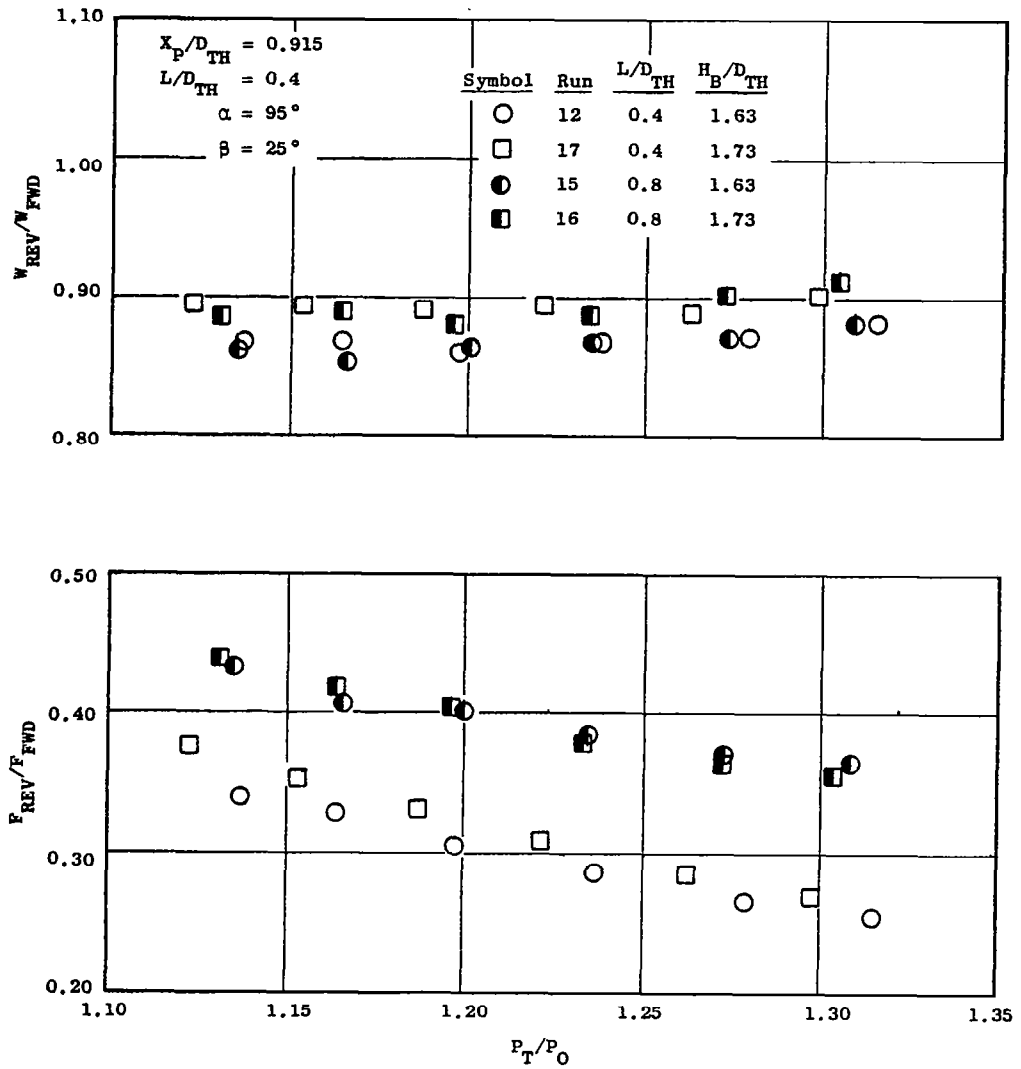

Figure 38. Effect of Blocker Height on Reverse Thrust and Airflow Characteristics at L/D_{TH} = 0.4 and 0.8.

Table 6. Reverser Parametric Test Matrix.

Trimmed Cut Line, QCSEE Pivot									
Run No.	$\frac{X_P}{D_{TH}}$	α°	β°	$\frac{H_B}{D_{TH}}$	$\frac{L}{D_{TH}}$	Inlet	Blast Shield	Skirt	Skirt Angle, φ°
40	0.865	95	25	1.63	0.4	Bellmouth	On	Nominal	45
41	0.865	95	25	1.63	0.4	Bellmouth	On	Tabbed	45
39	0.865	95	25	1.63	0.4	Bellmouth	On	Tabbed	0
42	0.865	95	25	1.63	0.2	Bellmouth	On	Tabbed	45
43	0.865	95	25	1.63	0.8	Bellmouth	On	Tabbed	45
46	0.865	95	35	1.63	0.4	Bellmouth	On	Nominal	45
45	0.865	95	35	1.63	0.4	Bellmouth	On	Tabbed	45
44	0.865	95	35	1.63	0.2	Bellmouth	On	Tabbed	45
37	0.865	105	15	1.63	0.4	Bellmouth	On	Nominal	45
36	0.865	105	15	1.63	0.4	Bellmouth	On	Tabbed	45
38	0.865	105	15	1.63	0.4	Bellmouth	On	Tabbed	0
35	0.865	105	15	1.63	0.2	Bellmouth	On	Tabbed	45
32	0.865	105	25	1.63	0.4	Bellmouth	On	Nominal	45
33	0.865	105	25	1.63	0.4	Bellmouth	On	Tabbed	45
31	0.865	105	25	1.63	0.4	Bellmouth	On	Tabbed	0
34	0.865	105	25	1.63	0.2	Bellmouth	On	Tabbed	45
51	0.865	105	35	1.63	0.4	Bellmouth	On	Tabbed	45
50	0.865	105	35	1.63	0.4	Bellmouth	On	Tabbed	0
29	0.865	115	15	1.63	0.4	Bellmouth	On	Nominal	45
27	0.865	115	15	1.63	0.4	Bellmouth	On	Tabbed	45
28	0.865	115	15	1.63	0.4	Bellmouth	On	Tabbed	0
30	0.865	115	15	1.63	0.2	Bellmouth	On	Tabbed	45
48	0.865	115	25	1.63	0.4	Bellmouth	On	Nominal	45
47	0.865	115	25	1.63	0.4	Bellmouth	On	Tabbed	45
49	0.865	115	25	1.63	0.4	Bellmouth	On	Tabbed	0

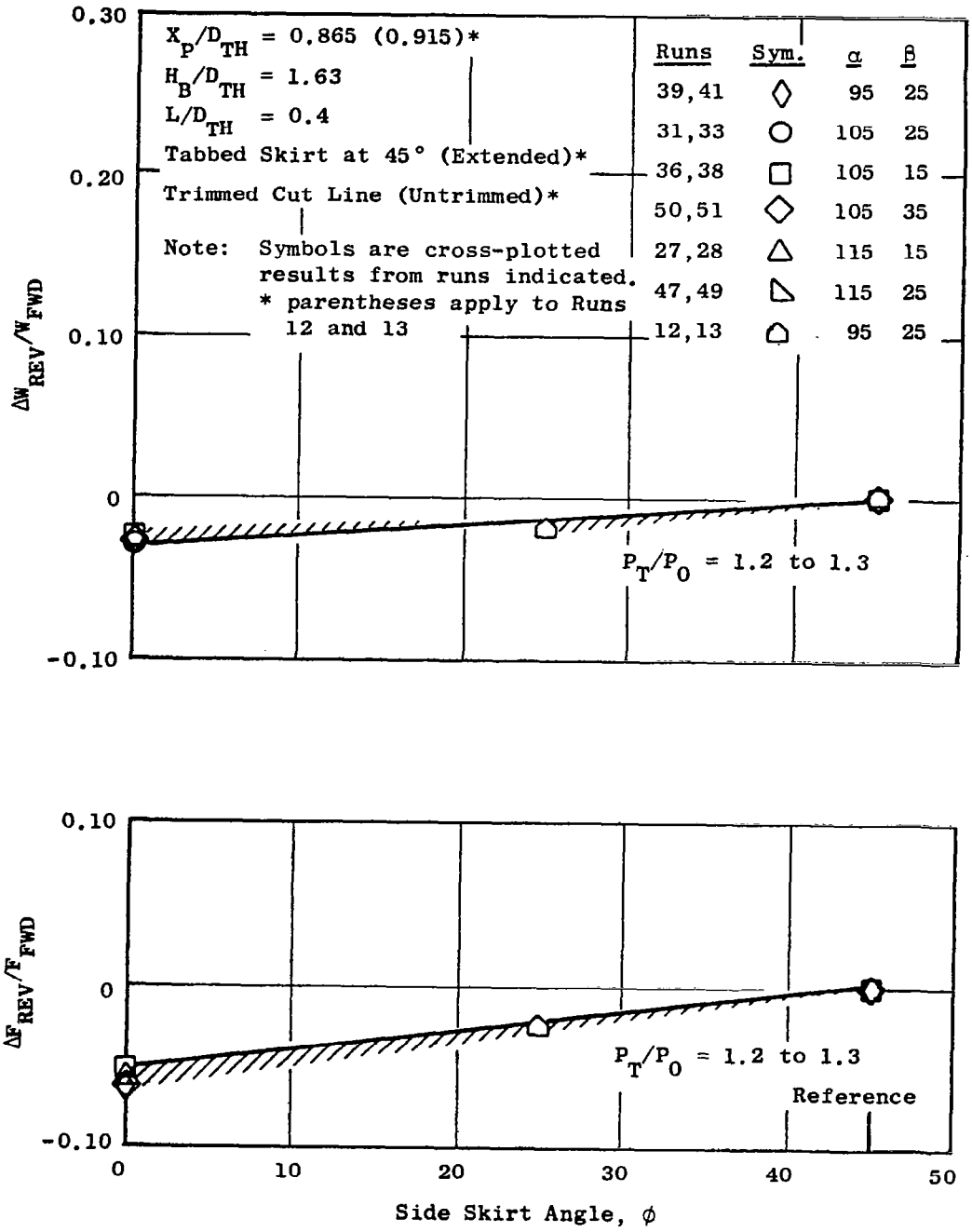

Figure 39. Change in Reverse Thrust and Airflow Characteristics with Side Skirt Angle.

6.3.2 Blocker Inclination Angle Effects

Figure 40 presents the effect of blocker door angle on reverser performance. Note from this figure that the most significant improvement to both airflow ratio and reverse thrust ratio occurs between blocker door angles of 95° and 105°, with little additional improvement above 105°, except as indicated from effectivity data taken on the short, 15° lip. As shown, the reference blocker door angle was chosen as 105°.

6.3.3 Lip Length Ratio Effects

Reverser effectivity was strongly influenced by increased lip length ratio, while airflow ratio was found to be relatively unaffected. Figure 41 shows these effects. Note particularly the change (0.135) in reverse thrust ratio between the lip length ratios of 0.2 and 0.4. Also observe the apparent secondary effects attributable to blocker door angle and low lip angle. A substantial reverse thrust increase also was realized for lip length ratios of 0.8, secondary effects of blocker angle and lip angle were not investigated here, however.

6.3.4 Lip Angle Effects

Blocker lip angle, which was varied between 15° and 35°, showed only moderate effects on airflow ratio and reverse thrust ratio as indicated by Figure 42. The greatest reverse thrust change was observed in decreasing lip angle from 35° to 25°, ignoring the secondary effects shown, with little additional reverse thrust benefit from a further angle decrease to 15°. Airflow ratio change was linear throughout the range of angles tested.

6.4 OTHER PERFORMANCE EFFECTS

Reverser development effort concluded with tests of a cut-back lip configuration (see Figure 6) evaluated alternately with bellmouth, flight-type inlet, blast shield, ground plane simulation (QCSEE full-scale tests will be conducted with the nozzle and reverser hardware mounted inverted so that the reverser will discharge groundward), and reingestion pipe installed (Figure 43). The reingestion pipe was scaled to model size from full-scale drawings of a pipe used for reingestion shielding in General Electric full-scale outdoor tests.

The configurations evaluated in these investigations are given in Table 7. Test results are presented on Figures 44 and 45.

6.4.1 Lip Cutback Effects

Figure 44 shows that both reverse thrust and airflow ratios are essentially unaffected by lip cutback for the 35° lip configuration investigated.

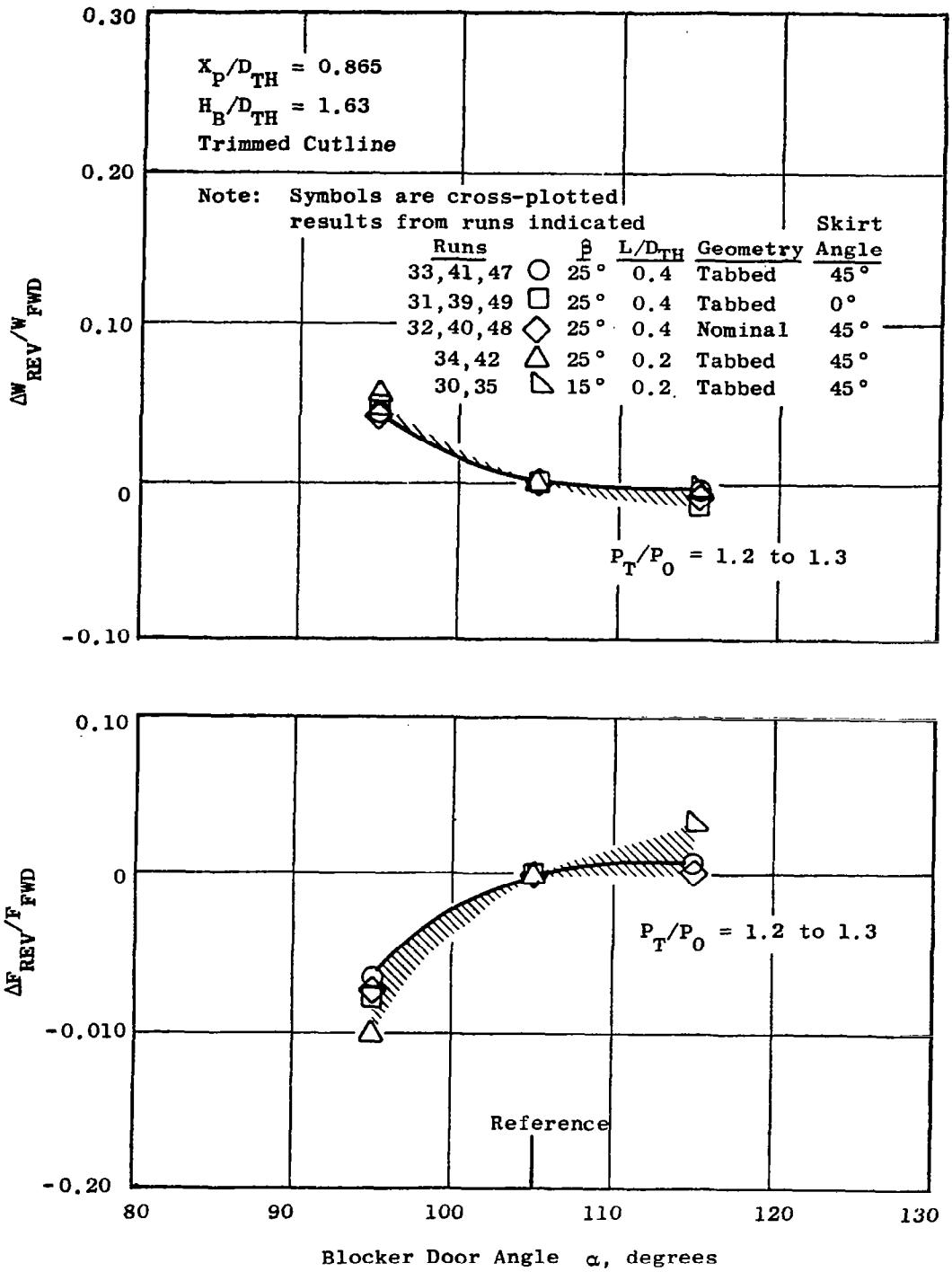

Figure 40. Change in Reverse Thrust and Airflow Characteristics with Blocker Door Angle.

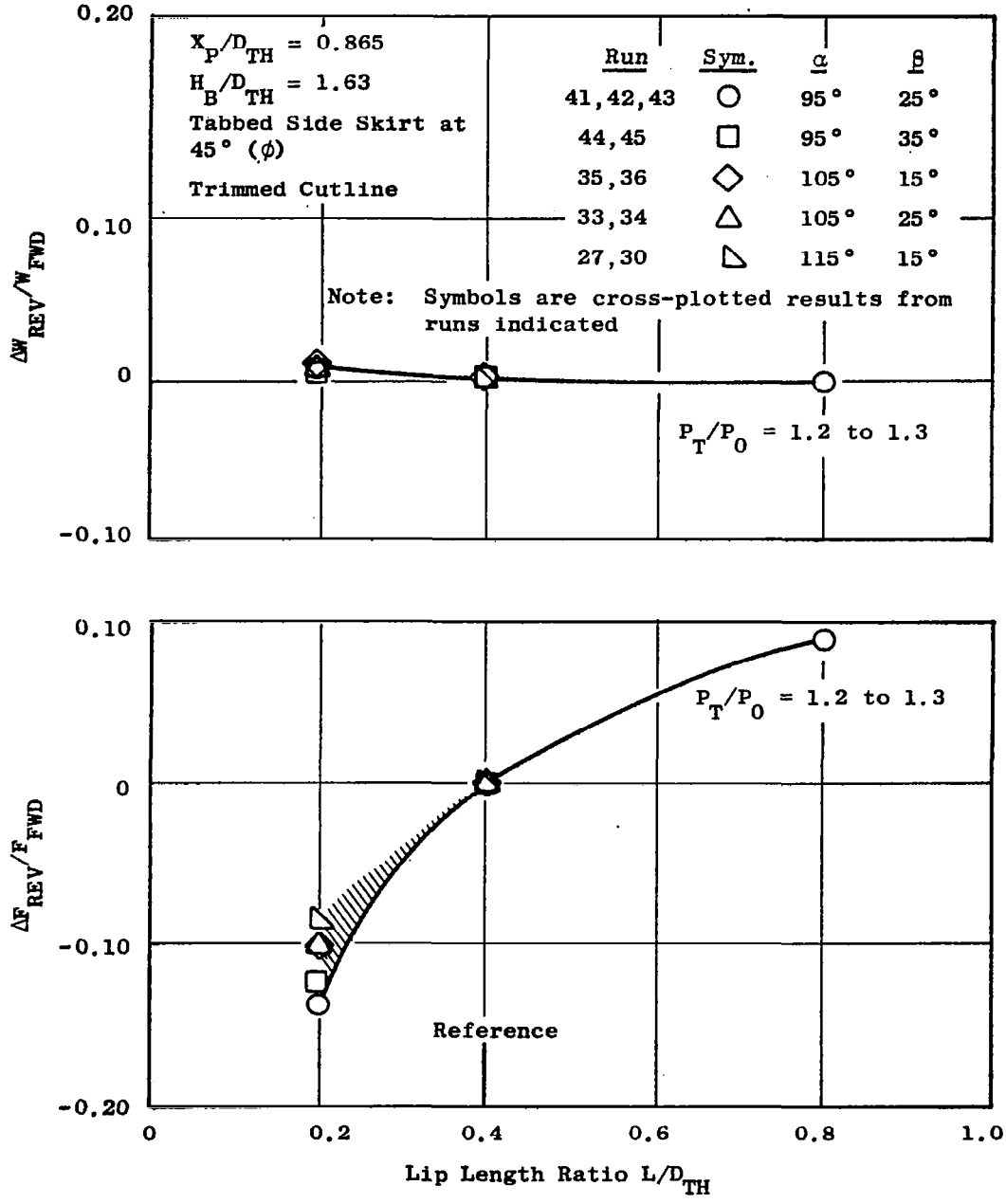

Figure 41. Change in Reverse Thrust and Airflow Characteristics with Lip Length Ratio.

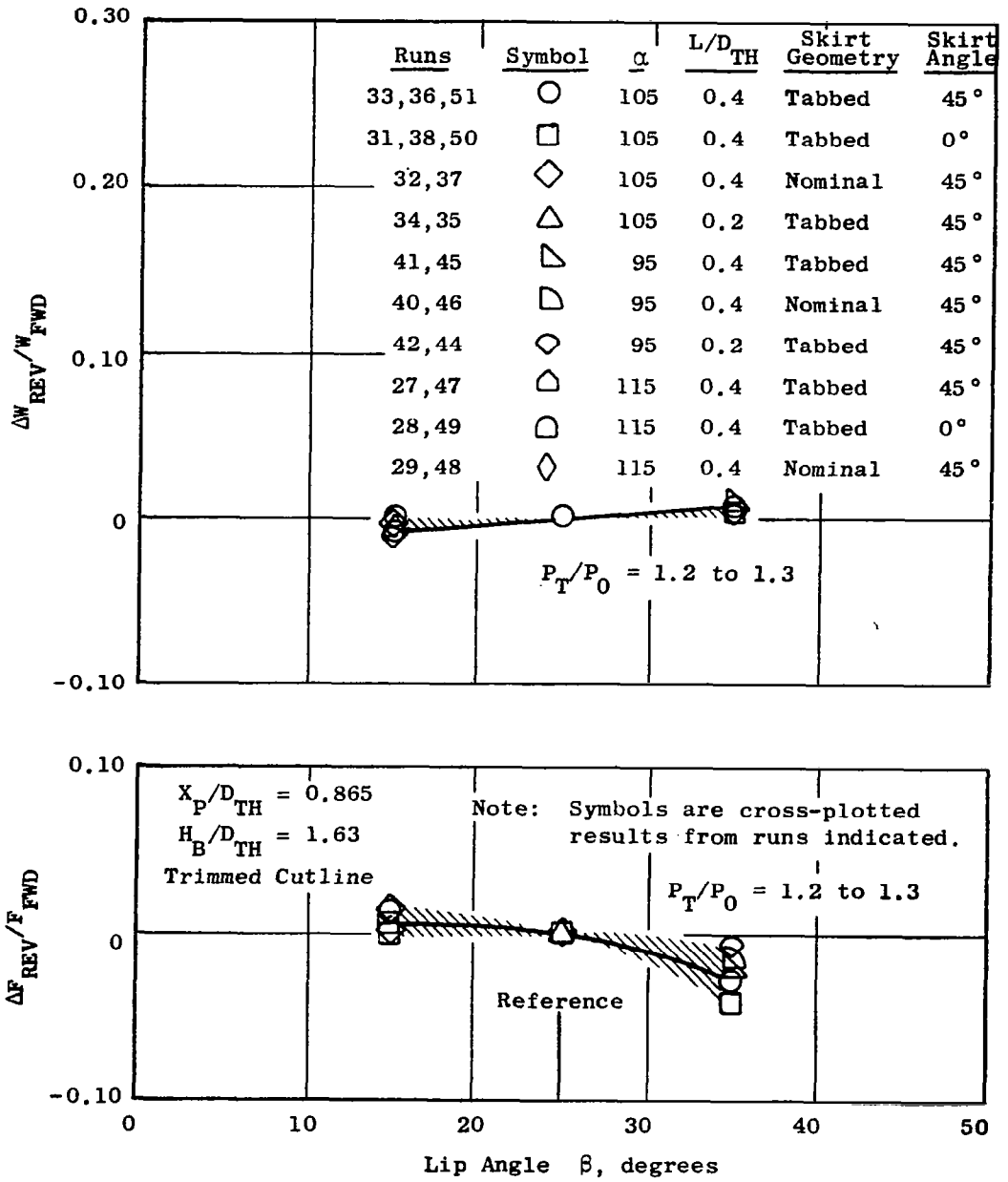

Figure 42. Change in Reverse Thrust and Airflow Characteristics with Lip Angle.

GROUND PLANE LOCATION

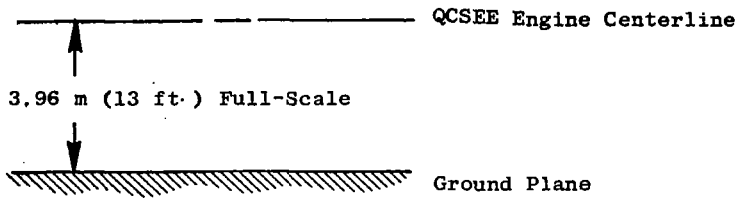

INLET PIPE

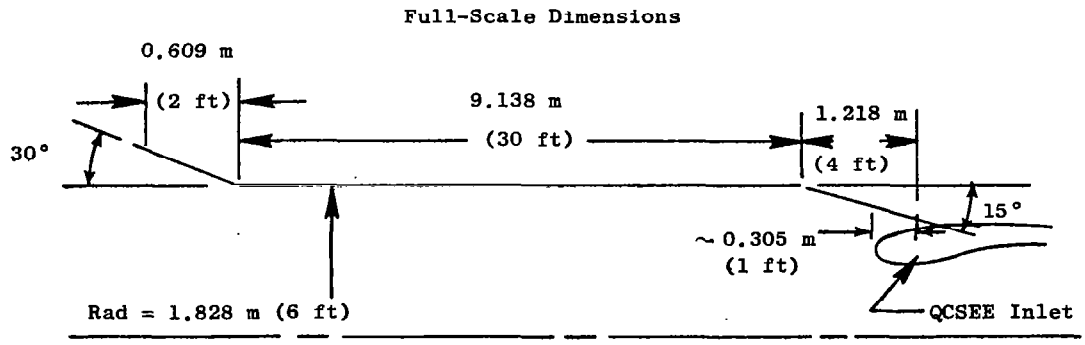

Figure 43. Reingestion Pipe, Full Scale.

Table 7. Supplementary Reverser Test Configurations.

Run No.	Trimmed Cut Line, QCSEE Pivot									
	X_P/D_{TH}	$\alpha°$	$\beta°$	H_B/D_{TH}	L/D_{TH}*	Inlet	Blast Shield	Skirt	Skirt Angle $\phi°$	
52	0.865	105	35	1.63	0.4	Bellmouth	On	Tabbed	45	
53	0.865	105	35	1.63	0.4	Bellmouth	Off	Tabbed	45	
54	0.865	105	35	1.63	0.4	Flight	Off	Tabbed	45	
55	0.865	105	35	1.63	0.4	Flight	Off	Tabbed	45	ground plane simulated
56	0.865	105	35	1.63	0.4	Flight/Pipe**	Off	Tabbed	45	

* Lip cutback in accordance with Figure 6.

** Pipe installed over inlet to prevent reingestion from ground plane.

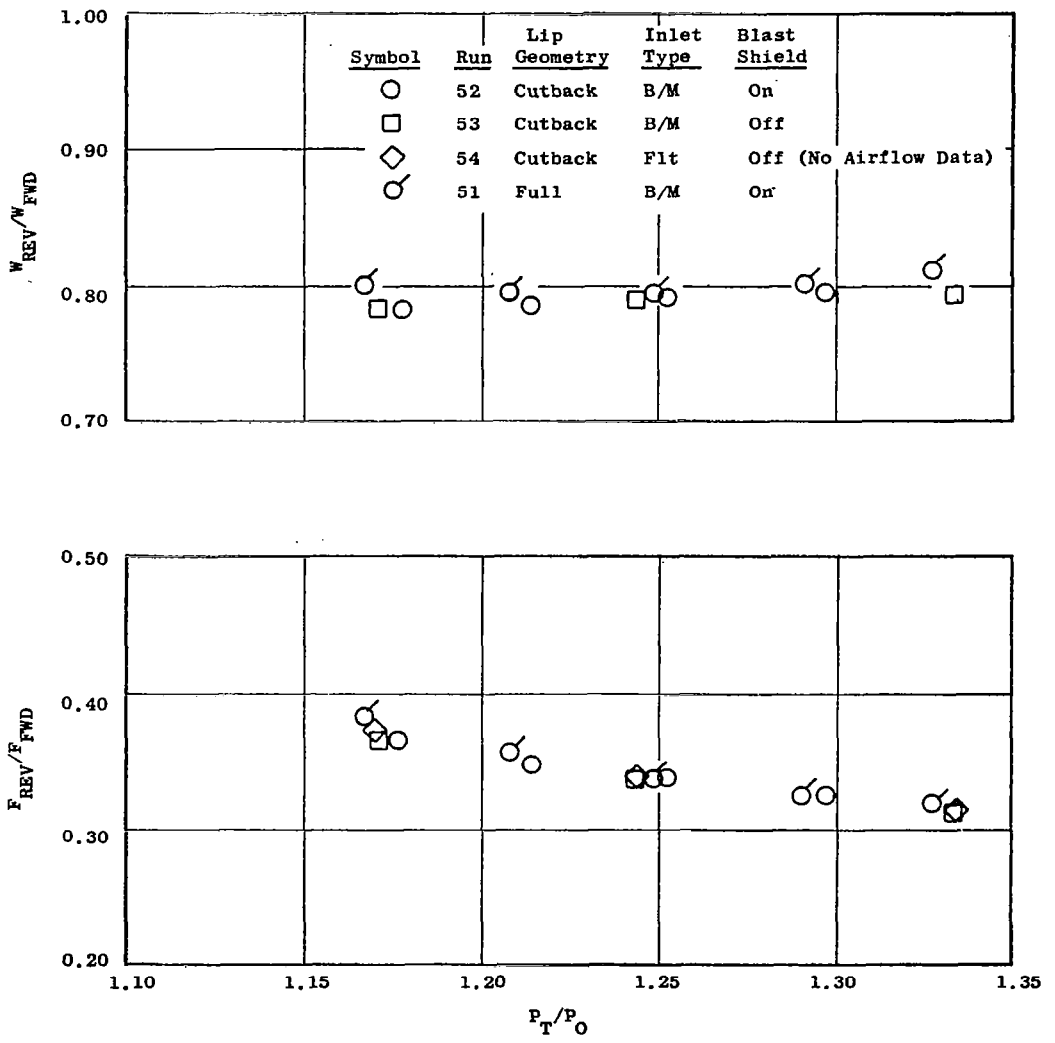

Figure 44. Effect of Lip Cutback on Reverse Thrust and Airflow Characteristics.

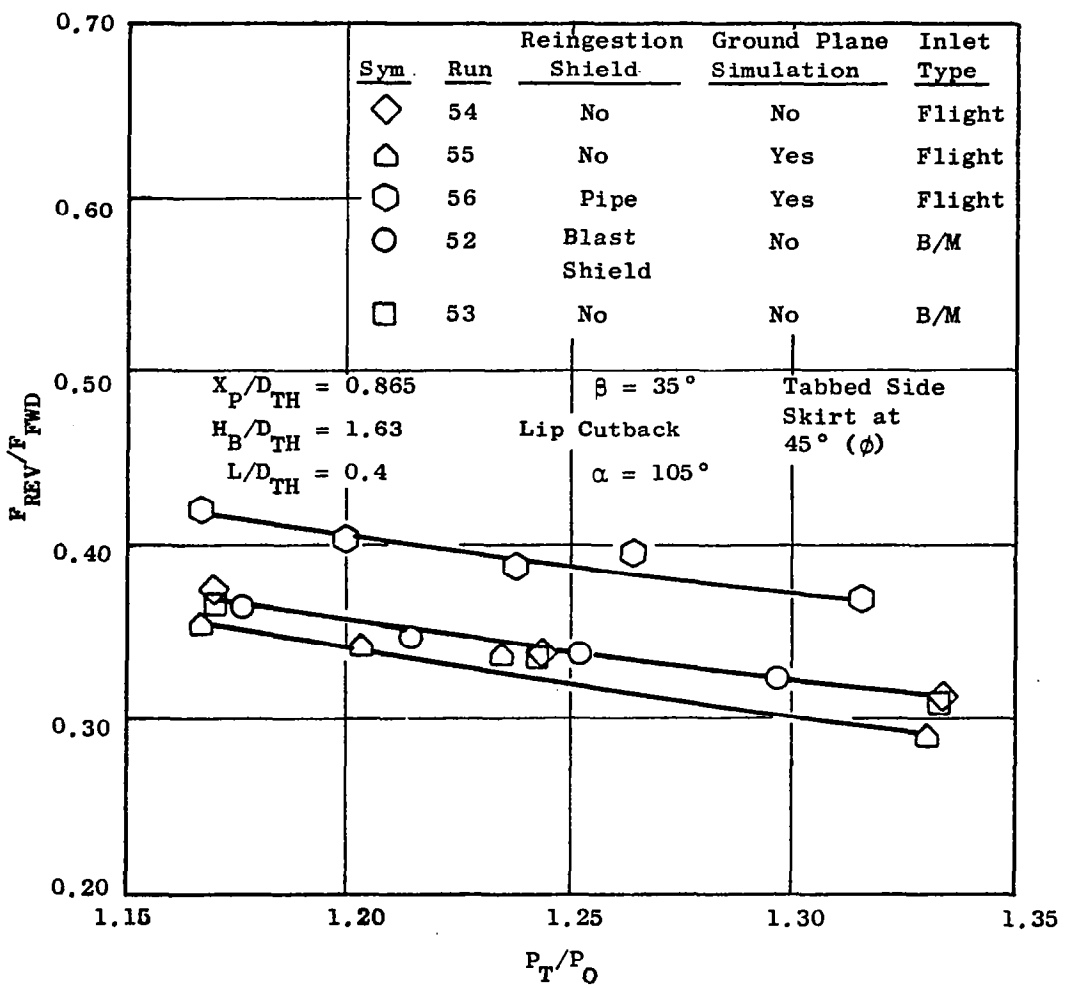

Figure 45. Effects of Ground Plane and Reingestion Shielding on Reverse Thrust.

The small differences in measured values which appear (comparing runs 51 and 52) are considered to be within test accuracy. As indicated on Figure 44, no airflow data were measured with the flight inlet.

6.4.2 Reingestion Shield Effects

Two types of reingestion prevention devices were used in these tests: 1) the blast shield (see Figure 7), and 2) the reingestion pipe shown on Figure 43.

The blast shield utilized was a simple flat plate attached to the facility and positioned between inlet and reverser, so that inlet and reverser flow fields were not adversely affected and installation around the model would not ground the force balance system (see Figure 7). A comparison of test runs 52 and 53 on Figure 44 shows no effect due to blast shield installation on either airflow or reverse thrust performance.

The reingestion pipe was installed over the inlet without grounding the force balance through an inlet/pipe contact; the pipe is attached to facility ground. A comparison of pipe-on and pipe-off data on Figure 45 (compare runs 52, 53, and 54 against the pipe installation run 56) shows a significant increase in measured reverse thrust ratio (about 0.05). This increase in reverse thrust is attributed to increased airflow inlet momentum (analogous to ram drag) at the face of the inlet inside the pipe. Had the pipe been coupled to the model or force balance instead of grounded to the facility test bench, the pipe body forces would have directly cancelled the inlet face momentum term, and test results would have fallen back in line with runs 52, 53, and 54. These reingestion pipe data indicate the approximate level of reverse thrust correction which must be made on full-scale outdoor reverser tests in QCSEE should a shield such as this be required. The level of correction observed is consistent with full-scale engine test experience with this type of reingestion shield.

6.4.3 Ground Plane Effects

A comparison of test results obtained with a flight-type inlet and without reingestion shields (Figure 45, runs 54 and 55) shows a reduction in reverse thrust ratio of about 0.02 when the ground plane is simulated. This reduction in reverser performance was attributed to reingestion from the ground of simulator exhaust flow directed groundward and forward by the inverted reverser simulation. This reduced performance condition indicates a potential requirement for conducting full-scale QCSEE reverser tests at the General Electric outdoor facility with a reingestion shield.

Similar airflow ratio effects with and without ground plane simulation could not be investigated because simulator airflow measurements were not made with the flight inlets tested here.

6.5 REVERSER CONFIGURATION RECOMMENDATIONS

Analysis of results obtained from reverser scale model testing has led to the selection of the recommended QCSEE reverser configuration shown on Figure 46. This configuration has a blocker inclination angle of 105° (model basis) with the blocker spaced at Xp/D_{TH} = 0.865; the blocker height ratio, H_B/D_{TH}, is 1.63. The recommended reverser lip angle is 25°, with a lip length ratio, L/D_{TH}, of 0.4. Tabbed side skirts were selected on the basis of side door clearance when stowing the reverser. The side skirts are rotated outward to 45°.

This recommended configuration geometry was tested as part of the reverser matrix evaluation; the test data for this model may be found in Appendix D as run 33. These data, in combination with other data in the reverser test matrix and the derivative curves from Section 6.0, were used to make up the scale model carpet plot performance curves on Figures 47 and 48.

The carpet plot data show reverser effectivities between 0.38 and 0.36 for pressure ratios between 1.2 and 1.3, respectively (Figure 47), with corresponding airflow ratios of 0.78 to 0.805 at the selected blocker angle and lip length ratio (105° α and 0.4 L/D_{TH}). Previous analysis of these data (Reference 2) has shown that this level of performance will enable the QCSEE reverse thrust requirement of 35% of takeoff thrust to be met, even when allowance is made for reverser blocker-door leakage losses. QCSEE engine cycle studies (Reference 2) have further indicated that adequate engine stability margins are maintained with these reverser airflow ratios, adjusted for blocker leakage flow rates, to permit satisfactory experimental engine testing.

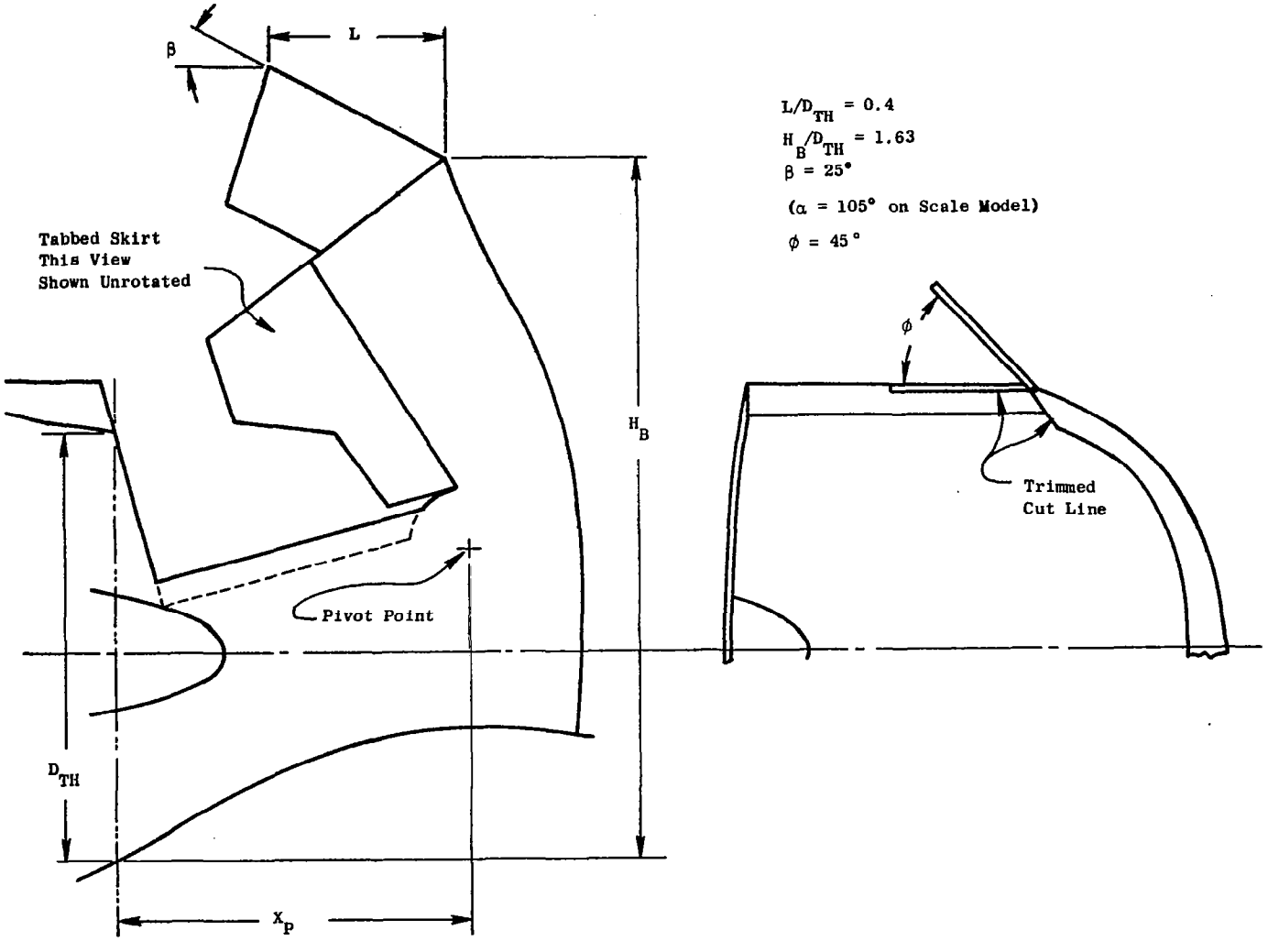

Figure 46. OTW Reverser Configuration Recommendation.

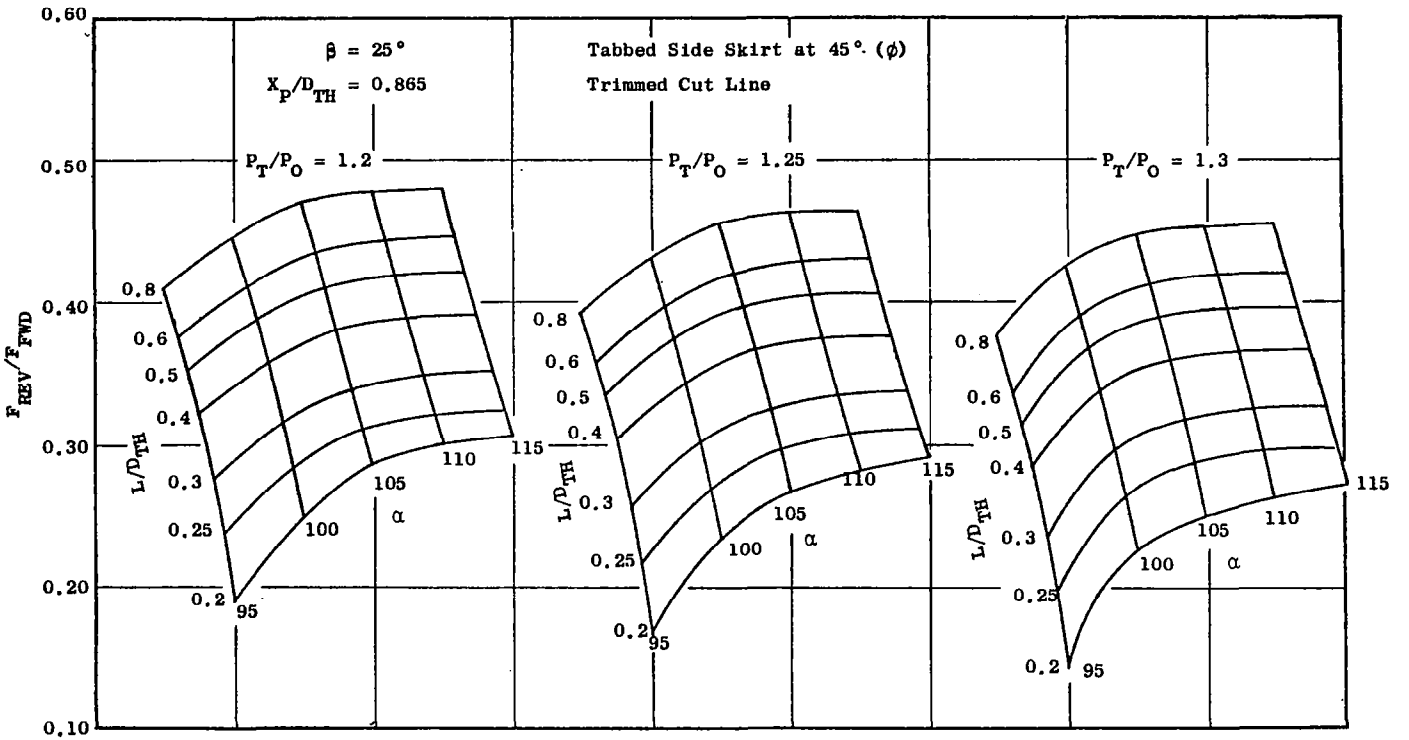

Figure 47. Effect of Lip Length Ratio and Blocker Door Angle on Reverse Thrust Performance for Various Pressure Ratios.

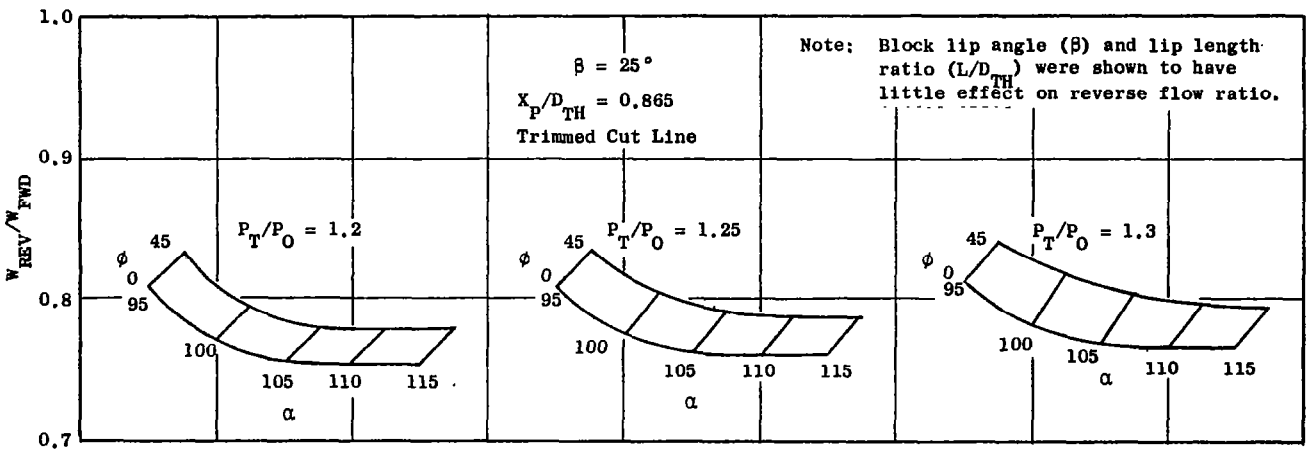

Figure 48. Effect of Side Skirt Angle and Blocker Door Angle on Airflow Performance for Various Pressure Ratios.

SECTION 7.0

CONCLUSIONS

- Scale-model static tests have defined an Over-the-Wing "D" nozzle and a reverser exhaust system which meet the cycle area requirements at takeoff, provide acceptable cycle effective area in reverse thrust, and meet the 35 percent reverse thrust objective established for the Quiet Clean Short-Haul Experimental Engine (QCSEE) Program.

- The QCSEE nozzle side door area variation concept demonstrated acceptable area variation capability, but internal flow separation, experienced at side door angles beyond the 25° door setting required for takeoff/cycle area, sets an upper limit on area variation capability.

- The nozzle side door concept demonstrated good flow-spreading characteristics for low speed powered-lift performance.

- Recontouring the nozzle roof (top) and floor internal flow lines to increase the flow kickdown angle provided 3 to 4 degrees more downward exhaust flow direction onto the wing surface relative to the baseline, and showed promise for meeting the objective 60 degrees of flow turning during powered-lift approach operation.

- Recontouring the nozzle internal flowpath reduced nozzle flow coefficients moderately, relative to the baseline at both takeoff and cruise positions, with reductions generally ranging between 0.01 to about 0.03.

- Wing surface proximity showed only a moderate reduction in flow coefficient, with about 0.01 reduction observed at takeoff settings and up to 0.026 for cruise, as evidenced from flat plate wing configuration testing.

- Velocity coefficients for baseline and recontoured nozzles were shown to be in general agreement levelwise, with the data spread between configurations ranging up to 0.02.

- Velocity coefficients were not significantly affected by side door position or wing presence, except for the cruise nozzle positions, which showed increases relative to takeoff settings of about 0.04, on the average, with the simulated wing attached. These increases resulted from less wing scrubbing friction and from reduced non-axial flow thrust losses when the side doors were closed.

- The QCSEE reverser concept was found to have a low effective discharge area relative to the engine cycle takeoff requirement, with measured scale-model reverse-to-forward mode airflow ratios between 0.80 and 0.90, generally, and with the recommended configuration at 0.80. A study of QCSEE engine stability under these operating conditions indicated acceptable safety margins for demonstration testing, however.

- Increasing the blocker door axial spacing ratio was found to be an ineffective means of increasing the reverse-to-forward-mode airflow ratio over the range of increased spacing ratio investigated (0.823 to 1.017); airflow ratio improved by 0.075 while reverse thrust ratio decreased a comparable amount.

- The blocker door height ratio increase from 1.63 to 1.73 showed some small improvement in airflow ratio and reverse thrust with increases up to about 0.02 observed for both.

- Rotating the blocker door forward to increase the blocker inclination angle from 95° to 105° significantly affected reverse thrust ratio (increased by about 0.08) and airflow ratio (decreased approximately 0.05). Further rotation to 115° inclination angle showed little additional change in reverser performance.

- Extended and tabbed side skirts, rotated outward 45°, produced significant improvement in reverse thrust ratio (0.1 to 0.12 increase) relative to the nominal skirt baseline case, with outward rotation of the side skirt contributing about half the amount. Correspondingly, only a little change in airflow ratio was observed from side skirt extension and tabbing.

- Increased lip length ratio was found to have a strong favorable effect on reverse thrust ratio with the greatest improvement (better than 0.10) in the lip length range between 0.2 and 0.4. Reverse-to-forward-mode airflow ratio was essentially insensitive to lip length ratio variations.

- Decreasing the lip angle produced only moderate improvement in reverse thrust ratio, with the greatest change (0.04) between 25° and 35°. Decreasing lip angle from 25° to 15° showed little additional reverse thrust improvement. In the range investigated, lip angle variation did not significantly influence airflow ratio.

SECTION 8.0

NOMENCLATURE

A_8	-	Nozzle discharge area
A_{eff}	-	Nozzle effective flow area
A_{15}	-	Calibration nozzle upstream area
C_d	-	Nozzle flow coefficient = W_8/W_i
C_V	-	Nozzle velocity coefficient = $F_{resultant}/F_i$
D	-	Diameter
D_{TH}	-	Reverser reference dimension (13.97 cm)
F_i	-	Ideal thrust based on P_T/P_0 and W_8
$F_{resultant}$, F_{FWD}	-	Resultant nozzle thrust = $\sqrt{H_V^2 + H_X^2}$
F_{REV}	-	Reverse thrust
H_B	-	Blocker door height, reverser
H_V	-	Normal scale force
H_X	-	Axial scale force
K_{PT}	-	Nozzle total pressure correction factor
L	-	Lip length, reverser
N_F	-	Fan speed
P_0	-	Ambient pressure, bellmouth total pressure
P_2	-	Static pressure, bellmouth wall
P_{TM}	-	Measured nozzle total pressure
P_T	-	Adjusted nozzle total pressure = $K_{PT}P_{TM}$
R	-	Radius
T_0	-	Ambient temperature, bellmouth total temperature
W_2	-	Bellmouth airflow
W_T	-	Simulator drive airflow
W_8, W_{REV}, W_{FWD}	-	Nozzle and reverser total airflow
W_i	-	Ideal airflow, based on P_T/P_0 and A_8
X_F	-	Blocker door spacing dimension
X_P	-	Blocker door pivot spacing dimension
ΔC_d	-	Change in flow coefficient
ΔC_V	-	Change in velocity coefficient

NOMENCLATURE (Concluded)

ΔP_T	-	Adjustment to measured nozzle total pressure
P_T/P_0	-	Nozzle pressure ratio
F_{REV}/F_{FWD}	-	Reverser effectivity, reverse thrust ratio
$\Delta F_{REV}/F_{FWD}$	-	Change in reverser effectivity
W_{REV}/W_{FWD}	-	Reverse thrust airflow ratio
$\Delta W_{REV}/W_{FWD}$	-	Change in reverse thrust airflow ratio
α	-	Blocker door inclination angle
β	-	Reverser lip angle
β_E	-	Effective exhaust flow angle (reverser) = $\tan^{-1}(H_V/H_X)$
θ	-	Calibration nozzle cone half angle
θ_j	-	Exhaust flow angle (nozzle) = $\tan^{-1}(H_V/H_X)$
ϕ	-	Reverser side skirt rotation angle
Θ_E	-	Angle between engine axis and wing chord

APPENDIX A

PRELIMINARY STATIC TURNING PERFORMANCE DATA AND TEST METHODOLOGY

NASA LANGLEY TEST METHODOLOGY
OTW EXHAUST SYSTEM STATIC TURNING AND
TURNING EFFICIENCY DETERMINATION

1. DETERMINE BARE NOZZLE KICKDOWN ANGLE

TEST CONFIGURATION

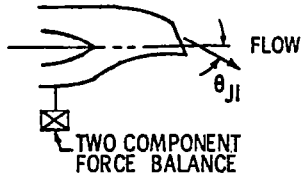

FORCE DIAGRAM

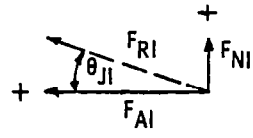

F_{NI} = MEASURED NORMAL FORCE

F_{AI} = MEASURED AXIAL FORCE

F_{RI} = CALCULATED RESULTANT GROSS THRUST = $\sqrt{F_{NI}^2 + F_{AI}^2}$

θ_{J1} = CALCULATED KICKDOWN ANGLE = $TAN^{-1}\ F_{NI}/F_{AI}$

2. DETERMINE INSTALLED NOZZLE PERFORMANCE (WITH FLAT PLATE WING)

TEST CONFIGURATION

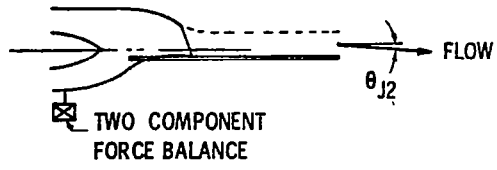

FORCE DIAGRAM AT
PLATE TRAILING EDGE

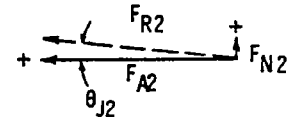

- FLAT PLATE SIMULATES CRUISE WING SCRUBBING DRAG
- PROVIDES CORRECT NOZZLE BACKPRESSURE FLOW FIELD

F_{A2} = MEASURED AXIAL FORCE

F_{N2} = MEASURED NORMAL FORCE (IDEALLY ZERO WITH PERFECT PLATE ALIGNMENT)

F_{R2} = CALCULATED INSTALLED GROSS THRUST = $\sqrt{F_{N2}^2 + F_{A2}^2} = T$

θ_{J2} = CALCULATED FLOW ANGLE = $TAN^{-1}\ F_{N2}/F_{A2}$ (~1° FOR TESTS)

NASA LANGLEY TEST METHODOLOGY (CONT'd)

3. DETERMINE ENGINE / WING FLAP SYSTEM LIFT AND DRAG CHARACTERISTICS

TEST CONFIGURATION

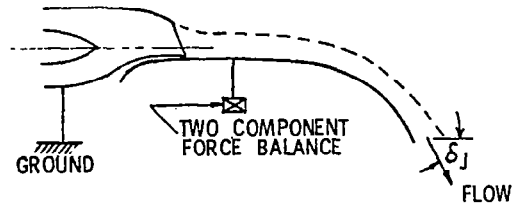

- NOZZLE DECOUPLED FROM WING
- NOZZLE BACKPRESSURED BY WING PRESENCE
- WING FLAP IN POWERED LIFT MODE

BALANCE FORCE DIAGRAM

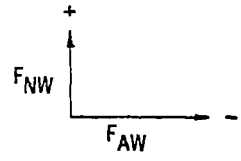

CONTRIBUTING WING SURFACE FORCES

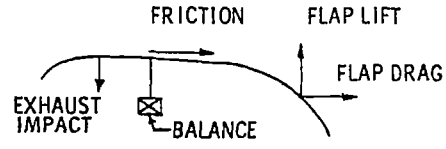

FOR THE REAL INSTALLED CASE WHERE ENGINE AND WING ARE COUPLED, THE EXHAUST IMPACT FORCE IS CANCELLED BY THE NOZZLE KICKDOWN FORCE:

WHERE KICKDOWN FORCE = F_{R2} SIN θ_{JI} (COMBINATION OF STEPS 1 & 2)

AND NET AXIAL FORCE IS THE SUM OF THE NOZZLE FLAT PLATE AXIAL FORCE (STEP 2) AND THE WING DRAG FORCE (STEP 3)

- ENGINE/WING SYSTEM LIFT = $F_{N3} = F_{NW} + F_{R2}$ SIN θ_{JI}
- ENGINE/WING SYSTEM AXIAL FORCE = $F_{A3} = F_{R2}$ COS $\theta_{JI} + F_{AW}$

NASA LANGLEY TEST METHODOLOGY - CONT'D

4. COMPUTATION OF STATIC TURNING ANGLE AND TURNING EFFICIENCY

FROM PROPULSION / LIFT SYSTEM NET FORCE ELEMENTS (STEP 3)

SYSTEM LIFT = $F_{N3} = F_N$

SYSTEM AXIAL FORCE (NET THRUST) = $F_{A3} = F_A$

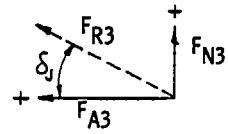

JET FLOW ANGLE (TURNING ANGLE) AT FLAP TRAILING EDGE

$$\delta_J = \text{TAN}^{-1} \; F_{N3}/F_{A3}$$

ENGINE / WING SYSTEM RESULTANT FORCE AT FLAP TRAILING EDGE

$$F_{R3} = \sqrt{F_{N3}^2 + F_{A3}^2}$$

SYSTEM STATIC TURNING EFFICIENCY

$$\eta = \frac{F_{R3}}{F_{R2}}$$

PLOTTED PARAMETERS

$$\frac{F_N}{T} \; ; \; \frac{-F_A}{T}$$

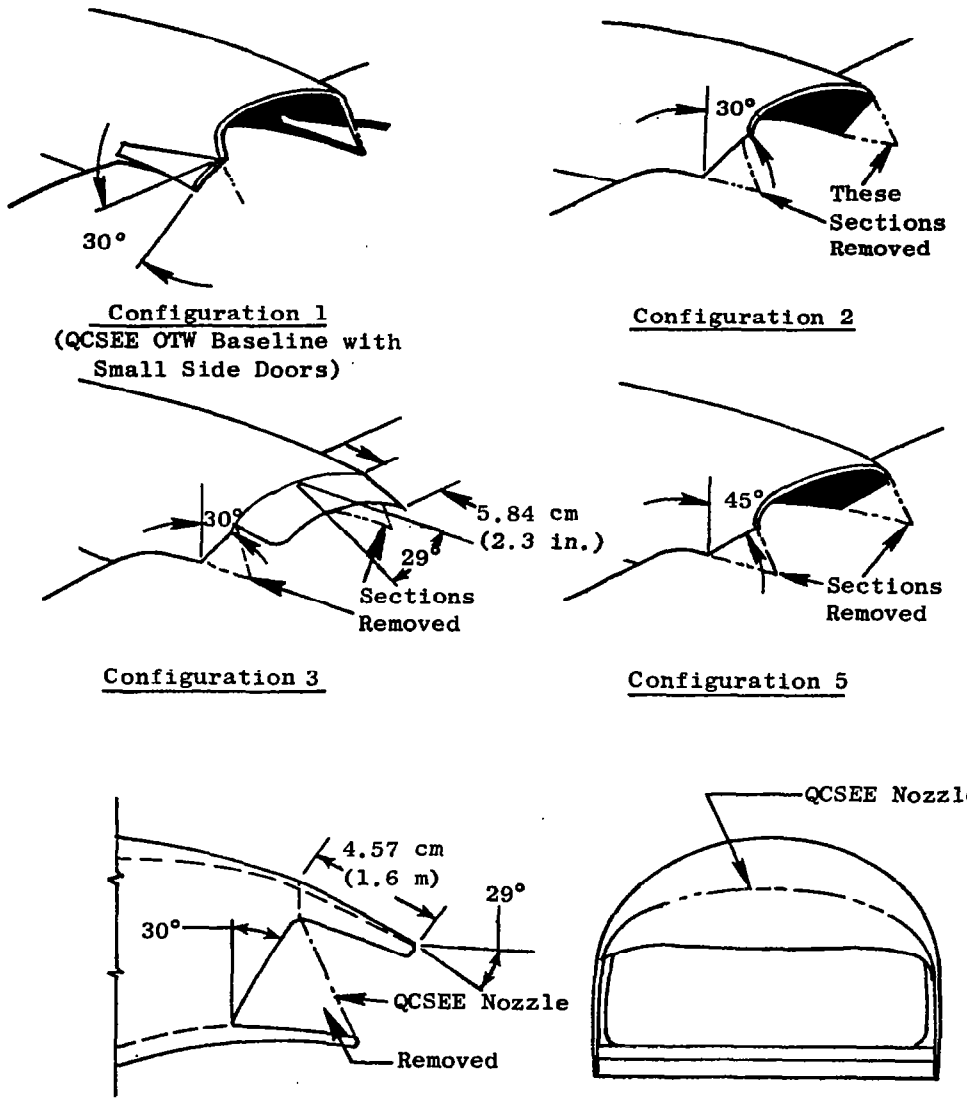

Figure 49. Preliminary Exploratory Test Configurations for Static Turning Performance.

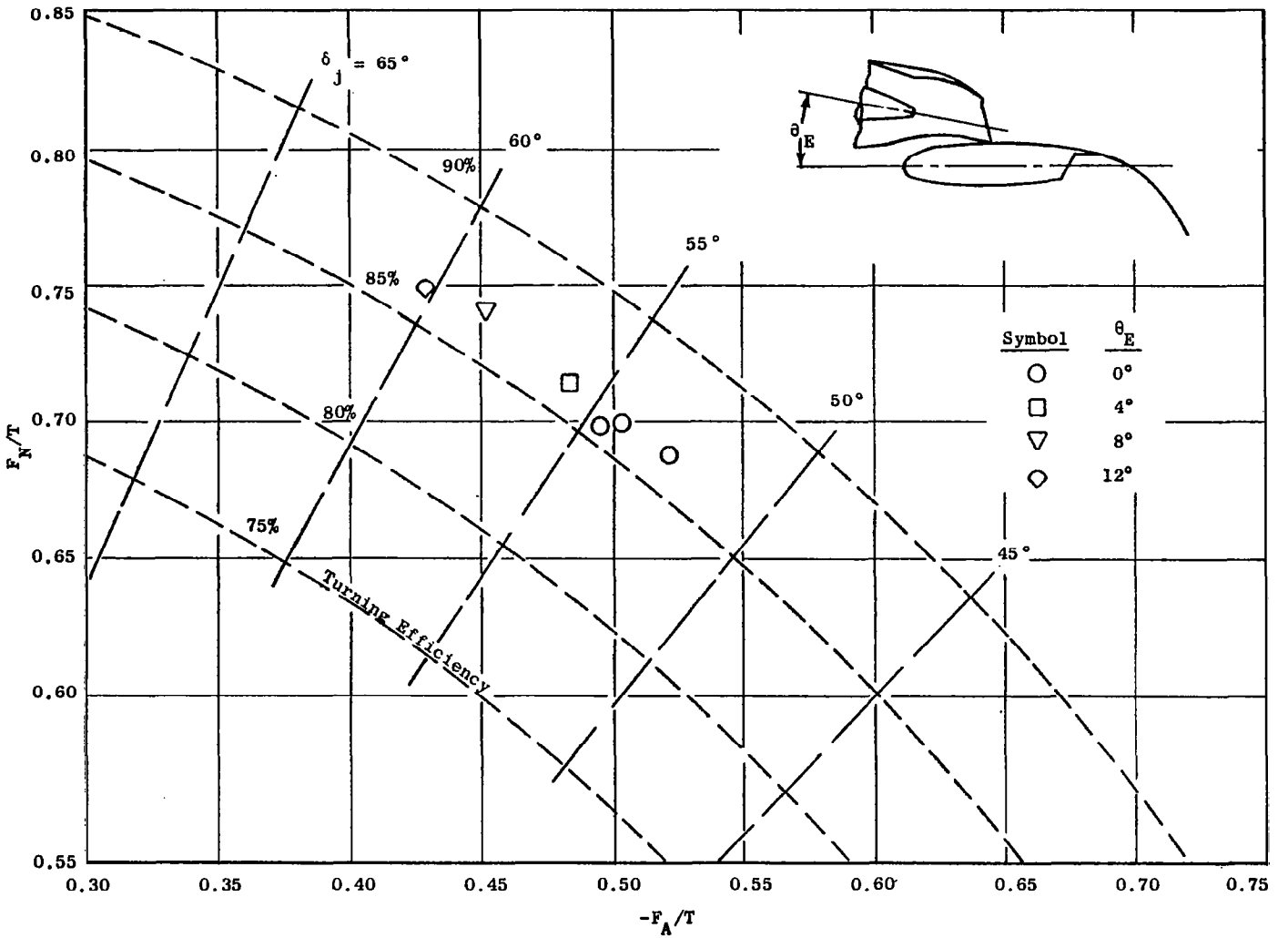

Figure 50. Preliminary Static Turning Performance, Configuration 1, QCSEE OTW Baseline Nozzle.

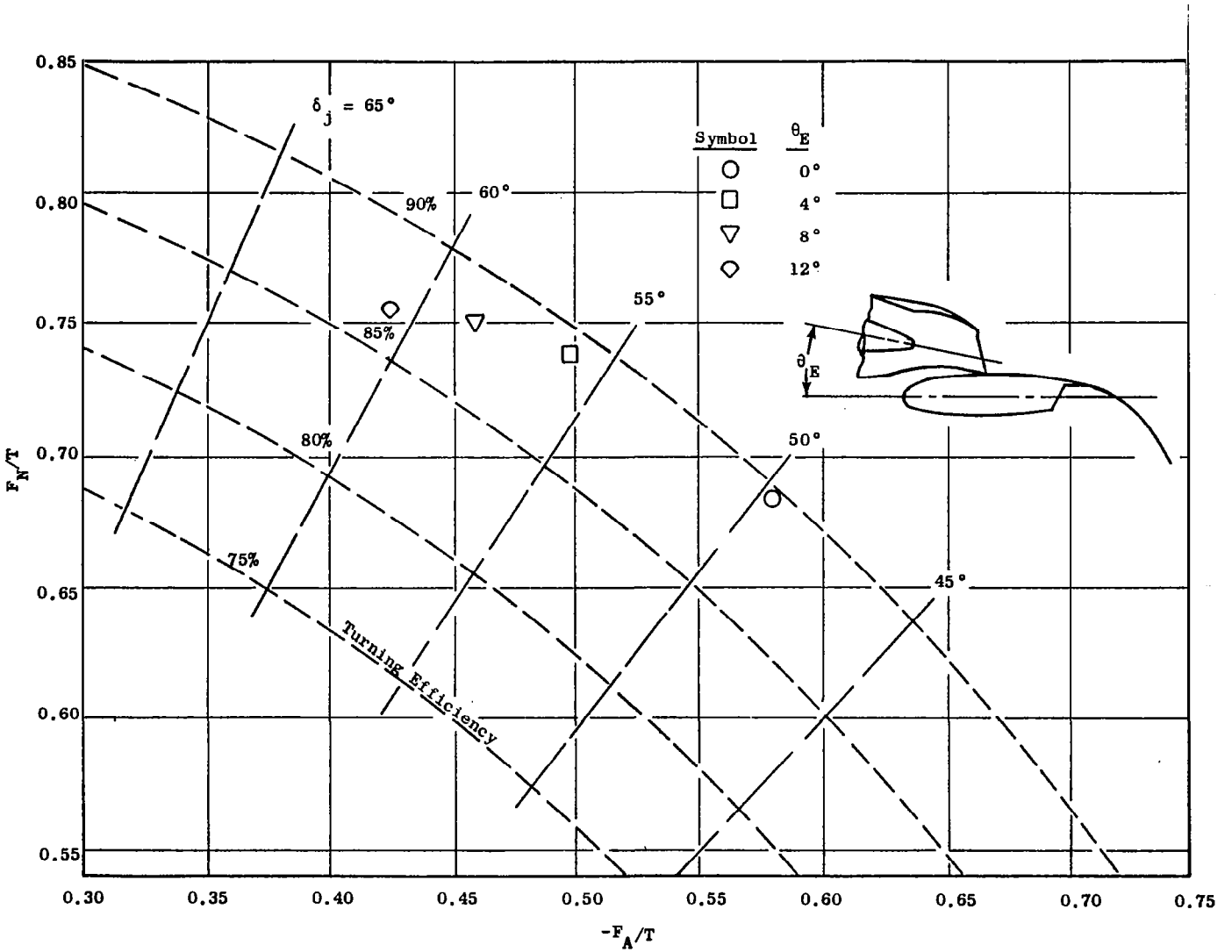

Figure 51. Preliminary Static Turning Performance, Configuration 2.

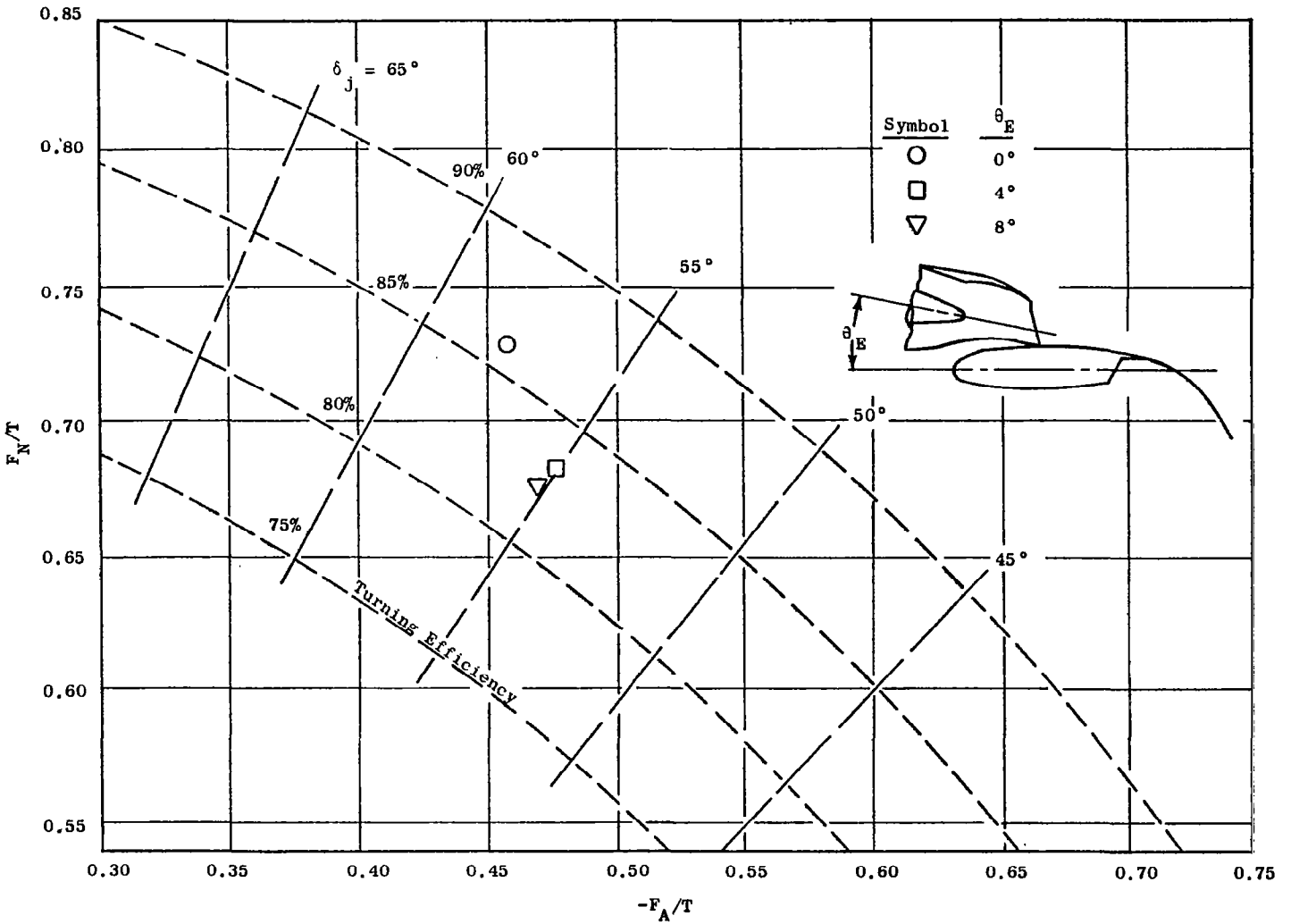

Figure 52. Preliminary Static Turning Performance, Configuration 3.

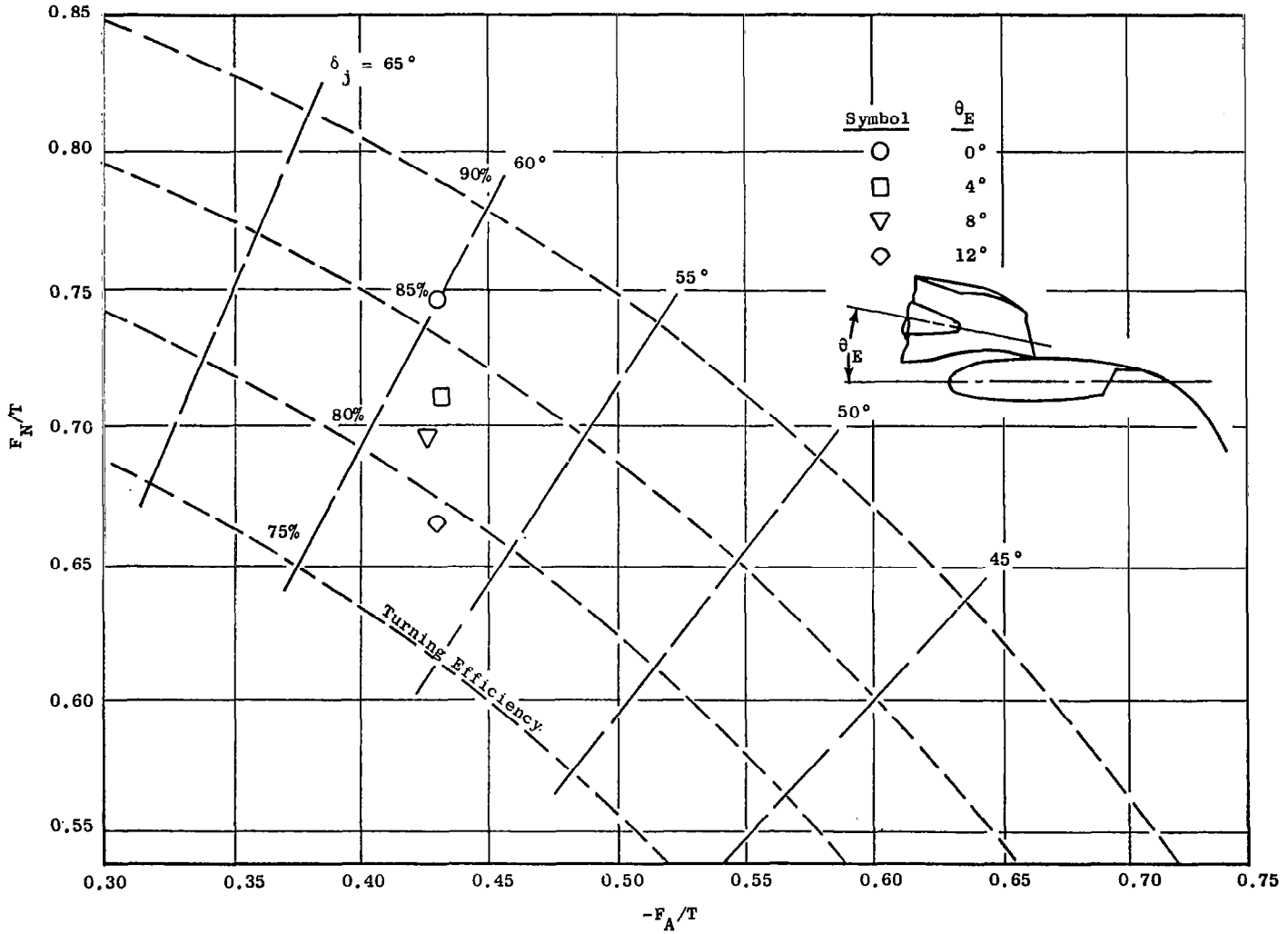

Figure 53. Preliminary Static Turning Performance, Configuration 4.

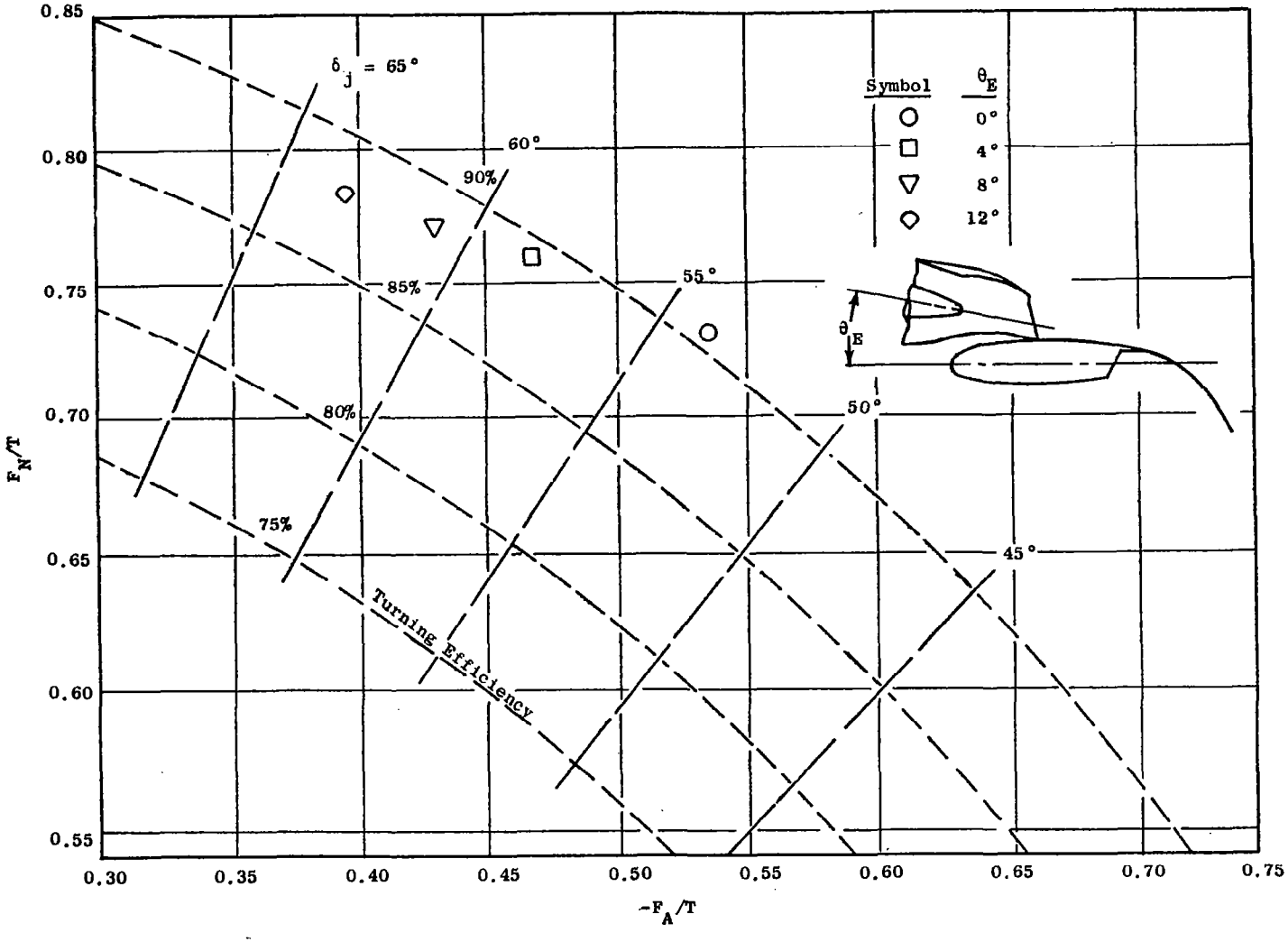

Figure 54. Preliminary Static Turning Performance, Configuration 5.

Symbol	Nozzle	Side Doors
◇	Baseline	Large, 25°
△		Small, 60°
●	RC-1	Large, 25°
		Small, 60°

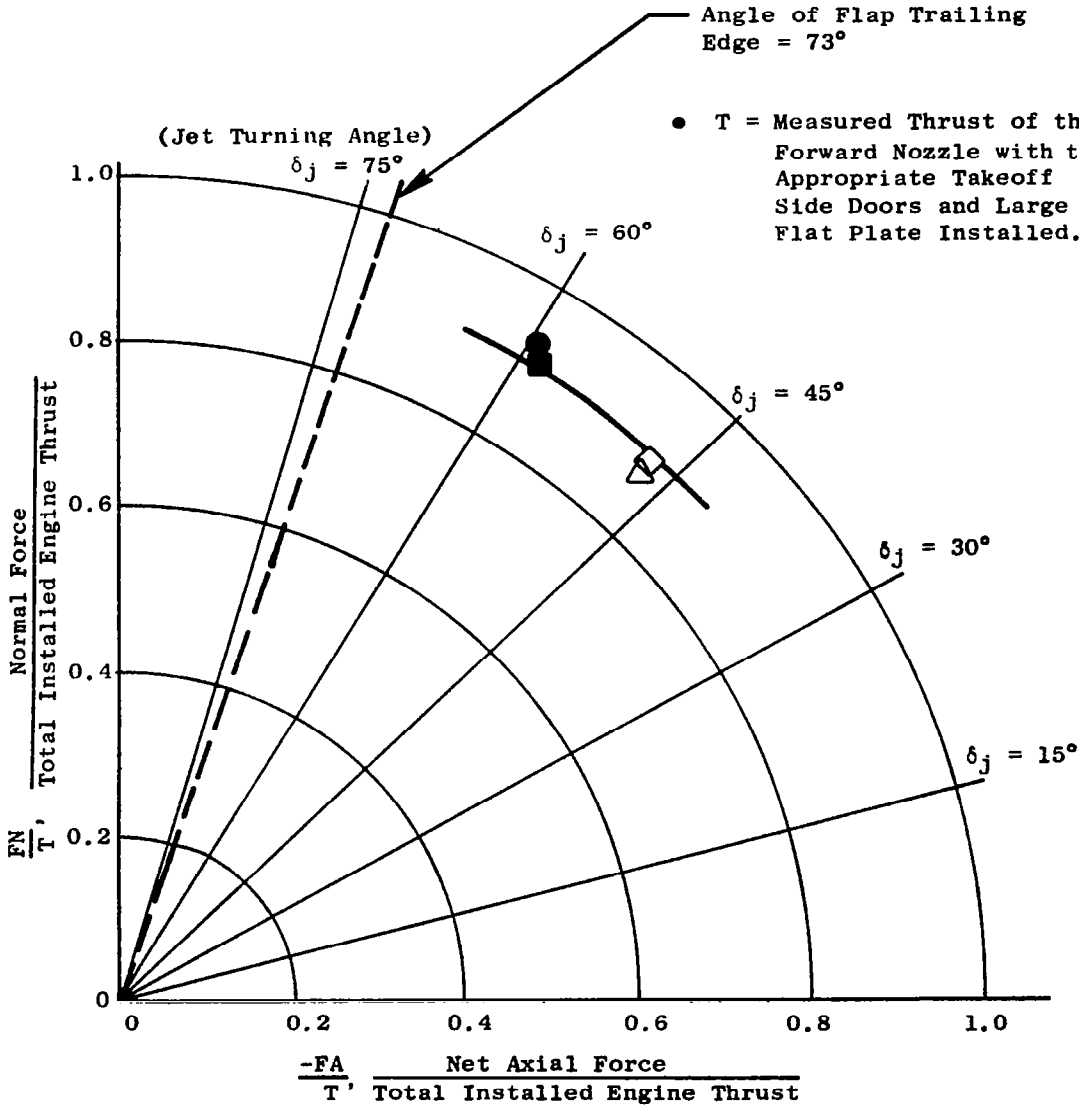

Figure 55. Preliminary Static Turning Performance, Baseline and Recontoured Nozzle, RC-1.

APPENDIX B

DATA REDUCTION SUMMARY

APPENDIX B

DATA REDUCTION SUMMARY

Inlet Parameter

P_0	-	Ambient pressure, inlet total pressure,	N/m^2 (lbf/in.^{2})
T_0	-	Ambient temperature, inlet total temperature,	K (° R)
P_2	-	Bellmouth wall static pressure,	N/m^2 (lbf/in.^{2})
M_2	-	Bellmouth Mach number	
W_2	-	Mass flow, bellmouth,	kg/sec (lbm/sec)
$\frac{W_2\sqrt{\theta}}{\delta}$	-	Mass flow, corrected to standard day conditions,	kg/sec (lbm/sec)

Simulator Parameters

N	-	Simulator fan speed,	rpm
$N/\sqrt{\theta}$	-	Fan speed corrected to standard day temperature,	rpm
ΔW	-	Simulator turbine drive mass flow,	kg/sec (lbm/sec)
T_W	-	Temperature at drive air flow meter,	K (° R)
P_W	-	Pressure at drive air flow meter,	N/m^2 (lbf/in.^{2})

Nozzle and Reverser Parameters

P_T, P_{TM}	-	Nozzle total pressure,	N/m^2 (lbf/in.^{2})
$P_T/P_0, P_{TM}/P_0$	-	Nozzle pressure ratio	
T_T	-	Nozzle total temperature (assumed T_0),	K (° R)
H_X	-	Balance force, axial component,	N (lbf)
H_V	-	Balance force, normal component,	N (lbf)
H_R	-	Resultant force, $\sqrt{H_X^2 + H_V^2}$,	N (lbf)
W_8, W_{REV}, W_{FWD}	-	Total mass flow, $W_2 + \Delta W$,	kg/sec (lbm/sec)
W_i	-	Ideal nozzle mass flow based on P_T/P_0,	kg/sec (lbm/sec)

DATA REDUCTION SUMMARY (Concluded)

F_i	-	Ideal thrust based on W_8 and P_T/P_0,	N (lbf)
C_d	-	Nozzle flow coefficient	
V_i	-	Nozzle ideal velocity based on P_T/P_0,	m/sec (ft/sec)
C_V	-	Nozzle resultant velocity coefficient, H_R/F_i	
A_{e8}	-	Nozzle effective flow area,	m^2 ($in.^2$)
θ_j	-	Nozzle flow angle,	degrees
β_E	-	Reverse effective efflux angle,	degrees
W_{REV}/W_{FWD}	-	Airflow ratio	
F_{REV}/F_{FWD}	-	Reverser effectivity, or reverse thrust ratio,	H_{XREV}/H_{RFWD}

Inlet Flow Calculations

- $W_2 = g\sqrt{\frac{\gamma}{RT_0}}\ C_2\ A_2\ P_0\ M_2\ (1 + \frac{\gamma - 1}{2}\ M_2^2)^{-3}$

  where: g is gravitational constant, 9.8066 m/sec^2 (32.174 ft/sec^2)

  γ = 1.4

  R = gas constant, 287.04 $m^2/sec/sec/K$ (1716.322 $ft^2/sec/sec/^\circ R$)

  C_2 = bellmouth flow coefficient, (0.987, based on analysis of boundary layer)

  A_2 = bellmouth area, 0.0153 m^2 (23.758 $in.^2$)

  P_0 = ambient pressure, N/m^2 ($lbf/in.^2$)

  and M_2 = bellmouth Mach number

  $$M_2 = \sqrt{\frac{2}{\gamma - 1}\left[(P_0/P_2)^{\frac{\gamma - 1}{\gamma}} - 1\right]}$$

  and P_2 = bellmouth average static pressure (from four measurements)

- $(W_2)_{corr} = W_2\sqrt{\theta_2}/\delta_2$

  where: $\theta_2 = T_0/288.2$ K, and 288.2 K is standard day temperature

  and: $\delta_2 = P_0/101.325\ kN/m^2$, and 101.325 kN/m^2 is standard atmospheric pressure

Simulator Calculations

- $(N)_{corr} = N/\sqrt{\theta_2}$

  where N is fan rotational speed, electrical pickup

  $\theta_2 = T_0/288.2$ K

- $\Delta W = f(T_W, P_W)$ and rotating vane-type flowmeter electrical signal

Nozzle Performance Calculations

- $H_R = \sqrt{H_X^2 + H_V^2}$

- $\theta_j = \tan^{-1} |H_V/H_X|$
- $W_8 = W_2 + \Delta W$
- $P_T/P_0 = K_{PT}(P_{TM}/P_0)$

  where: P_{TM}/P_0 is the manifolded rake nozzle total-pressure ratio

  K_{PT} is a total-pressure ratio bias correction factor used to adjust measured total pressure from an equal area average value to a mass-weighted average. This factor was established from comparison of round calibration nozzle data with NACA data reported in Report 933.

- $F_i = \frac{W_8}{g} V_i$

  where: $V_i = M_i \sqrt{\gamma R T_T}$

  and: $M_i = \sqrt{\frac{2}{\gamma-1}\left[(P_T/P_0)^{\frac{\gamma-1}{\gamma}} - 1\right]}$

  and: T_T is assumed equal to T_0

- $A_{e8} = \frac{W_8\sqrt{T_T}(A/A^*)}{P_T K}$

  where: K is the choked flow ($M_i = 1.0$) value

  for the flow function $\frac{W\sqrt{T_T}}{P_{TA}} = M_i \frac{g\sqrt{\gamma/R}}{\left(1 + \frac{\gamma-1}{2} M_i^2\right)^{\frac{\gamma+1}{2(\gamma-1)}}}$

  and: $A/A^* = M_i \left[\frac{1 + \frac{\gamma-1}{2}}{1 + \frac{\gamma-1}{2} M_i^2}\right]^{\frac{\gamma+1}{2(\gamma-1)}}$

- $W_i = g\sqrt{\frac{\gamma}{RT_T}} A_8 P_0 M_i \left(1 + \frac{\gamma-1}{2} M_i^2\right)^{-3}$

where: A_8 is the nozzle physical exit area consistent with the nozzle being tested

Round Nozzles	Nozzle Physical Exit Area, A_8
R_1	0.01503 m^2 (23.3 $in.^2$)
R_2	0.01348 m^2 (20.9 $in.^2$)
R_3	0.01193 m^2 (18.5 $in.^2$)
R_4	0.01032 m^2 (16.0 $in.^2$)
QCSEE Nozzles	0.01097 m^2 (17.0 $in.^2$)

(cruise position referenced)

and M_i is calculated as in F_i

- $C_V = H_R/F_i$
- $C_d = W_8/W_i$, or A_{e8}/A_8

Reverser Performance Calculation

- $W_8 = W_{REV} = [W_2 + \Delta W]_{REV}$

  Calculated in the same way shown under nozzle performance calculations.

- $P_T/P_0 = K_{PT}(P_{TM}/P_0)$
- $\beta_E = \tan^{-1}(H_V/H_X)$
- $$W_{REV}/W_{FWD} = \left[\frac{W_8\sqrt{\theta_2}}{\delta_2}\right]_{REV} \div \left[\frac{W_8\sqrt{\theta_2}}{\delta_2}\right]_{FWD}$$
$$= \left(\frac{W_{REV}}{W_{FWD}}\right)\sqrt{\frac{T_{O_{REV}}}{T_{O_{FWD}}}}\left(\frac{P_{O_{FWD}}}{P_{O_{REV}}}\right)$$

where: W_{FWD} is determined from a curve fit of the reference forward thrust test results evaluated at corresponding reverser test pressure ratios. The quation for W_{FWD} is given as:

$$W_{FWD} = -64.9239 + 145.8658\ (P_T/P_0)$$
$$-108.2791\ (P_T/P_0)^2 + 28.0100\ (P_T/P_0)^3$$

with units for flow expressed in kg/sec.

This method accounts for differences in ambient temperature and pressure between forward and reverse thrust tests by correcting both sets of data to sea level standard conditions.

- $$F_{REV}/F_{FWD} = \left(\frac{H_X}{P_0/\delta_2}\right)_{REV} \div \left(\frac{H_R}{\delta_2}\right)_{FWD} = \left(\frac{H_X}{H_R}\right)\left(\frac{P_{0_{FWD}}}{P_{0_{REV}}}\right)$$

where: H_R is the resultant forward thrust reference value determined from a curve fit of forward thrust test data evaluated at corresponding reverse test pressure ratios. The equation for H_R is given by:

$$H_R = -2326.1662 + 2310.9103\ (P_T/P_0)$$

with units for H_R in newtons.

APPENDIX C

FORWARD THRUST TEST RESULTS

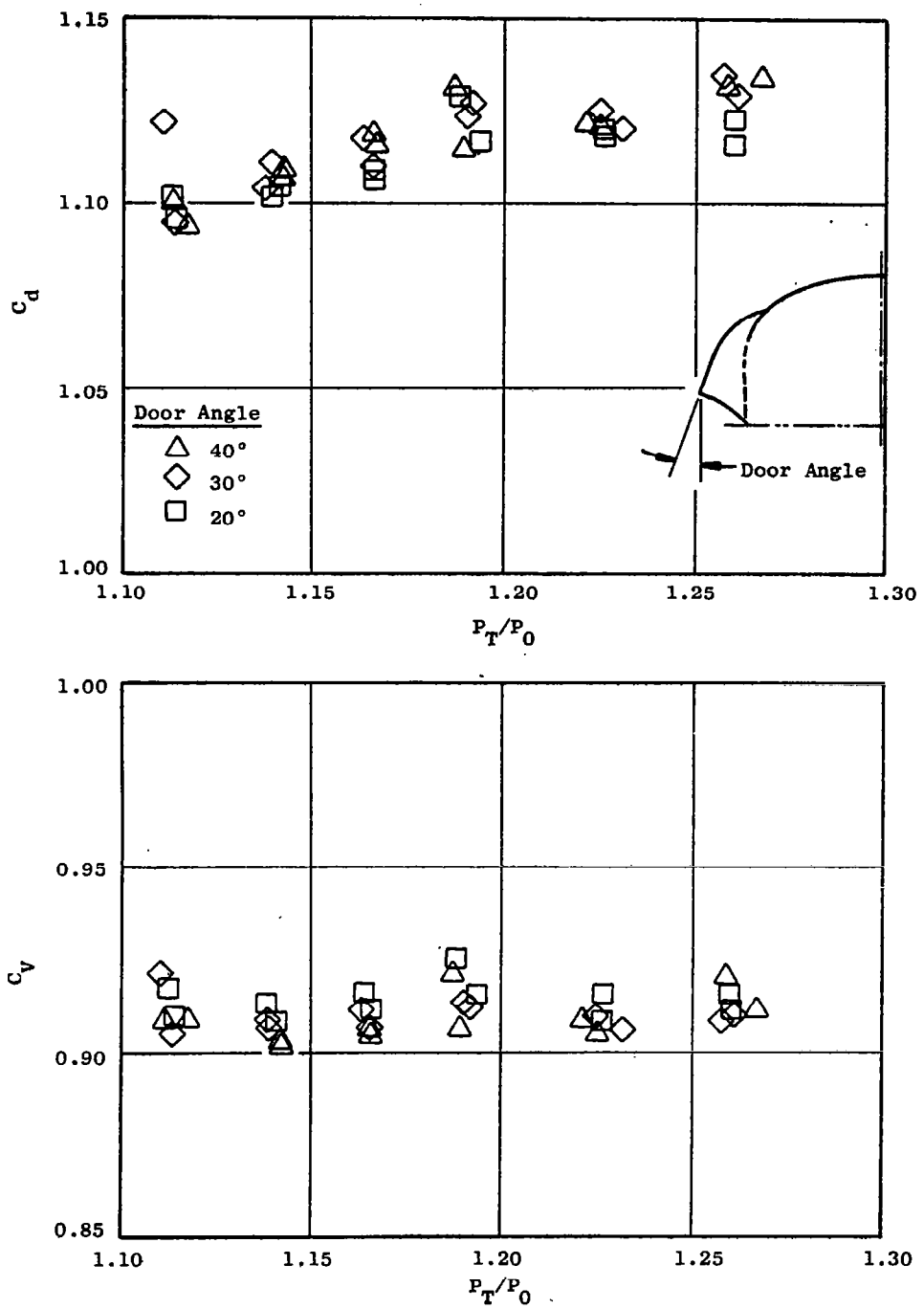

Figure 56. Effect of Nozzle Side Door Angle on Performance, QCSEE Baseline Configuration, Large Plate On.

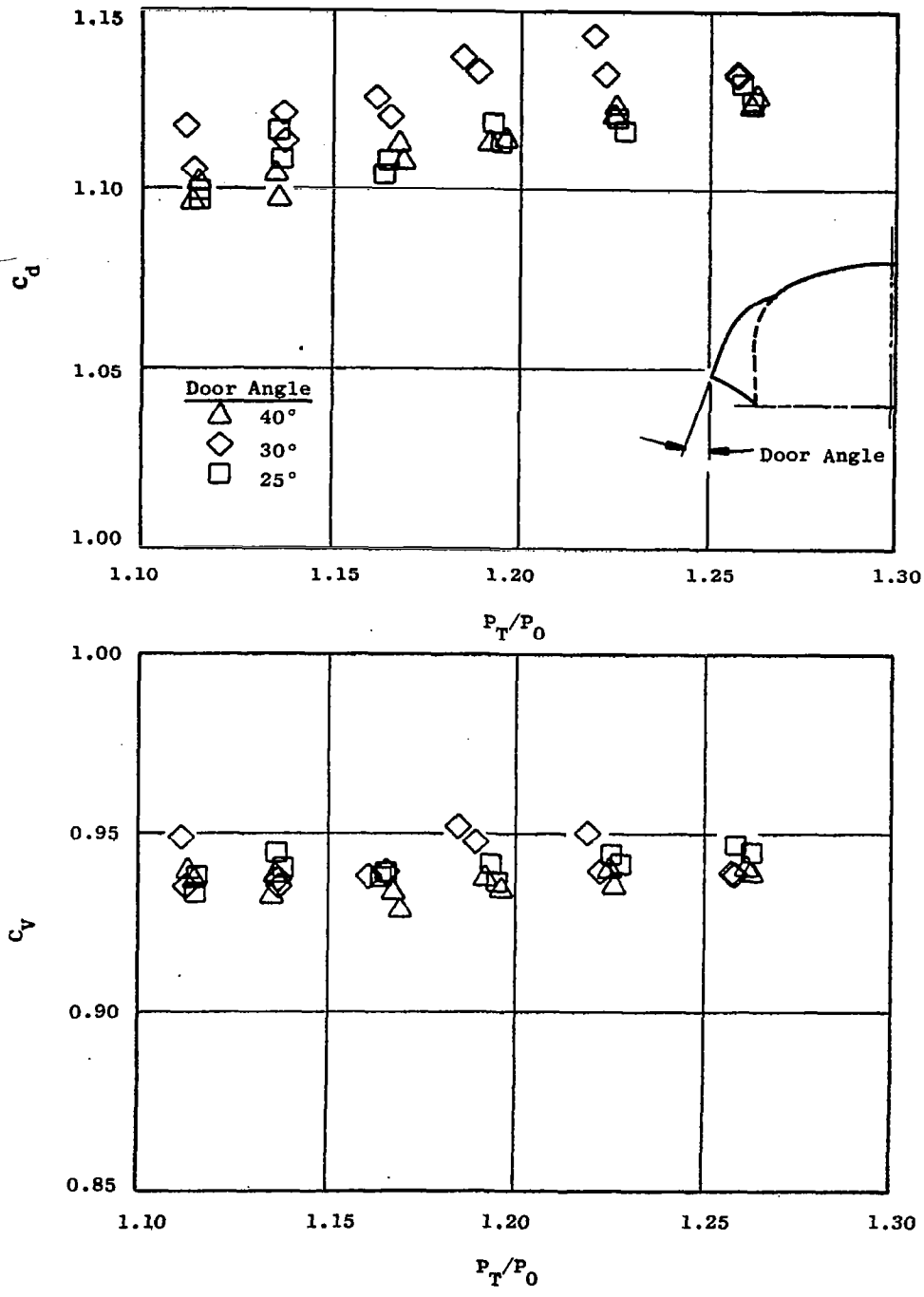

Figure 57. Effect of Nozzle Side Door Angle on Performance, QCSEE Baseline Configuration, Small Plate On.

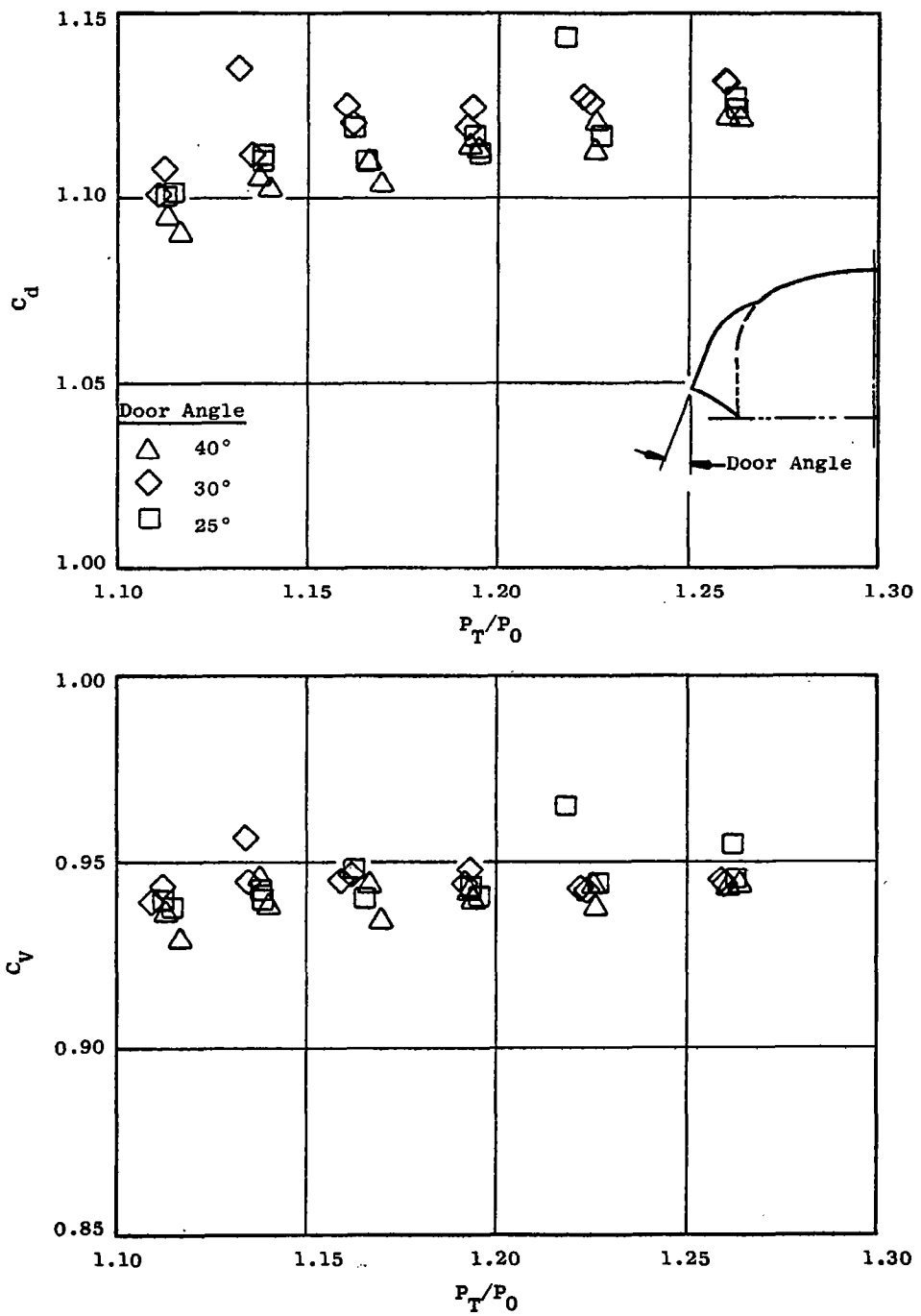

Figure 58. Effect of Nozzle Side Door Angle on Performance, QCSEE Baseline Configuration, Plate Off.

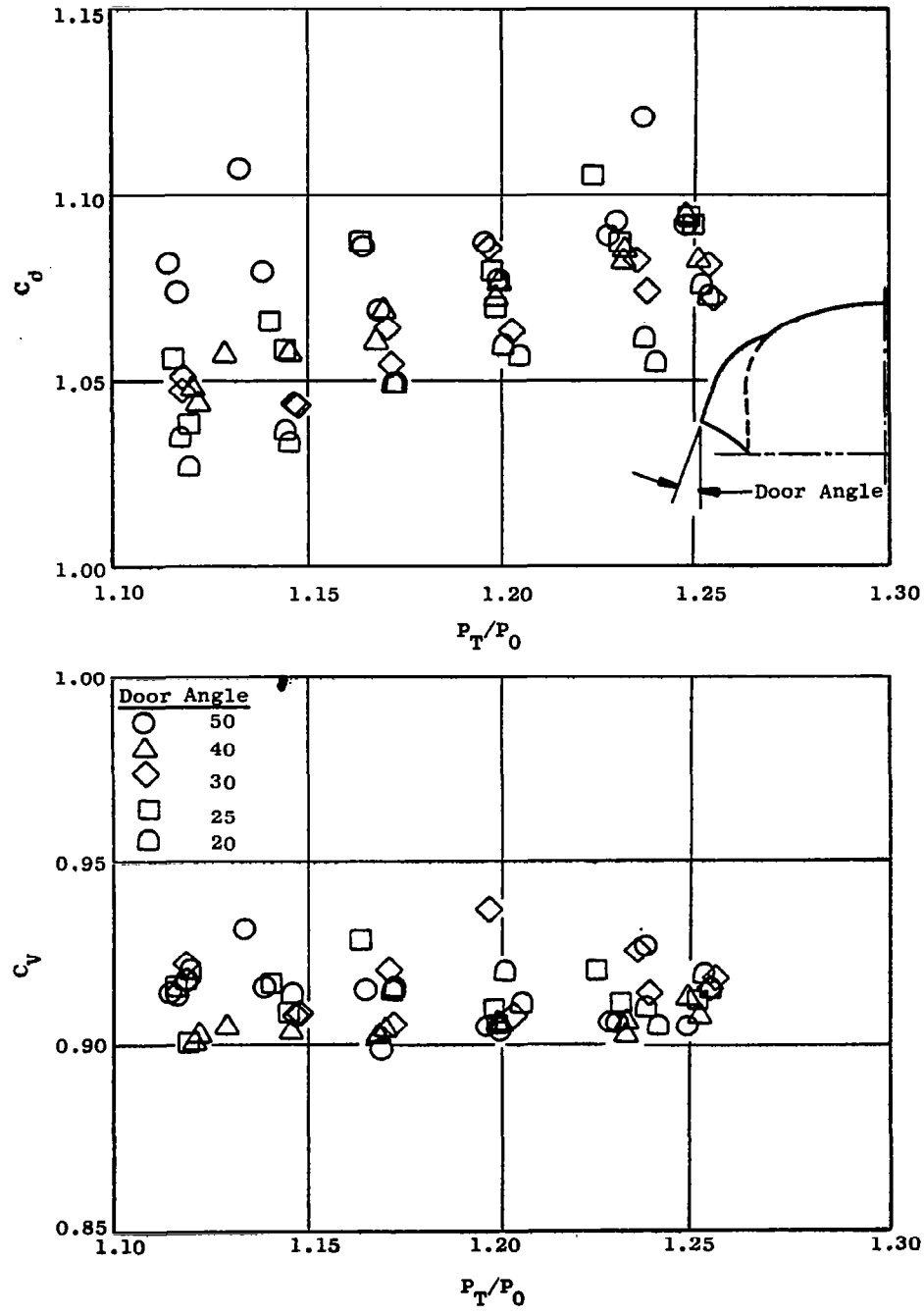

Figure 59. Effect of Nozzle Side Door Angle on Performance, RC-1 Configuration, Large Plate On.

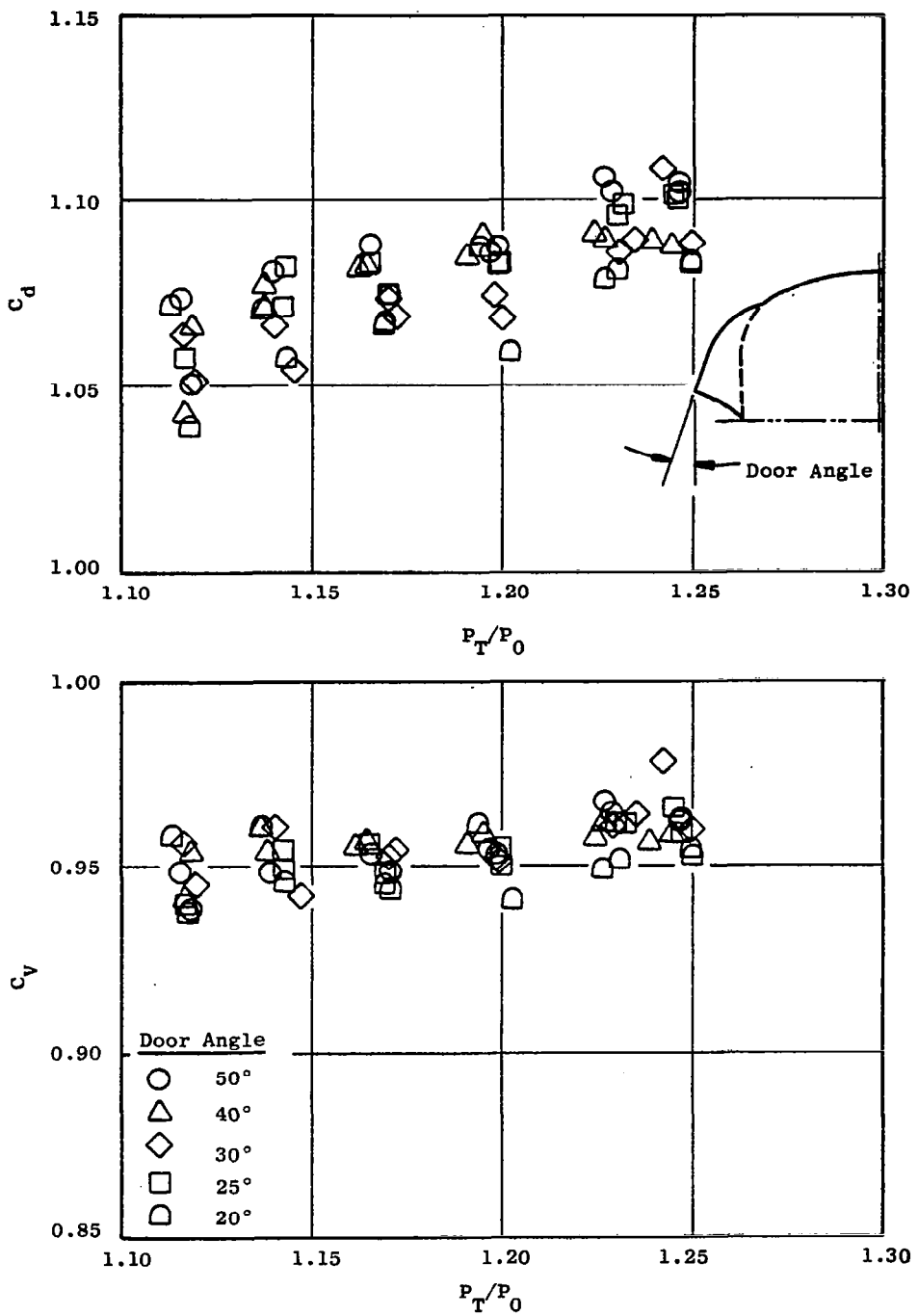

Figure 60. Effect of Nozzle Side Door Angle on Performance, RC-1 Configuration, Small Plate On.

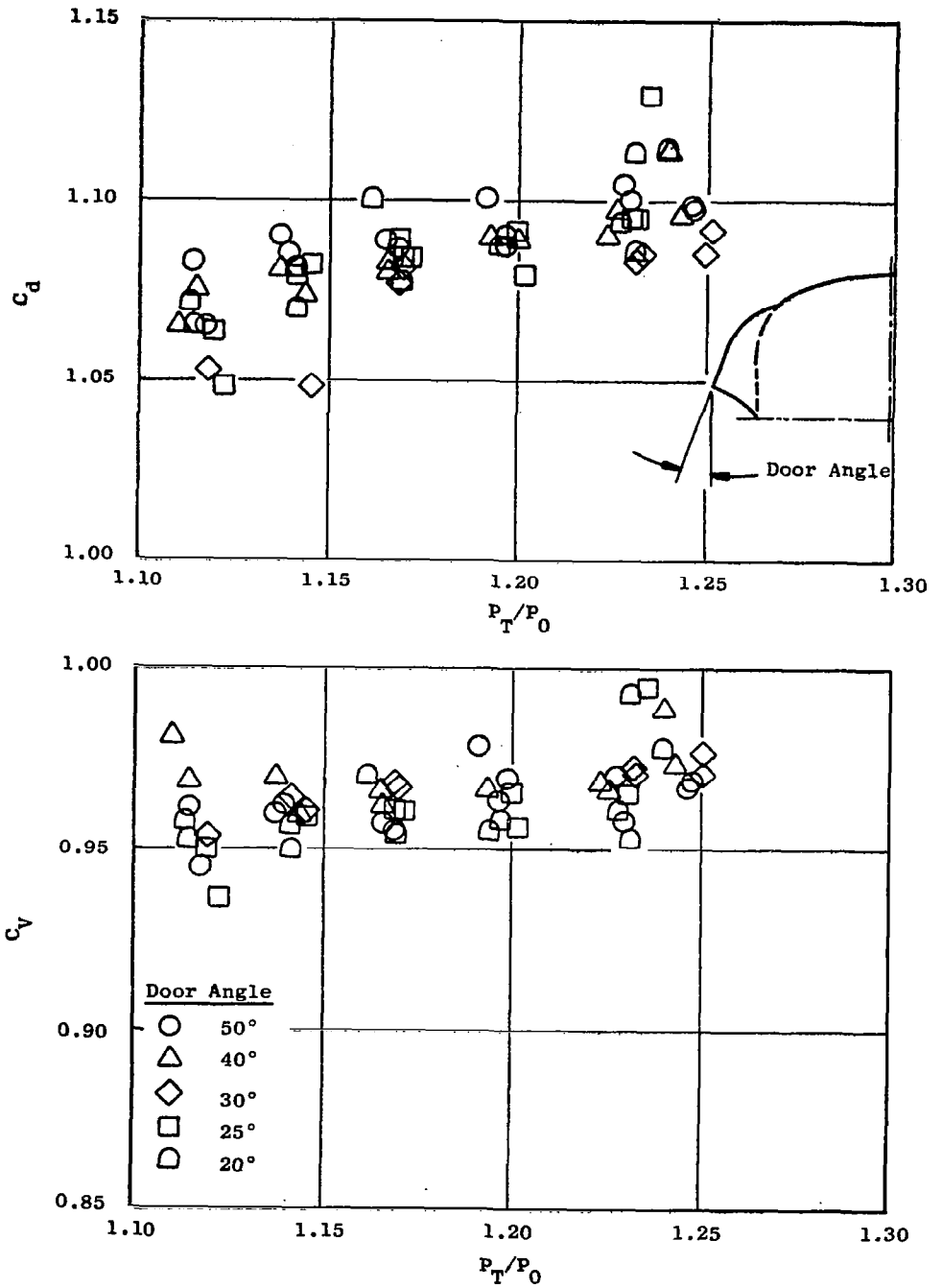

Figure 61. Effect of Nozzle Side Door Angle on Performance, RC-1 Configuration, Plate Off.

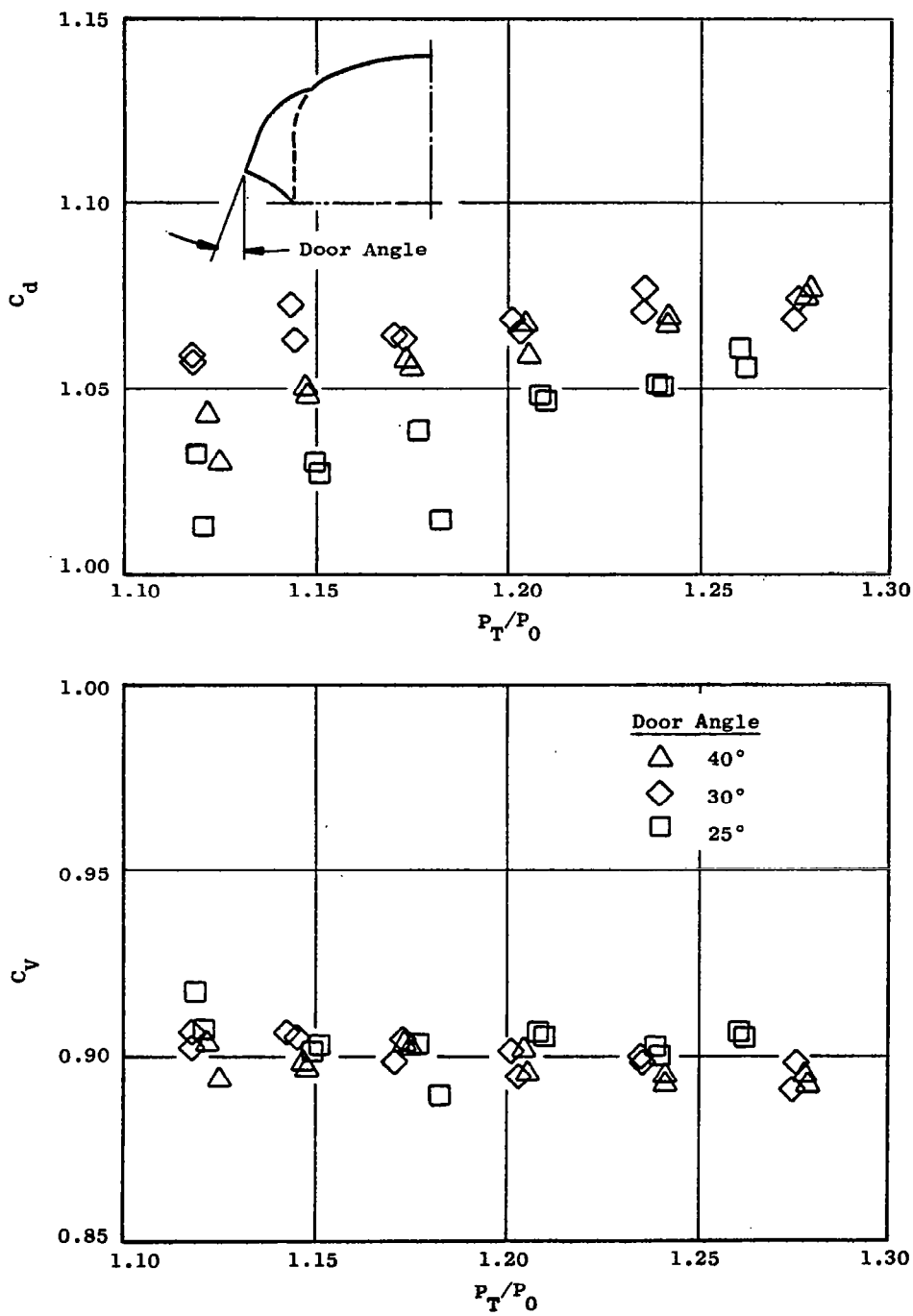

Figure 62. Effect of Nozzle Side Door Angle on Performance, RC-2 Configuration, Large Plate On.

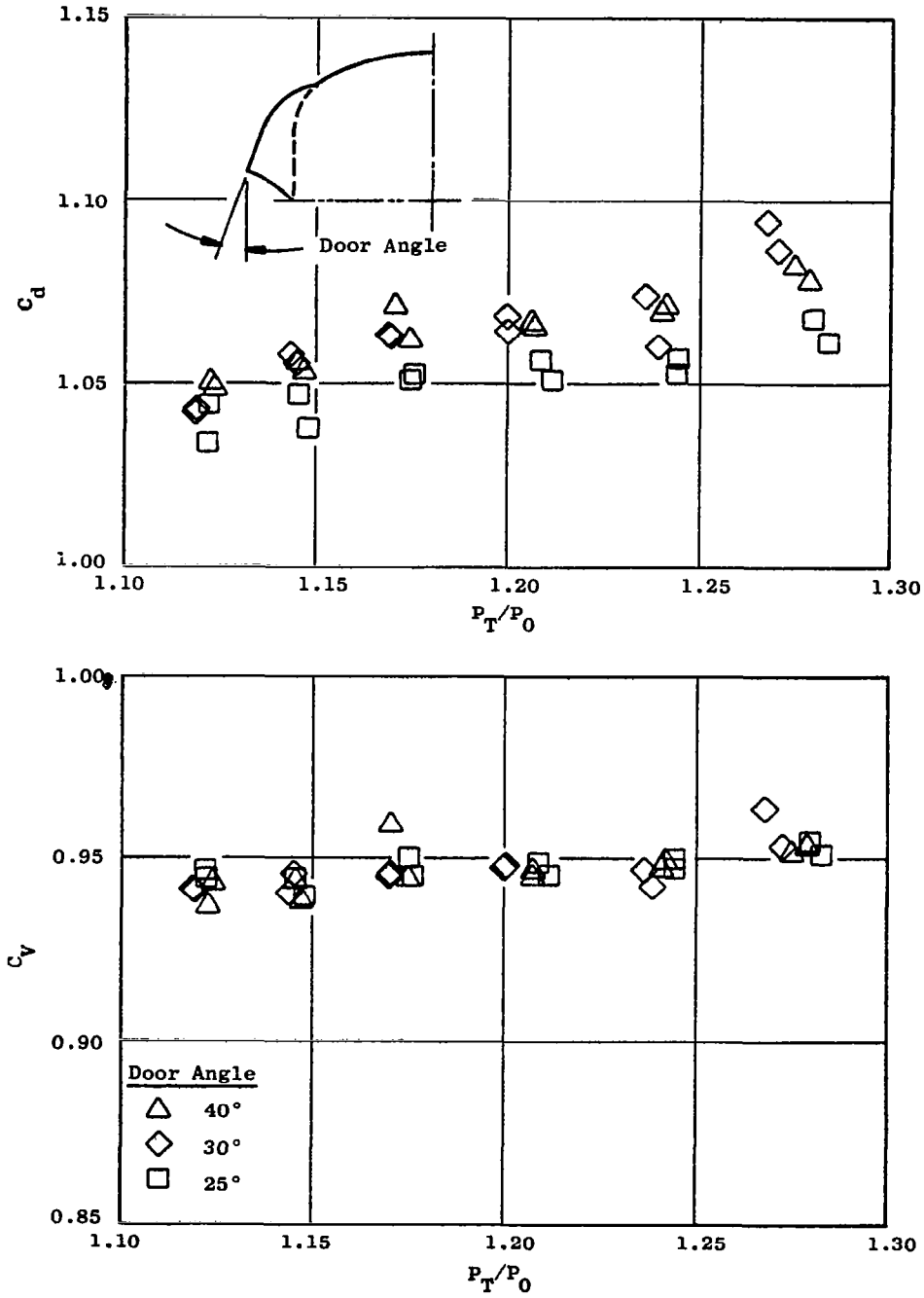

Figure 63. Effect of Nozzle Side Door Angle on Performance, RC-2 Configuration, Small Plate On.

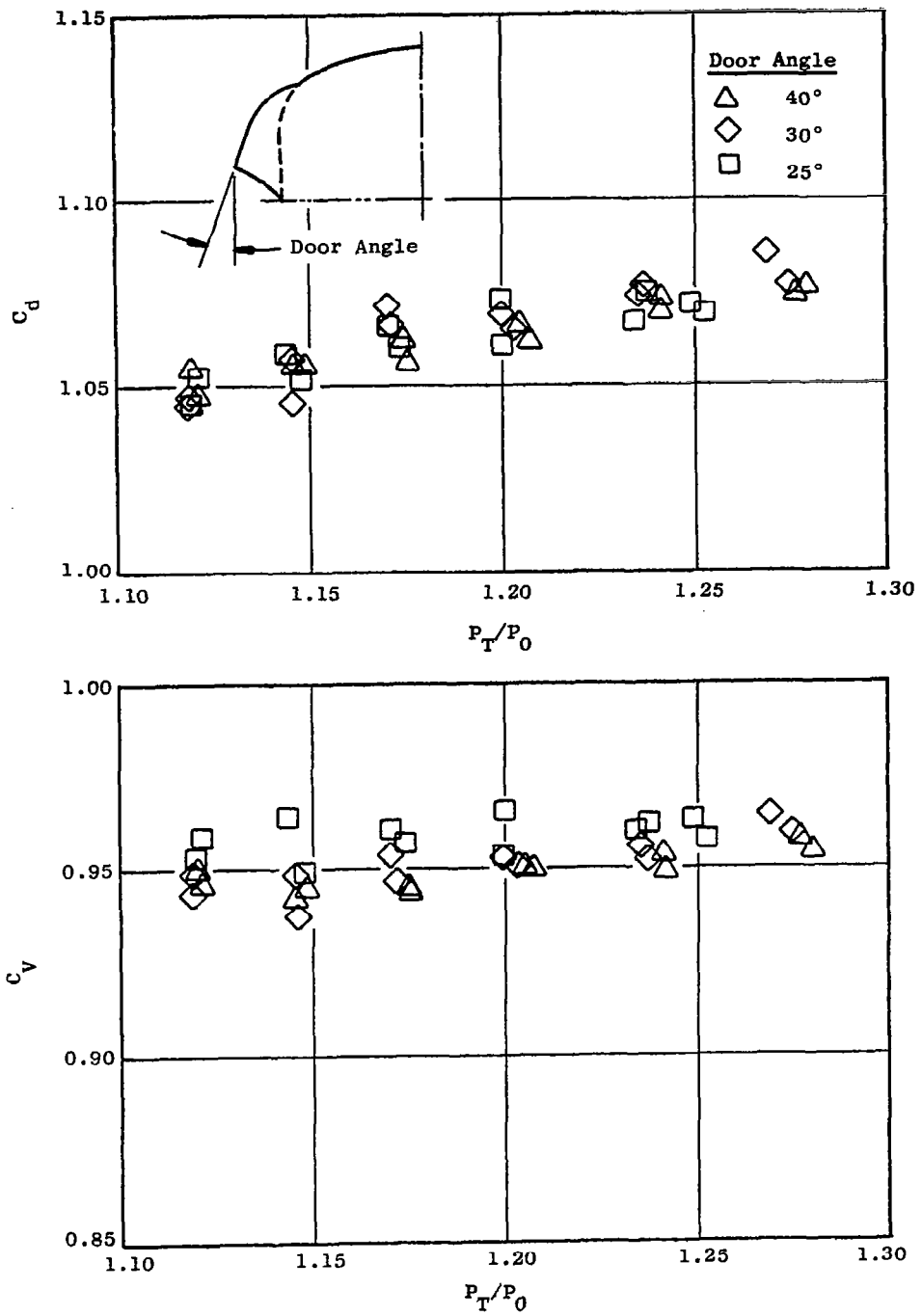

Figure 64. Effect of Nozzle Side Door Angle on Performance, RC-2 Configuration, Plate Off.

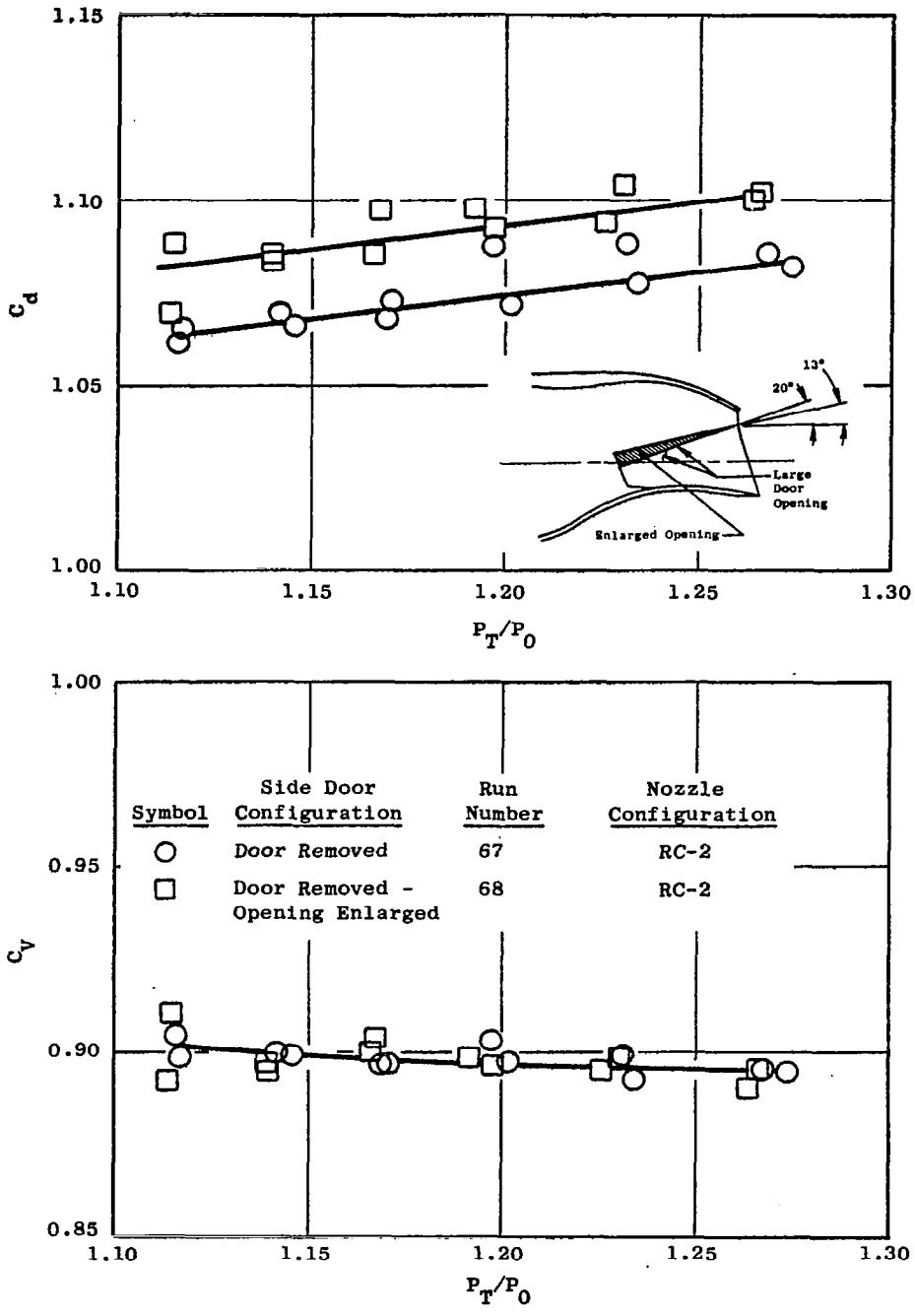

Figure 65. Effect of Side Door Removal, Large Plate On.

APPENDIX D

REVERSE THRUST TEST RESULTS

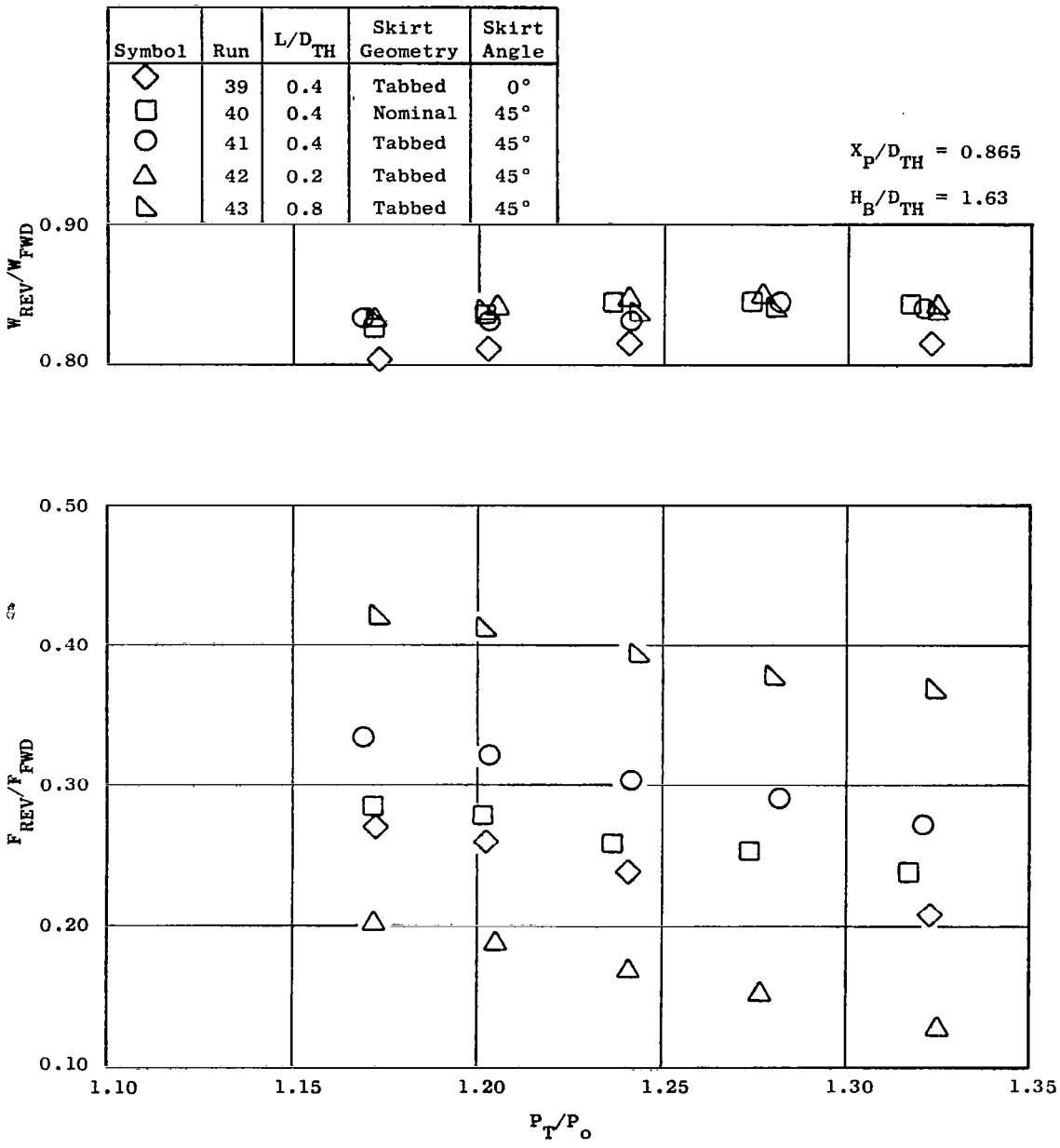

Figure 66. Effect of Lip Length Ratio and Side Skirt Configuration on Reverse Thrust and Airflow, α = 95°, β = 25°.

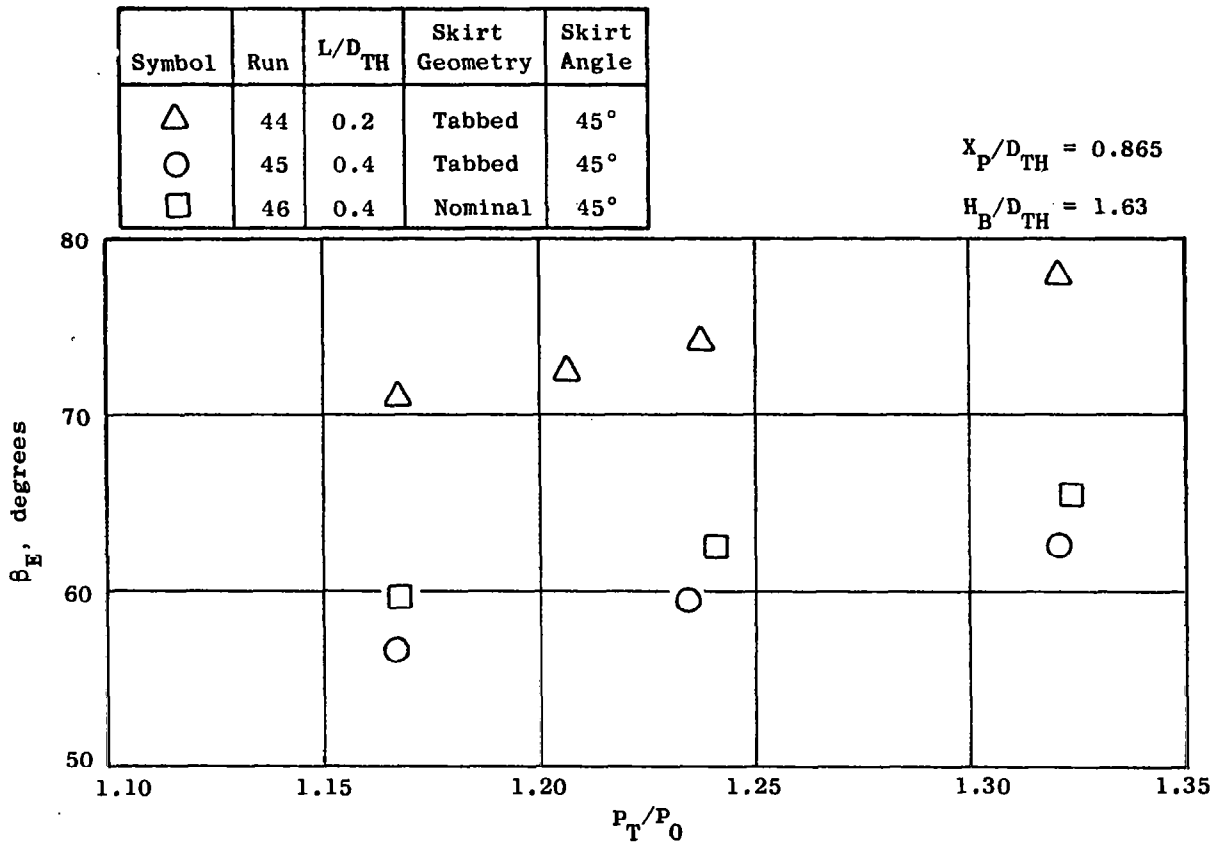

Figure 69. Effect of Lip Length Ratio and Skirt Configuration on Effective Efflux Angle, $\alpha = 95°$, $\beta = 35°$.

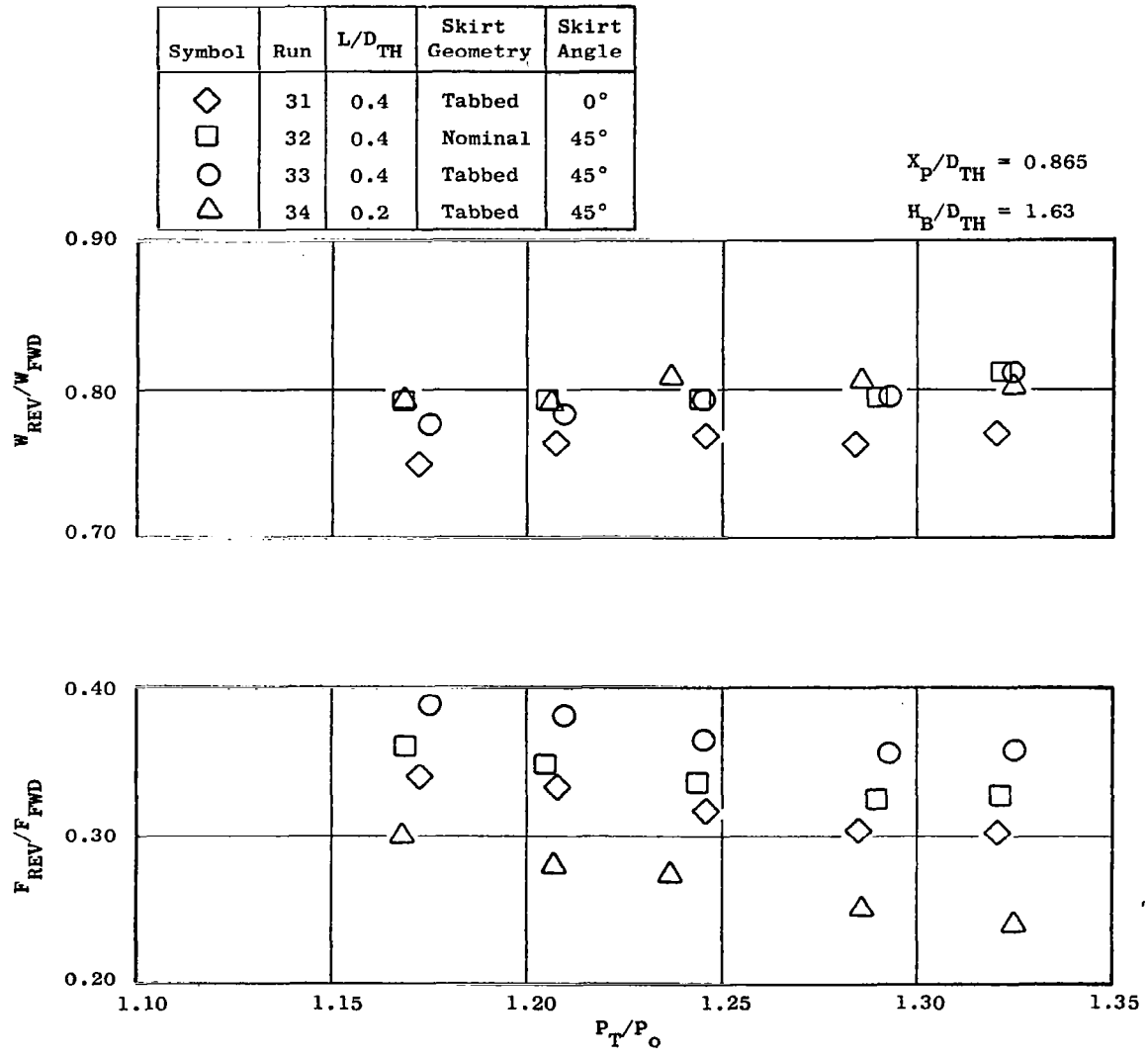

Figure 70. Effect of Lip Length Ratio and Side Skirt Configuration on Reverse Thrust and Airflow, α = 105°, β = 25°.

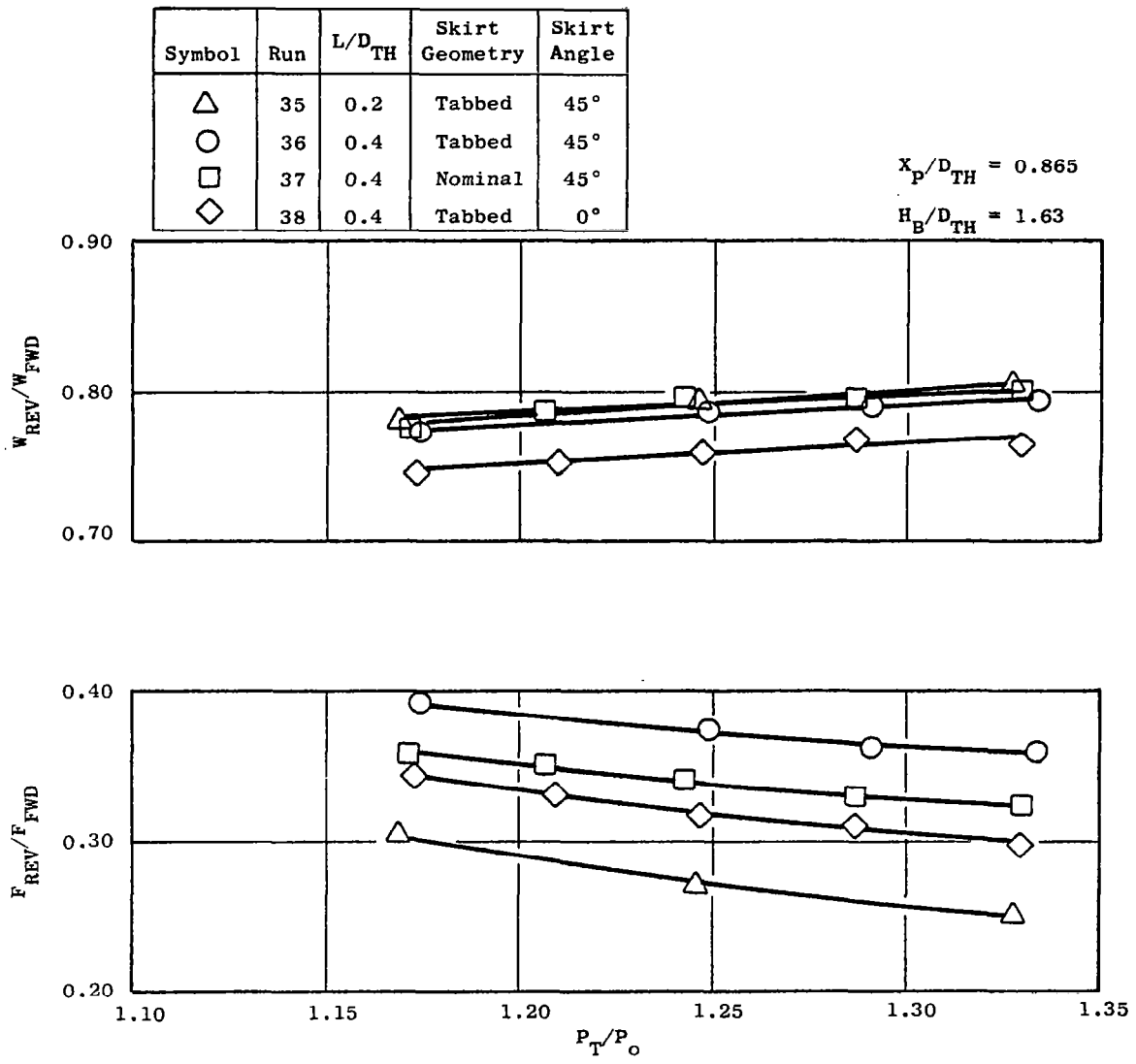

Figure 71. Effect of Lip Length Ratio and Side Skirt Configuration on Reverse Thrust and Airflow, α = 105°, θ = 15°.

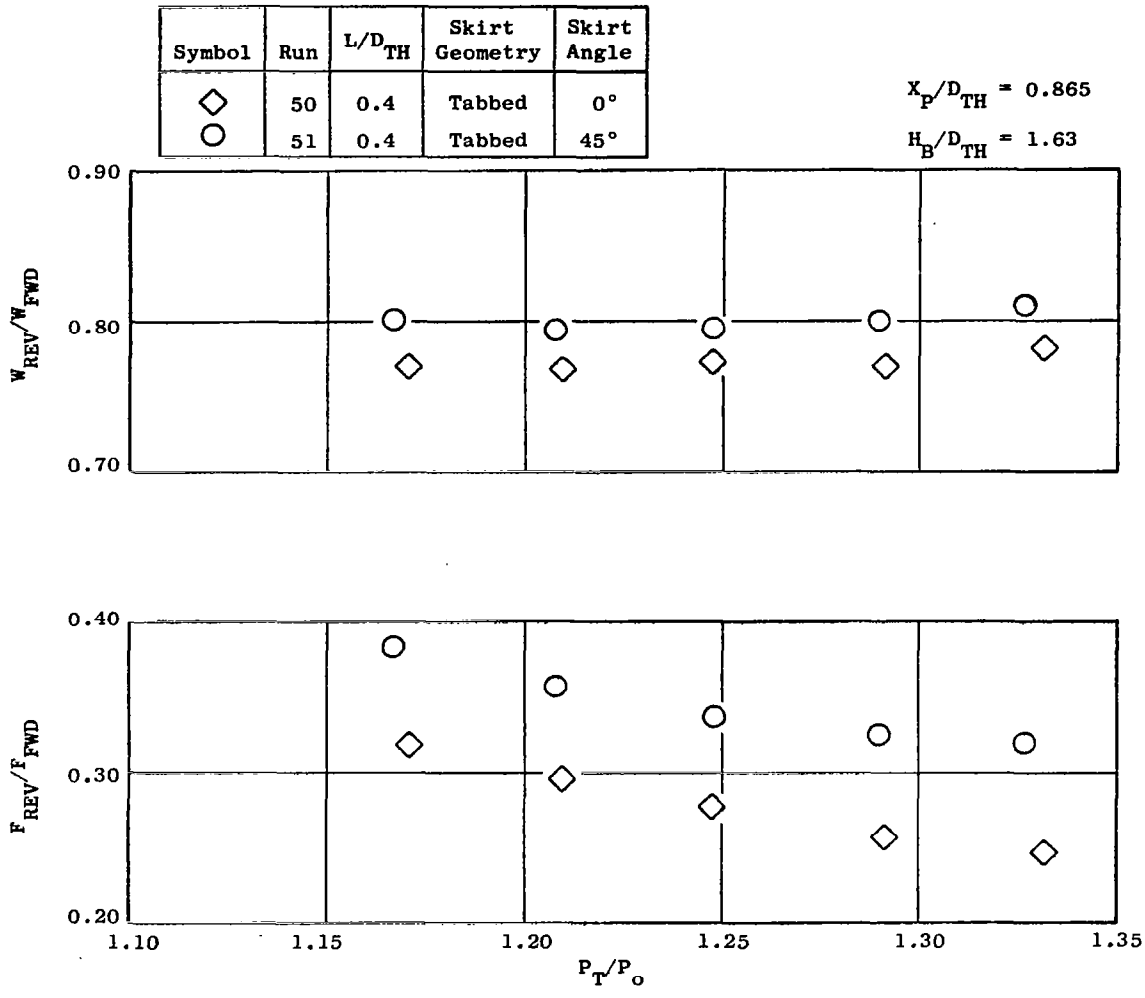

Figure 72. Effect of Tabbed Side Skirt Angle on Reverse Thrust and Airflow, $\alpha = 105°$, $\beta = 35°$.

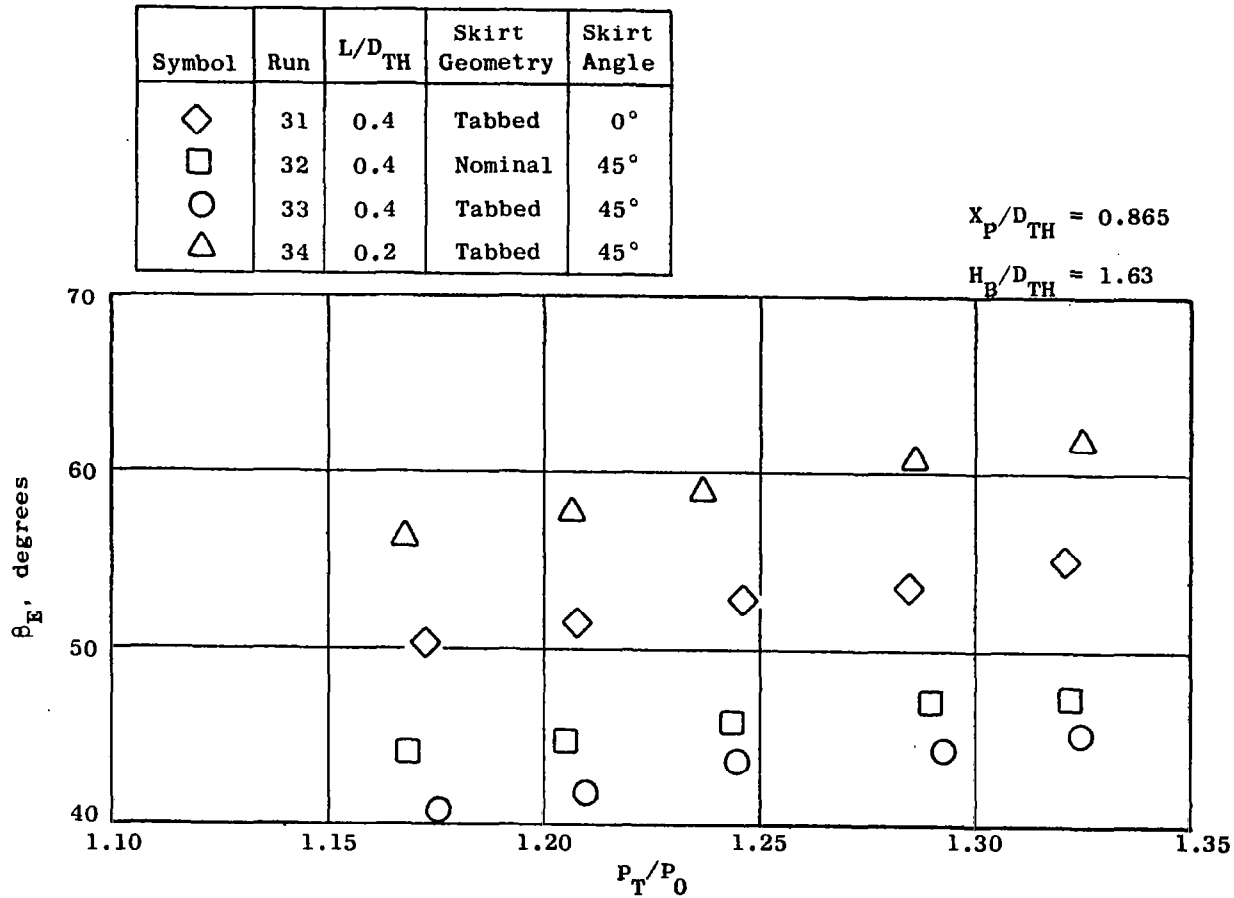

Figure 73. Effect of Lip Length Ratio and Side Skirt Configuration on Effective Efflux Angle, $\alpha = 105°$, $\beta = 25°$.

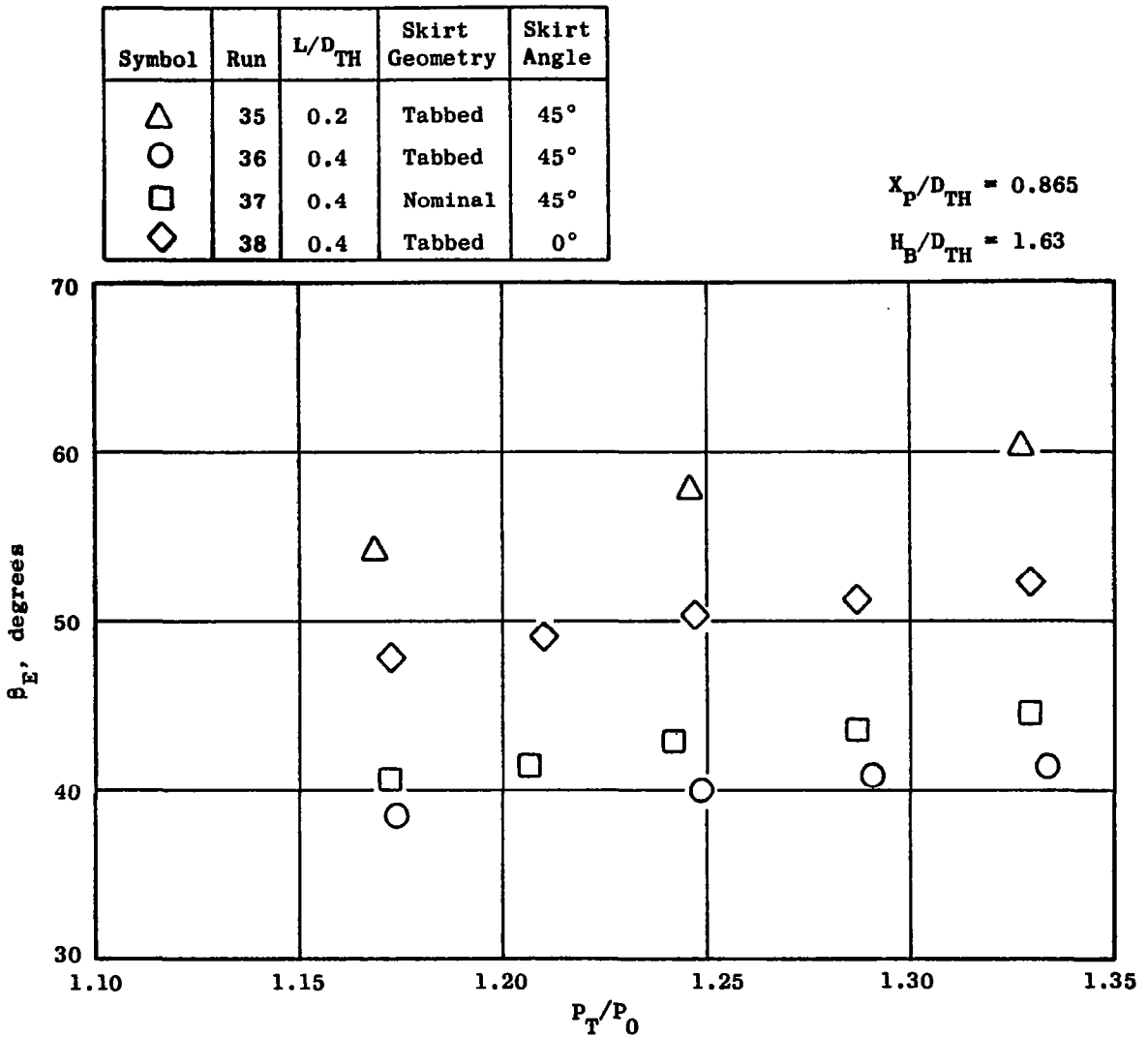

Figure 74. Effect of Lip Length Ratio and Side Skirt Configuration on Effective Efflux Angle, $\alpha = 105°$, $\beta = 15°$.

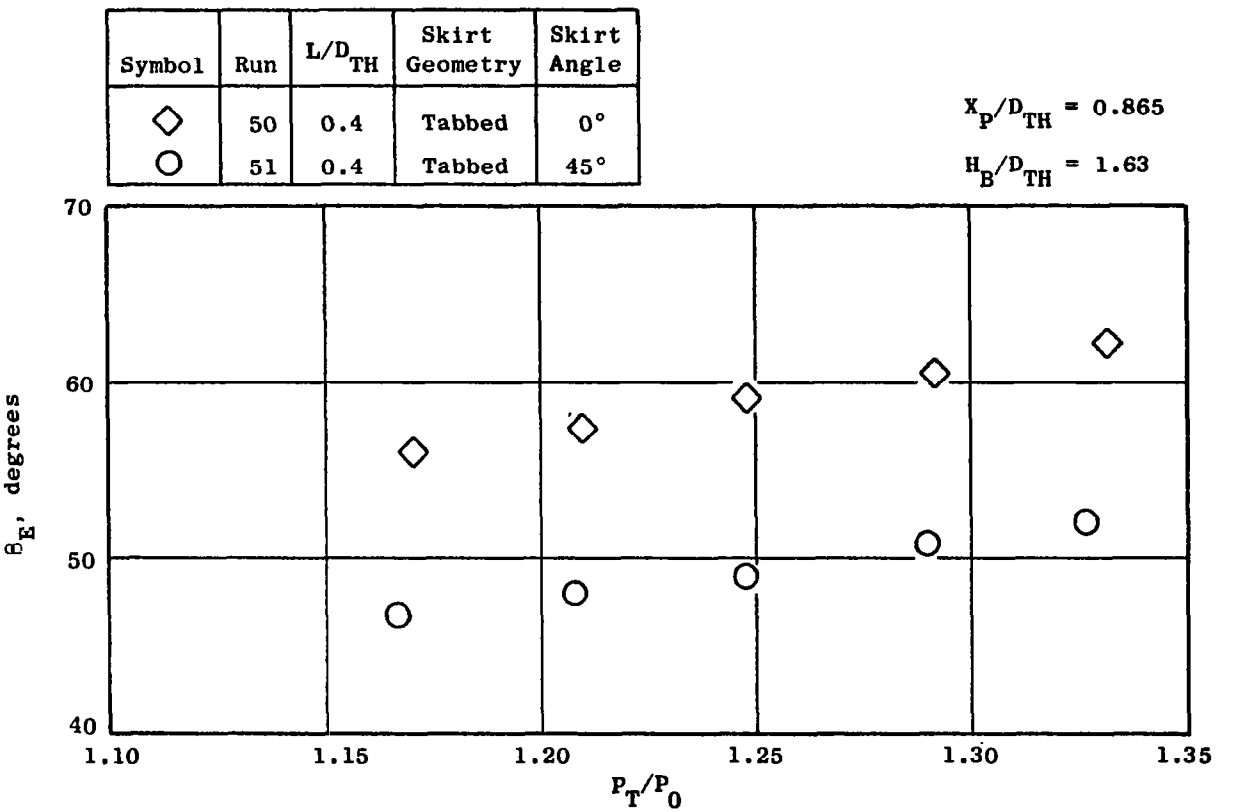

Figure 75. Effect of Tabbed Side Skirt Angle on Effective Efflux Angle, $\alpha = 105°$, $\beta = 35°$.

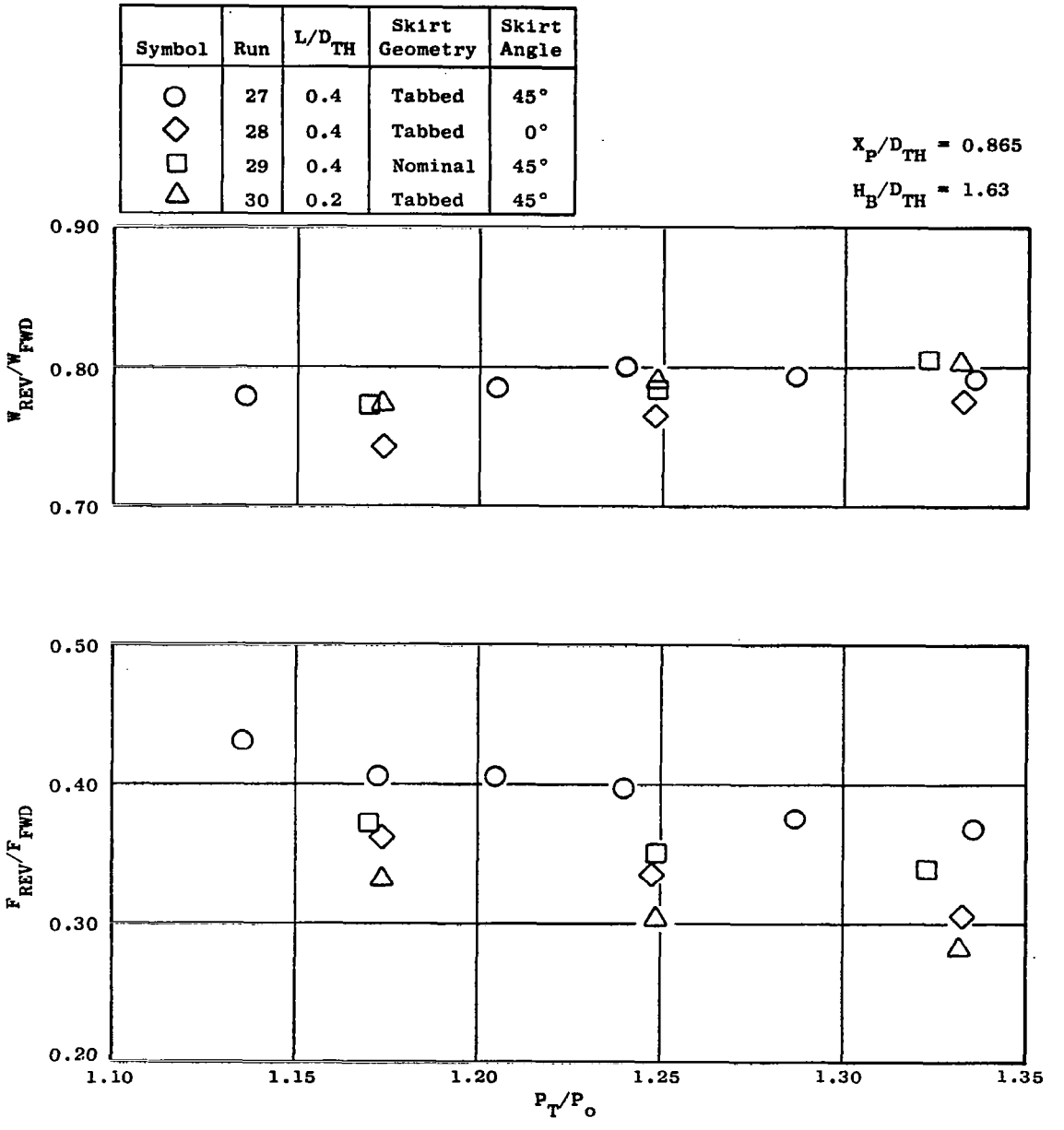

Figure 76. Effect of Lip Length Ratio and Side Skirt Configuration on Reverse Thrust and Airflow, $\alpha = 115°$, $\beta = 15°$.

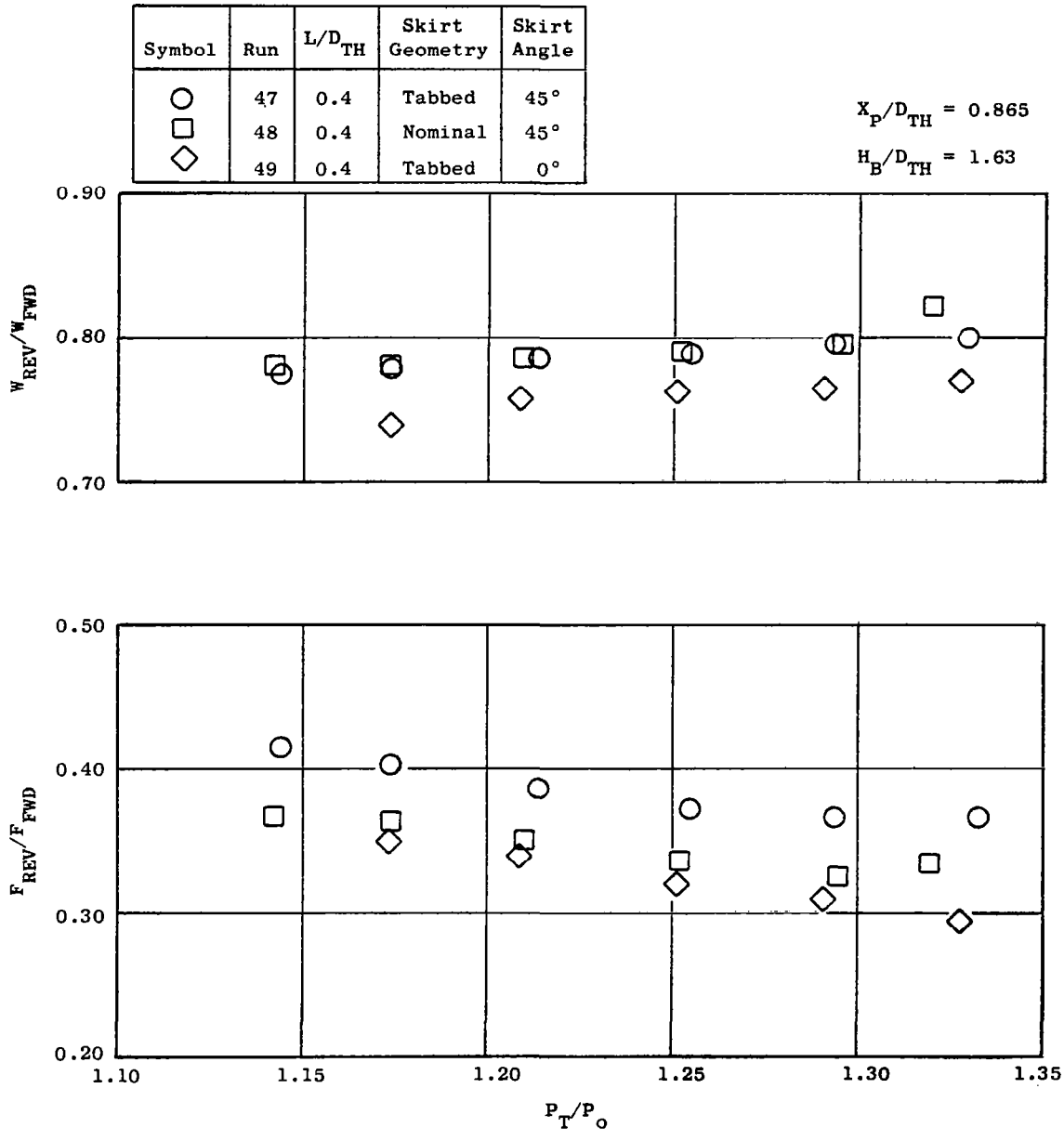

Figure 77. Effect of Side Skirt Configuration on Reverse Thrust and Airflow, α = 115°, β = 25°.

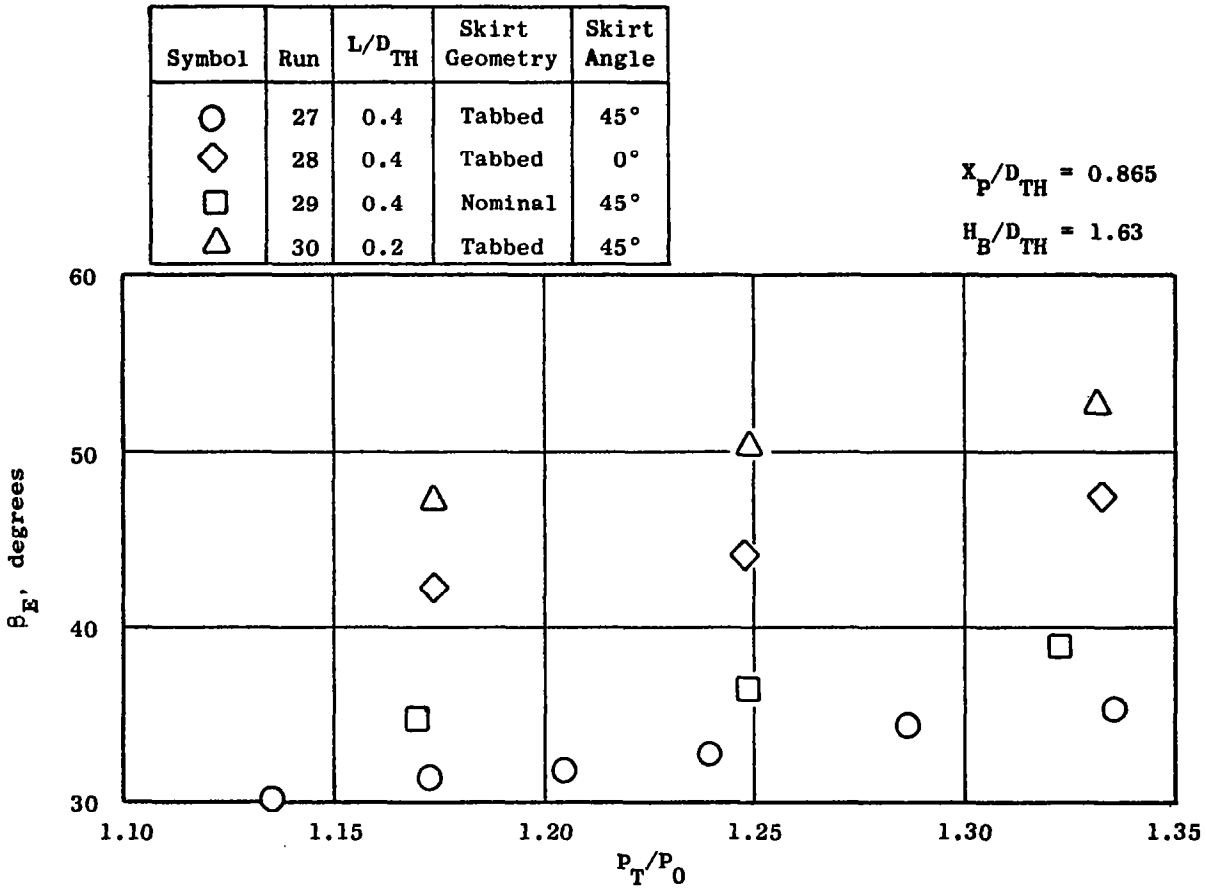

Figure 78. Effect of Lip Length Ratio and Side Skirt Configuration on Effective Efflux Angle, $\alpha = 115°$, $\beta = 15°$.

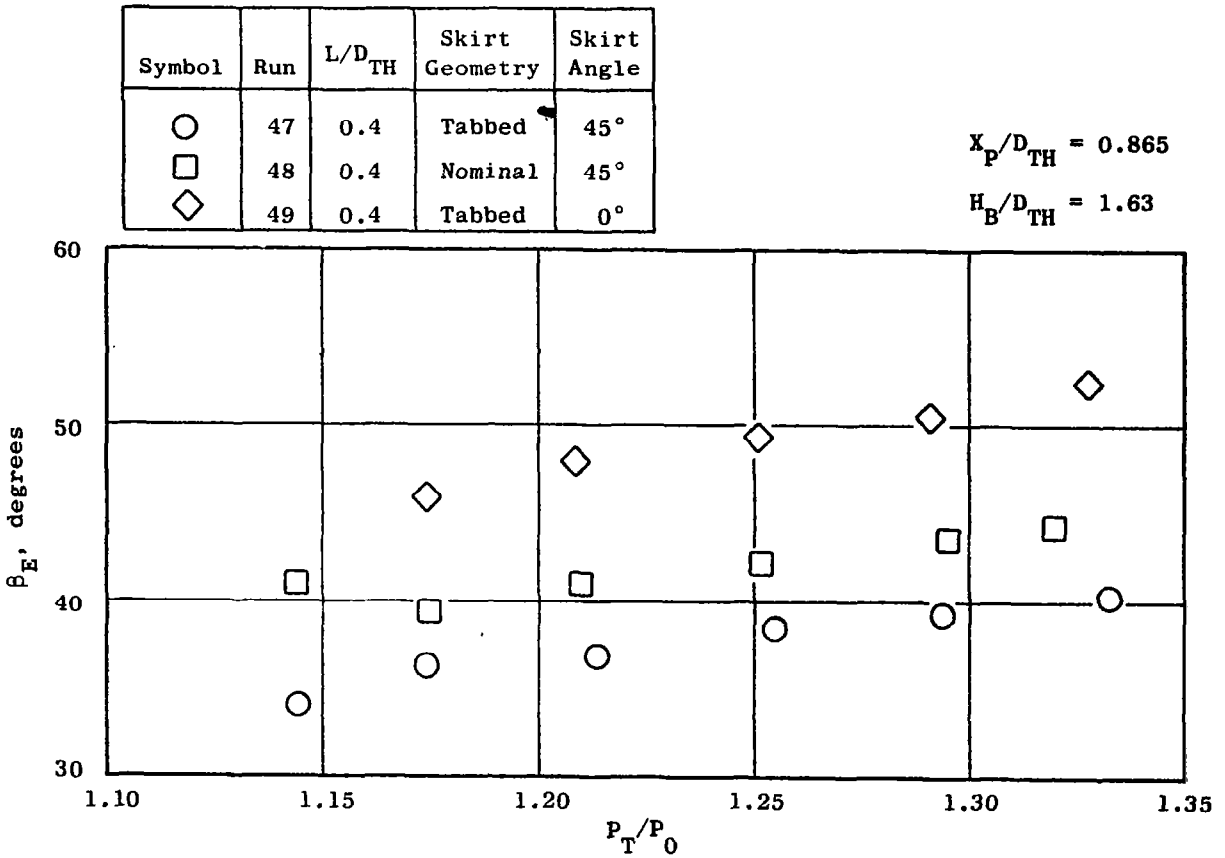

Figure 79. Effect of Side Skirt Configuration on Effective Efflux Angle, $\alpha = 105°$, $\beta = 25°$.

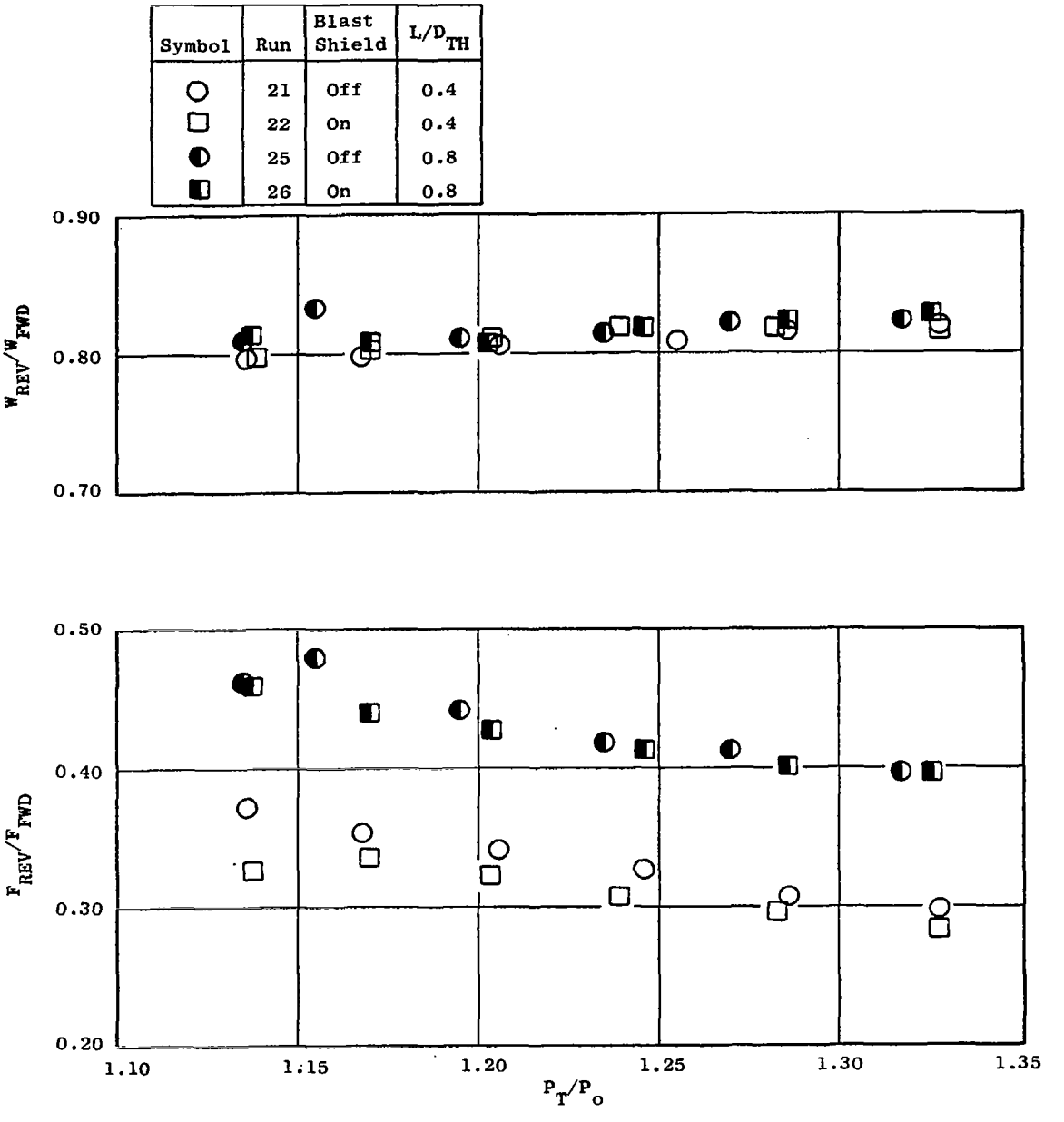

Figure 80. Effect of Blast Shield on Reverse Thrust and Airflow Characteristics.

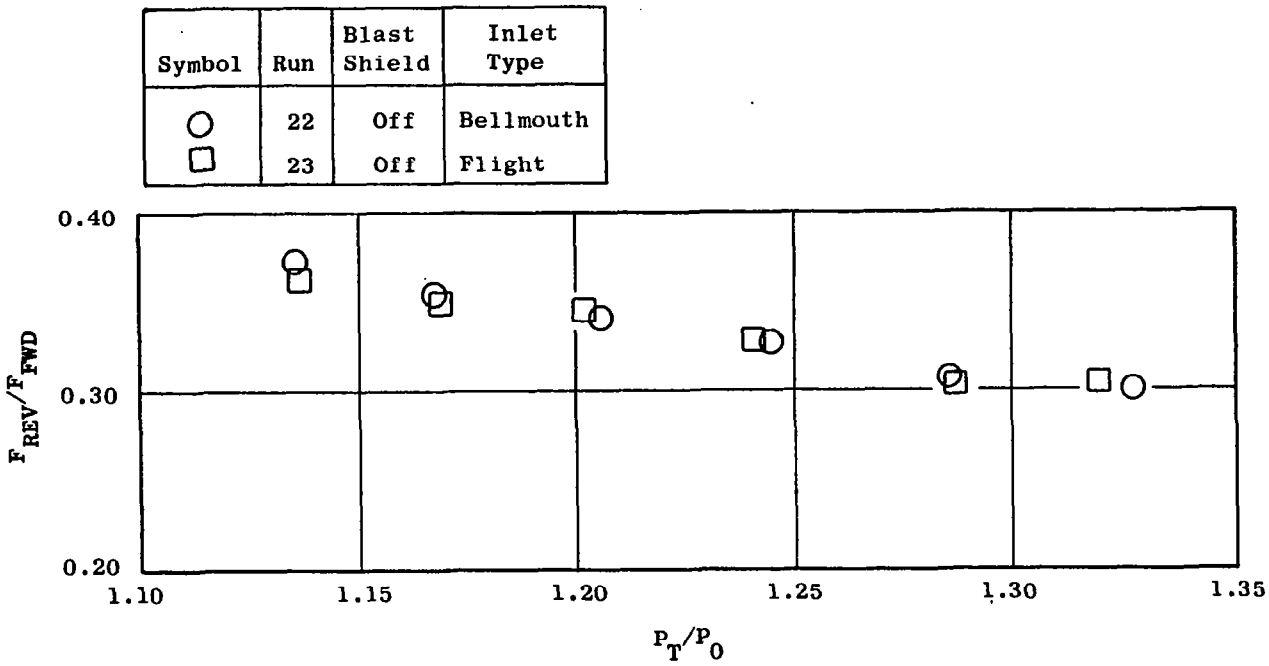

Figure 81. Effect of Inlet Type on Reverse Thrust.

SECTION 9.0

REFERENCES

1. Grey, R.E., and Wilsted, H. Dean; "Performance of Conical Jet Nozzles in Terms of Flow and Velocity Coefficients," National Advisory Committee for Aeronautics Report 933, 1949.

2. Quiet Clean Short-Haul Experimental Engine (QCSEE) Over-the-Wing (OTW) Final Design Report, NASA CR134848, May 1976.